Title	Long-term mechanical performance of geothermal diaphragm walls in stiff clay
Author(s)	Dai, Quanwei; Li, Zili
Publication date	2019-09-16
Original citation	Dai, Q. and Li, Z. (2019) 'Long-term mechanical performance of geothermal diaphragm walls in stiff clay', Tunnelling and Underground Space Technology, 94, 103113 (21pp). doi: 10.1016/j.tust.2019.103113
Type of publication	Article (peer-reviewed)
Link to publisher's version	http://www.sciencedirect.com/science/article/pii/S0886779819304663 http://dx.doi.org/10.1016/j.tust.2019.103113 Access to the full text of the published version may require a subscription.
Rights	**© 2019, Elsevier Ltd. All rights reserved. This manuscript version is made available under the CC BY-NC-ND 4.0 license.** https://creativecommons.org/licenses/by-nc-nd/4.0/
Embargo information	Access to this article is restricted until 24 months after publication by request of the publisher.
Embargo lift date	2021-09-19
Item downloaded from	http://hdl.handle.net/10468/8620

Long-term mechanical performance of geothermal diaphragm walls in stiff clay

Quanwei Dai[1], Zili Li[2√]

[1]Mr Quanwei Dai

Civil, Structural & Environmental Engineering, School of Engineering,

University College Cork, Cork, Ireland.

daiquanwei@yahoo.com

[2]Dr. Zili Li

Civil, Structural & Environmental Engineering, School of Engineering,

University College Cork, Cork, Ireland.

zili.li@ucc.ie

[√]Corresponding Author: Civil Engineering Building, College Road, Cork, T12 YN60, Ireland.

zili.li@ucc.ie

ABSTRACT

Diaphragm wall equipped with ground heat exchangers is one type of thermo-active foundations, which harness the energy stored by the ground for heating and/or cooling buildings. Past investigations on geothermal diaphragm walls mainly focused on the thermal performance, but paid little attention on their mechanical response to geothermal energy operation. This paper conducts thermo-hydro-mechanical (THM) finite element analyses to investigate the long-term performance of geothermal diaphragm walls in stiff clay. The numerical analyses take account of both the station excavation process in short-term and long-term behaviour of the diaphragm wall. The long-term soil-structure interaction simulation includes three scenarios, examining the effects of ground consolidation, external thermal solicitations and seasonal geothermal operation, respectively. A comparison between the mechanical behaviour of the geothermal diaphragm wall and that of the same wall without geothermal activation indicates that geothermal operation may have an impact on structural serviceability issues (e.g. thermal-induced concrete cracks) although unlikely cause critical safety problems. In particularly, the ground settlement near the station is very sensitive to the stiffness degradation of the stiff clay during geothermal operation, while specific attention should be given to the structural performance at the connections between the wall and slabs due to thermo-induced additional stress concentration.

KEYWORDS

Geothermal foundation

Diaphragm wall

Long-term mechanical behaviour

Long-term ground settlement

Thermo-hydro-mechanical analysis

1 Introduction

Geothermal energy is a type of renewable energy generated and stored under the ground surface with the potential to reduce fossil energy consumption. It has attracted increasing attention from the engineering community all over the world. For most European countries, the seasonal ground temperatures remain relatively constant at a certain depth, e.g. 10-15°C down to a depth of approximately 50 m (Brandl, 2006, Adam and Markiewicz, 2009). The utilisation of this shallow geothermal energy allows heat exchange with the ground for cooling and heating civil infrastructures: in winter, heat is extracted from the ground to satisfy heating needs, whereas heat is injected into the ground during summer for cooling demands. Over the last few decades, the technologies for the exploitation of low enthalpy geothermal energy have been developed significantly, especially thermo-active underground structures.

Unlike conventional ground heat exchanger (GHE) systems, e.g. earth collectors or borehole heat exchangers, thermo-active ground structures are more cost-effective and environmentally friendly (Brandl, 2006). This technology embeds heat exchanger pipes into underground structural elements such as slabs, anchors, tunnel lining, pile foundations and diaphragm walls, enabling the structural system to absorb geothermal resources and sustain loads at the same time. The main benefits of thermo-active structures include: preventing groundwater pollution, saving drilling cost, boosting heat transfer efficiency, and reducing underground space occupation.

In the past, the majority of past investigations and practices of thermo-active structures focused on energy piles (Bourne-Webb et al., 2009, Brandl, 1998, Brandl, 2006, Gashti et al., 2014, Jeong et al., 2014, Knellwolf et al., 2011, Laloui et al., 2006, Ouyang, 2014, Suryatriyastuti et al., 2012). Recently, growing attention has been attracted to other thermo-active structures, for example, diaphragm walls (Amis et al., 2010, Coletto and Sterpi, 2016, Di Donna et al., 2017, Sterpi et al., 2017, Sun et al., 2013, Xia et al., 2012, Sterpi et al., 2014, Rammal et al., 2016, Barla et al., 2018). Diaphragm walls are widely adopted as earth retaining structures for deep pit foundations, such as metro stations or high-rise building foundations; given the same concrete volume, diaphragm wall may provide relatively larger heat-exchanging contact area with surrounding ground than piles, which in turn enhance the heat exchange efficiency (Brandl, 2006).

Despite the increasing research outcomes on the thermal performance study of geothermal diaphragm walls (Adam and Markiewicz, 2009, Brandl, 2006, Di Donna et al., 2017, Sun et al., 2013, Xia et al., 2012, Barla et al., 2018), the study on the mechanical aspect of energy walls is still scarce, even though some investigations have been made recently (Bourne-Webb et al., 2016, Coletto and Sterpi, 2016, Rui, 2014, Rui and Yin, 2018, Barla et al., 2018, Sterpi et al., 2017, Rammal, 2017, Dong et al., 2018). Mimouni and Laloui (2015) conducted a full-scale experimental site with four energy test piles, and indicated that differential displacements between conventional and energy piles could induce potential damage to the supported superstructure in stiff soil layers. Even though their results showed that the magnitudes of differential ground movements due to energy piles are significantly low, it's still essential to examine the undetermined mechanical performance due to energy diaphragm walls. The analysis of a geothermal diaphragm wall can be more complicated than an energy pile, in terms of the surrounding ground conditions. The pile foundation of a building is usually entirely embedded in soil, whereas some part of a diaphragm wall is exposed to the air. The heating and cooling operation causes the soil and the concrete to expand and shrink, respectively. As a result, the thermal-operation induced differential displacement between the soil side and the soil-free side of the wall may affect the performance of the diaphragm wall in the long run.

Bourne-Webb et al. (2016) pointed out that the mechanical response (displacement and bending moment) of the thermal wall from the geothermal operation is limited, on the basis of a 2D symmetrical thermo-hydro-mechanical numerical model. Rui (2014) programmed in-house 2D finite element codes to investigate both the short-term and long-term THM responses of energy walls for the first time, based on a well-documented thermal diaphragm wall project in London. Later, Rui and Yin (2018) concluded that the effect of the geothermal operation on the long-term wall movement magnitude was small considering seasonal variations. Meanwhile, Barla et al. (2018) also conducted 2D TH analyses to investigate the thermal-induced mechanical effects on the wall in terms of the computed horizontal displacement and bending moment along the wall using a FLAC model. Further to 2D numerical analysis, Coletto and Sterpi (2016) and Sterpi et al. (2017) conducted a 3D numerical TH model to predict the wall movement and internal forces (axial force and bending moment) and indicated that the computed results is within the acceptable range of geotechnical safety. Rammal (2017) investigated the impact of various thermal solicitations and different soil thermo-mechanical properties on the structural performance (e.g. internal structural forces) of geothermal diaphragm walls in Paris metropolitan underground stations, and provided some recommendations for the industrial designers. In addition, Dong et al. (2018) found a thermal-induced increase of axial strain in the wall and earth pressure at the soil-wall interface through both experimental and numerical modelling approaches. Most of past studies, however, usually consider soil-structure THM interaction in an idealised simplistic scenario (e.g. one-layer homogenous soil), but seldom compare the computed retaining wall behaviour against reliable field measurements. Due to lack of comprehensive field data of energy walls, the proposed finite element models could hardly be well validated and therefore may have difficulty in accurately predicting the geothermal retaining wall behaviour in the long term.

This paper mainly focuses on the investigation of the long-term performance of geothermal diaphragm walls in relation to the mechanical behaviour of structural elements and ground response. In this study, a THM numerical model using HSS model is performed based on the construction and design records from London Dean Street Station reported by Rui (2014). The finite element analysis considered the whole life of London Dean Street Geothermal Station: from station construction in the short term to long-term geothermal operation. In particular, the thermal effects due to external thermal solicitations (e.g. air temperature seasonal variation, soil temperature and station temperature) and seasonal geothermal operation were examined by specific modelling scenarios, respectively.

2 Project overview

Di Donna et al. (2017) collected the existing records of constructed geothermal diaphragm walls from studies available from the UK, Austria and China. Although some past studies have provided details of the energy efficiency, the field data on the mechanical performance of energy wall projects are rather rare, especially for the long term. Up to date, to the authors' best knowledge, only Rui (2014) reported some comprehensive monitoring data of the horizontal geothermal wall movement at the construction stage in London Dean Street Station Project. The field measurements at the short-term construction stage were used to test Rui (2014)'s finite element model, followed by the prediction of long-term wall behaviour, whereas there remain some major limitations in his study: 1) numerical accuracy; 2) model validation; and 3) various mechanical aspects.

- Compared with sophisticated commercial finite element software, Rui (2014) wrote his own in-house thermo-hydro-mechanical codes for soil-structure THM interaction.

Since his code is not yet open-source, the predicted diaphragm wall behaviour in his study can hardly be reproduced by other researchers without using the codes. There remains an arguable uncertainty of his FE code with regard to the accuracy and numerical stability if it has not yet been comprehensively examined by some international peers and / or independent third party.

- In order to match the field measurements, Rui (2014) purposely zeroed the computed wall displacements at the toe but failed to explain the reason in details. There is lack of justification, to the authors' best knowledge, for such intentional modification on the basis of past diaphragm wall studies.
- In terms of THM soil-structure interaction in the long term, Rui (2014) only focused on diaphragm wall behaviour and temperature-variation-induced soil volume change, but paid little attention on adjacent ground settlement and structural behaviour of the train station and other important mechanical behaviour, which may be sensitive to geothermal operation.

Considering the aforementioned limitations, this study conducted thermo-hydro-mechanical (THM) analysis to evaluate whole-life behaviour of geothermal station using sophisticated PLAXIS finite element software. The computed results of short-term wall displacements due to station construction are compared against the field measurements, followed by specific investigation of both geothermal diaphragm wall performance and ground response in the long term. The overview of this project is described as follows:

In London, there has been some energy foundations adopted in new or redeveloped station boxes. Dean Street Station is one of these geothermal boxes, known as the second thermal wall project in the UK, with 500 kW geothermal capacity. The station is located at the intersection of Dean Street and Oxford Street (red block C & D in Figure 1), consisting of two main boxes with different base levels. A combination of thermal piles and thermal walls has been installed in the station.

The station box was constructed using bottom-up method. Prior to the pit foundation excavation, a 1-meter-thick diaphragm wall trench (up to 41m depth) was constructed around the excavation site. 40-m-long absorber pipes were attached to the reinforcement cage and lowered into the trench (0.25 m from the soil-side surface of the wall), and later grouted together with the steel cage to form geothermal diaphragm wall panels. The foundation pit was designed to be 28.9 m in depth and excavated following 5 stages as shown in Figure 2. Three temporary props and one slab were constructed to support the excavation for each stage. Due to access constraints at the site, the lowest prop was omitted during excavation as to save construction time and cost. After excavated to the designated elevation, slabs were cast from the base of the station, and the temporary props were replaced by slabs to form a five-level station box.

3 Finite element model

3.1 Model geometry

For simplicity, a 2D plane strain THM analysis of London Dean Street Station is conducted using finite element software PLAXIS 2D (Brinkgreve et al., 2018), as shown in Figure 3. In PLAXIS, a fully coupled flow-deformation (i.e. soil-fluid coupled) and thermal transient calculations is adopted for long-term geothermal soil-structure interaction. The diaphragm wall around the station is set to be wished in place and the initial stress state (i.e. geostatic phase) for the short-term simulation is generated by the K0 procedure available in PLAXIS, while the initial stress balance for the long-term model is set automatically after the final phase of the short-term model. The excavation block is 32 m wide and 28.9 m deep, surrounded by 1-m-thick and 41-m-deep diaphragm wall panels. The diaphragm wall is mostly embedded in low-permeability clay including 23-m-thick London Clay and 9-m-thick Lambeth Group Clay. The model boundary is 160 m deep and extended 144 m laterally from excavation edges to both sides. The structural members used during construction are shown in refined mesh block of Figure 3: three temporary props (green in the figure, 1 m thickness), five slabs (grey in the figure, 1 m thickness) and a base slab (2 m thickness).

The model consists of 10011 15-node triangular elements. For better accuracy, the finite element meshes around the excavation pit are refined, whereas coarser meshes are adopted away from the station as to save computational cost. Besides, the geothermal operation mode in this paper is considered as symmetrical operation mode (the geothermal systems at both sides of the diaphragm wall are activated), whereas the model in this study is conducted as a full-scale model instead of a symmetric half-scale one, on the purpose of facilitating future study on asymmetric geothermal operation mode.

3.2 Boundary conditions

The water level is set to be 3 m below ground surface, while the pore pressure distribution is assumed to be hydrostatic prior to soil excavation. During station construction, the clayey soil layers (e.g. London clay and Lambeth Group) are assumed in undrained condition, whereas drainage is allowed at all model boundaries for long-term thermo-hydro-mechanical coupled analysis after construction. The hydraulic boundary conditions inside the station are set to be impermeable throughout soil excavation and long-term consolidation. The maximum negative pore pressure is controlled within -100 kPa to avoid suction cavitation; negative pore pressure lower than -100 kPa will result in perfect vacuum condition with zero absolute pressure in the soil, which is prohibitively unlikely to happen.

At the side and bottom boundaries of the model, the horizontal and vertical displacements are fixed. The dimension of this FE model is 10 times greater than the excavation site (see Figure 3) as to minimise the boundary effect on the numerical results. The top boundary is free to move, allowing possible ground settlements to be induced by excavation, consolidation and temperature variations.

For simplicity, no adiabatic boundaries have been imposed at the contact with the external air inside the station. The heat transfer among the whole model is controlled by the thermal properties of the material, e.g. thermal conductivity. The configuration of thermal boundaries is illustrated in Figure 3. All side boundaries except the top boundary set to be an initial temperature, 12°C, same as the soil temperature, corresponding to the soil constant temperature at a depth 10-12m in Europe (Brandl, 2006), whilst the temperature of the top thermal boundary is varying with seasons. The temperature inside the station is kept constant at 18°C all year round, all the thermal boundaries inside the station and along the slabs set as 18°C when activated at the start. In this figure, the heat exchanger pipes inside the diaphragm are modelled as a plane element together with two thermal boundaries, which is able to generally consider the equivalent effect of 3D spaced heat exchange tubes by thermal function in the PLAXIS 2D model. The top thermal boundary and these two heat-exchanging boundaries are controlled by thermal functions inside PLAXIS. In Fully coupled flow-deformation analysis, the temperature set for each boundary or material block is only used to initialize the temperature at the beginning of the long-term simulation, while the temperature afterwards change time-dependently (Brinkgreve et al., 2018).

3.3 Material properties

3.3.1 Structural properties

The temporary props for construction stages are made of 1-m-diameter hollow steel tubes, modelled as node-to-node anchors, while slabs and diaphragm walls are modelled as concrete polygon entities in PLAXIS. Compared to plate elements, the use of the concrete clusters for walls and slabs enables to simulate the temperature variations inside the geothermal diaphragm wall and slabs more realistically. The material properties of anchors and concrete are listed in Table 1 and Table 2, respectively. For simplicity, the solid thermal expansion mode is set to be linear.

Due to creep and relaxation over time, Young's modulus of diaphragm wall is assumed to be 26GPa (70% of the original 37GPa for the C50/60 concrete) for the short-term construction stage, while 19GPa (50% of the original value) was adopted for the long-term analysis as advised in CIRIA C580 by Gaba et al. (2003). For simplicity, the stiffness of slabs at both construction and long-term stages remains constant at 26GPa.

3.3.2 Soil properties

In terms of soil properties on site, Rui and Yin (2018) indicated that the use of non-linear elastic model for clayey layers (i.e. London Clay and Lambeth Group) in their FE model can predict short-term wall displacement in better agreement with the field measurements than that by linear elastic model. Similar findings are also noted in this study. To simulate soil-structure interaction realistically without compromising computational cost, this FE analysis adopted Hardening soil model with small-strain stiffness (HSS) model for the nonlinear elastoplastic behaviour of clayey soil and Mohr-Coulomb (MC) model for nonclayey soils near the ground surface. The mechanical and thermal properties for soil layers are listed in Table 3 and Table 4, respectively. Linear thermal expansion coefficients are assumed for all soil materials in the numerical simulation. In addition, the specific material properties of HSS models are listed in Table 5.

Most soil properties listed in Table 2, Table 3 and Table 4 were based on Crossrail design guideline (Rui, 2014). For better accuracy, the parameter c and ϕ for Lambeth Group were determined according to the upper bound data suggested by Hight et al. (2004). The parameters of HSS model were also calibrated against the experimental lab tests available in literature: both London Clay A3 and A2 were determined by matching the shear modulus with triaxial test data from Gasparre (2005); the HSS model parameters of both Lambeth Group UMC and LMC were calibrated by matching the shear modulus with the undrained young's modulus from Hight et al. (2004).

3.4 Geothermal scenarios

3.4.1 Construction phase and long-term phases

This study aims to evaluate the influence of geothermal operation on the mechanical performance of structural elements and surrounding ground response. In general, the mechanical behaviour of geothermal diaphragm wall system is mainly governed by three factors: consolidation, external thermal solicitations (e.g. air temperature seasonal variation, soil temperature and station temperature) and geothermal operation. In order to separate these aspects and analyse the influence one after another, this study considered four modelling scenarios: one identical short-term scenario followed by three different long-term scenarios.

1A) Construction phase (HM): model validation stage, modelling the construction procedure and comparing the computed wall movement against the field motoring data;

2-A) Long-term phase A (HM): thermo-inactive scenario, evaluating the mechanical performance of geothermal diaphragm walls during long-term operation without any thermal solicitation, while only consolidation effect is activated;

2-B) Long-term phase B (THM): thermo-active scenario with no geothermal operation, evaluating the effect of seasonal temperature change on the mechanical behaviour of the structure, while both consolidation and external thermal solicitations are activated;

2-C) Long-term phase C (THM): thermo-active scenario with the geothermal operation, evaluating the effect of geothermal operation on the mechanical behaviour of the structure, while all three factors are activated.

3.4.2 Thermal boundaries

There is no thermal boundary activated during the short-term phase, as temperature change (e.g. hydration heat of cement during concrete construction stage) generally has a much lower impact on the short-term mechanical behaviour of the diaphragm walls than that induced by soil excavation. While the thermal boundary conditions of the three aforementioned long-term phases are various in terms of external thermal solicitations and geothermal operation as shown in Figure 4. In long-term A phase, all the thermal boundaries in the model are set to deactivate temperature with no consideration of thermal effects (see Figure 4(a)). In long-term B phase, all external thermal solicitations are activated, e.g. soil temperature, seasonal air temperature and station temperature. The thermal boundaries of the station box and the far-field soil in this study are set to be constant at 18°C and 12°C, respectively, assuming the temperature inside the station to be relatively invariant by the operation of ventilation system. The thermal boundary at the ground surface remains the same as the external air temperature subject to seasonal changes in London as shown in Figure 4(b). Long-term C phase is very similar to Long-term B phase, as shown in Figure 4(c) except that the temperature of heat exchange pipes inside the wall is activated, allowing the geothermal operation to affect the mechanical behaviour of the diaphragm wall.

Figure 5 shows the annual temperature range of London according to the local seasonal temperature variation (NOAA, 2018). The orange line in the graph represents the high level of temperature in London while the green line stands for the low level of temperature. For simplicity, this study adopts a step-fluctuating thermal function (Figure 5, dash line) to represent seasonal variations, cycling from 4°C for 6 months (winter cycle) to 23°C for 6 months (summer cycle), for both air temperature boundaries and heat exchange fluid inside the wall. The selection of maximum temperature variation range and the presumed step-shaped thermal function considers the mechanical behaviour of geothermal foundation in a potentially most critical scenario on a conservative side (Rammal et al., 2018), whereas the determination of temperature range and thermal function may vary for various projects across the world on a case-by-case basis, depending on the designer's engineering judgement. The heat exchange fluid inside the diaphragm wall is assumed to be constant all the way from the inlet entrance to the outlet exit, since the thermal efficiency is not the primary concern of this study.

4 Geothermal diaphragm wall behaviour

In this section, the computed short-term horizontal wall movement is compared against the field data to validate the FE model. Later, this FE model simulates thermo-hydro-mechanical (THM) soil-structure interaction to investigate long-term mechanical performance of the geothermal diaphragm wall system in five aspects: horizontal wall movement, vertical wall movement, ground settlement, basement heave and internal structural forces (normal force, shear force and bending moment). In all the output data, the sign convention are set as follows: 1) for soil pressures (including total stress, effective stress and pore water pressure), compressive stress is represented by positive / plus sign and tensile stress is negative; 2) for structural forces (N, Q and M), they are set to follow the general definitions of the structural mechanics. Normal force N presents as positive if in tension and negative for compression. While the shear force Q and bending moment M are positive if the material element is rotated in the counterclockwise direction, and negative for rotation in the clockwise direction.

4.1 Short-term diaphragm wall displacement

In London Dean Street Station project, the excavation-induced wall displacement was recorded by inclinometers, where its bottom was assumed to be fixed with zero displacement. Figure 6 compares the computed horizontal wall movements against the field measurements at four construction stages: the installations of Prop 2, Prop 3, Slab 2 and base slab. In general, the computed wall deflection shape matches with the field monitoring curves, whereas the maximum difference between them appears at the bottom of the wall at the last excavation stage (see Figure 6(d)).

Rui (2014) pointed out the wall movement at the bottom of the wall could hardly be measured by the inclinometers and therefore suggested to zero the computed displacements at the base of the wall. Nevertheless, the difference of the wall movement near the bottom of the wall between monitoring data and computed results is an universal problem observed by many researchers across the world (Cabarkapa et al., 2003, Hsieh et al., 2016, Lim et al., 2018, Nisha and Muttharam, 2017, Ou and Hsieh, 2011). Schwamb (2014) indicated the drawbacks of inclinometer measurement led to the underestimate of the movement at the bottom of the wall. The inclinometer can only obtain a relative deflection but not the absolute movement of the wall, as the displacement at the based point of the inclinometer can hardly be determined. There is a lack of justification to zero the wall movement at the toe.

Despite of the discrepancy between the computed results and field measurements, the FE model can generally simulate the short-term wall behaviour during excavation. Besides, the Customer Experience Executive of Transport for London Customer Services pointed out that the long-term field data was unable to be recorded in this case and difficult to collect over decades in practice. Therefore, this study predicts the thermal effect on the mechanical behaviour of geothermal diaphragm walls in the long term based on a short-term validated model rather than a long-term validated model.

4.2 Long-term train station behaviour

4.2.1 Long-term horizontal wall movement

Figure 7(a) shows the incremental horizontal displacement of the diaphragm wall after construction in the long term. The maximum incremental horizontal wall deformation of 6.8 mm towards the excavation side after 30 years is obtained below the base slab, which is as much as 31% of the maximum horizontal movement of 21.9 mm due to construction. Since substantial soil was excavated between Slab 2 and Base Slab within a short period of time (11.2 m depth of soil removed within 36 days), significant excess pore pressure was generated below the base slab after excavation. As soil consolidates with time, the ground below the base slab heaves up and in turn allows the adjoining D-wall to move towards the excavation side in the long term.

One significant movement (3.2 mm) towards the excavation side occurs at the depth of 21.4 m between Slab 2 and Slab 1, where a large amount of soil was excavated during construction as mentioned before. In addition, there are two notable horizontal movements towards the soil side, appearing between Slab 1 and Base Slab, and the bottom of the wall, 4.3 mm and 1.6 mm respectively. The lateral wall movement mode is very likely due to the combined effect of lateral soil pressure, excess pore water pressure dissipation and propping forces of the slabs.

Figure 7(b) shows the incremental horizontal movement of the wall under external thermal solicitations, which is generally consistent with the incremental wall deformation in Long-term A. The wall section above Base Slab shifts 1.2 mm towards the soil side immediately after construction, mainly due to the thermal expansion of the concrete slabs inside the station. When the thermal boundaries along the slabs (18°C) are activated in Long-term B, the 32-m-long slabs expand immediately, and pushes the part of the wall close to the station towards the soil side. There is negligible difference in wall displacement after 30 years between Long-term A and Long-term B below Base Slab. In general, the influence of external thermal solicitations on the incremental lateral movement of the wall is insignificant.

Figure 7(c) shows the incremental wall deformation during geothermal operation. Unlike the wall deflection behaviour in the first two scenarios, the part of wall movement above Slab 1 in Long-term C is significantly affected by the geothermal operation. The differential movement between Long-term B and Long-term C above Slab 1 starts to occur in the summer of the first operation year (1Y summer in the graph), where the wall section near the ground surface in

Long-term C moves 1.2 mm towards the excavation side in the opposite direction from with that in Long-term B. As mentioned earlier, the stiffness of soil layers at large shear stain level (over 0.0001) in HSS model is relatively small, hence, the wall deformation is sensitive to the mechanical change induced by the geothermal operation; that is, the soil stiffness degradation at particular site may notably affect the ground movements during geothermal operation. Nonetheless, the changes of wall deformation below Slab 1 are generally consistent with Long-term B, where the soil stiffness remains high at small strain level and as such little additional displacement is induced by the geothermal operation.

Furthermore, the wall movement also changes with seasonal operations. Above slab 5, the wall moves significantly towards the soil side in winters, approximately 0.8 mm greater than that in summers, while it gradually bends towards the excavation side between Slab 5 and Slab 4.

Figure 8 illustrates the mechanism for the temperature variation inside slabs and wall. In this particular thermal operation mode, there is little temperature variation for slabs, whereas a 14°C temperature variation develops along the wall thickness in winter (4°C near the soil side and 18°C near the station side). In winters, the soil side of the wall (4°C) shrinks, whereas the station side (18°C) expands as shown in

Figure 8. Consequently, the temperature change across the wall thickness causes differential thermal displacement and greater wall bending deflection towards the soil side than that in Long-term B. In summers, since the absorber fluid temperature (23°C) is closer to the station temperature (18°C), the temperature difference along the wall thickness is small and therefore the wall deflection is almost the same as the results from Long-term B. Below slab 5, the D-wall displacement is similar to that in Long-term B. As soil pressure increases along the depth of the wall, the geothermal operation becomes less influential on the changes in wall movements.

In summary, in Long-term A, the horizontal wall movement is mainly controlled by the hydro-mechanical effects (e.g. lateral soil pressure and excess pore water pressure). When the external thermal solicitation is activated in Long-term B without geothermal operation, the thermal expansion of the slabs pushes part of the diaphragm wall towards the soil side. During the geothermal operation in Long-term C, the geothermal operation has a great effect on the wall behaviour near the ground surface but becomes less influential with increasing soil depth.

4.2.2 Long-term vertical wall movement

In addition, the vertical deflection of the diaphragm wall during geothermal operation is evaluated in relation to the risk of differential movement to the surface building.

Figure 9(a) shows the change of vertical wall movement in Long-term A without thermal solicitation. During ground consolidation after construction, the entire wall heaves over the next 30 years up to 7.2 mm near the ground surface level. When the external thermal solicitations is activated in Long-term B, the entire wall heaves up 2.9 mm greater than that in Long-term A due to the thermal extension of the concrete as shown in Figure 9(b). In contrast, the geothermal operation in Long-term C results in cyclical wall vertical displacement as shown in Figure 9(c). The wall heaves up during summers but shrinks in winters: the differential vertical displacement within a single year can be as much as 7.8 mm over 30 years after construction. Compared to wall displacement in Long-term B, the geothermal operation in Long-term C greatly affects the wall vertical displacement; for example, the maximum wall displacement in Long-term C after 30 years can build up to 18.1 mm, 8mm greater than that in Long-term B. In practice, if the geothermal diaphragm walls around an excavation are not operated in the same mode, the differential vertical movement induced by geothermal operation may potentially cause serviceability problems (e.g. cracks), particularly at the structural connections, for example, between the wall and the slabs.

4.2.3 Long-term ground settlement

Geothermal operation will inevitably alter surrounding ground response and may in turn cause differential ground settlement, posing a risk to existing buildings nearby. According to the assessment method proposed by Burland and Wroth (1975), the assessment ratio of the relative settlement to the horizontal distance (Δ/L) will be particularly evaluated in the following discussion.

Wongsaroj (2005) suggested to analyse the ground settlement at a certain depth (e.g. 5 m) below the surface as to avoid the intervention from the temperature and seasonal changes in the air. Hence, this paper predicted the settlements at 5 m below the ground surface aiming to avoid any potential interference from the near-surface temperature change. During consolidation, temperature change may have an influence on the coupled thermo-hydro-mechanical behaviour of soil. Over large temperature variation between 0°C and 180°C, heating at a high temperature can increase soil stiffness and strength (Houston et al., 1985), whereas the thermal effect on soil deformability and shear strength is not appreciable if temperature variation becomes smaller within 60°C (Miliziano, 1992, Lingnau et al., 1995). In this study, the range of temperature variation is as small as within 20°C during geothermal operation, and as such the coupling of temperature and consolidation is considered to be negligible.

Figure 10(a) shows the incremental ground settlement after construction during ground consolidation. The incremental ground movement distribution is generally in line with the long-term ground settlement for clayey soil deposit predicted by Ou and Lai (1994); the ground heaves progressively with time as the excess pore water pressure dissipates during consolidation. The maximum incremental ground settlement builds up to 8.3 mm after 30 years since excavation at a distance of 12.2 m from the edge of the wall; as much as 0.6 times of the excavation-induced ground settlement (14.0 mm) at the same position. The maximum assessment ratio in Long-term A achieved after 10 years geothermal operation is 0.018% as calculated in the graph.

Figure 10(b) shows the changes in the long-term ground settlement under external thermal solicitations. In the first winter after construction, the incremental ground settlement adjacent to the wall rises to 3.3 mm (1Y winter in Long-term B) greater than 1.0 mm for 1Y winter in Long-term A. After 30 years since construction, the peak incremental long-term ground settlement in Long-term B can build up to 10.0 mm at a distance 7.6 m from the edge of the wall, which is 1.7 mm higher than that in Long-term A. Conversely, the maximum assessment ratio is not much affected by the thermal solicitations, which is 0.011% obtained at 10Y (similar for winter and summer) and slightly smaller than it in Long-term A.

Figure 10(c) presents the incremental ground settlement during geothermal operation. The peak ground settlement after 30 years in Long-term C is 9.0 mm at a distance 15.1 m from the edge of the wall, which is similar as it in Long-term B. However, the assessment ratio in Long-term C is distinctly different from the other two modelling scenarios. In this graph, the maximum ratio at 30Y winter goes up to 0.073%, which is almost 5 times greater than that in the other situations in Long-term A & B. In particular, significant ground settlement builds up near the edge of the wall due to the development of horizontal wall movement at the wall top section as discussed earlier. The seasonal geothermal operation has a notable effect on the ground movements near the diaphragm wall and the neighbouring buildings, although the assessment ratio generated by geothermal operation is still within the allowable deflection ratio (lower than 0.2%) according to Burland and Wroth (1975).

4.2.4 Long-term basement heave

In an underground structure, connections between the wall and slabs are supposed to distribute the vertical loads acting on the slabs (Gaba et al., 2003). Of particular interest is the base slab, which directly withstands the ground water and heave earth pressure underneath. Chan and Madabhushi (2017) pointed out that it is essential to design the substructure to withstand the pressure or accommodated heaving deflections before anticipated critical conditions occur in the long term. The long-term development of base slab heave is widely observed in deep basement embedded in clayey soil. For example, Chan et al. (2018) conducted geotechnical centrifuge testing on heave and pressure beneath base slab in excavation in over-consolidated clays, based on an 11-m-deep excavation project in London, which contains a total of 21 years of well-recorded heave monitoring data after construction. They noted that the development of heave with time was generally consistent with one-dimensional consolidation theory and estimated that long-term heave at the centre of the slab would reach 110 mm after excess pore water pressure dissipation for approximately 21 years. After that, the pore water pressure below the bottom basement will increase back to its hydrostatic value and together with a net change of 184kPa in total stress. In this study, the computed FE results of basement base case show similar deflection and stress development mechanism in consistent with the observed behaviour reported by Chan et al. (2018).

Figure 11 shows the development of long-term ground heave underneath the centre of the base slab (30.9 m below the ground surface) with square-root of time. Likewise, almost 80% consolidation has completed 30 years after the construction. Different from other behaviour aspects, the development of bottom centre movement and stresses of the base slab has included more phases, e.g. 40 years, 50 years, 60 years, 70 years and 80 years, in order to have a better present of the heaving mechanism. The rate and magnitude of heave displacement with time generally follows one-dimensional consolidation theory. Figure 12 shows the evolution of the stresses with time including total stress, pore water pressure and effective stress respectively under the centre of the base slab. After construction the effective stress reduces to zero very quickly within 14 days, while the total stress and pore water pressure changes gradually with the dissipation of excess pore water pressure. The total stress is increased by 46 kPa due to the self-weight of the installed base slab, while the pore water pressure immediately after construction (i.e. the start of long-term consolidation) is -100 kPa owing to suction cavitation effect. The long-term heave of basement is mainly due to the dissipation of excess pore water pressure, and developments of heave and stresses are very similar among the three long-term scenarios A & B & C.

Figure 13(a) shows the changes of vertical base slab movement in Long-term A. The base slab gradually heaves up with the dissipation of excess pore water pressure, up to a maximum value of 74.8 mm at the foundation centreline after 30 years. After the base slab installation, there generates massive excess pore water pressure below the base slab. In the long term, the pore water pressure below the base slab recovers progressively with the dissipation of excess pore water pressure, contributing significantly to the uplift of the base slab. Compared with the centre of base slab, the vertical movement of the base slab at the corners is much smaller due to the constraints by the wall, which is only 8.7 mm after 30 years.

If the external thermal solicitation is activated (Long-term B), Figure 13(b) shows that the computed vertical base slab movement is consistent with Long-term A, except that the maximum displacements at the centre and the corners slightly increase by 4.2 mm and 1.0 mm respectively after 30 years. Figure 13(c) presents the base slab movement during the geothermal operation, which relatively shrinks during winters whereas expands in summers. The maximum movement at the centre and the corners after 30 years are 84.2 mm and 17.1 mm, respectively, 6% and 58% greater than that in Long-term B. That is, geothermal operation may cause additional slab movements and therefore more serviceability issues (e.g. cracks) particularly at sensitive joint sections between the wall and the slabs.

4.2.5 Internal structural forces

Another concern of geothermal foundation is the thermal effect on the internal structural forces, including normal force (N), shear force (Q) and bending moment (M). Figure 14 & Figure 15 shows the internal structural forces inside the wall in Long-term A and Long-term B, respectively, where the green lines represent the total internal forces due to short-term excavation. Compared to the short-term internal forces, the incremental long-term internal forces above Base Slab are negligible for both Long-term A and Long-term B.

In contrast, Figure 16 shows that the internal forces above Base Slab oscillate with the seasonal geothermal operation for Long-term C, and the maximum long-term differential value builds up greater than the short-term excavation-induced forces. Nevertheless, considering the large the wall bending stiffness of (10^6 kN•m^2/m) and the oscillating internal forces (10^3 kN/m for N, 10^2 kN/m for Q and 10^2 kN•m/m for M), the geothermal-operation-induced oscillation effect is small and negligible.

Some notable stress concentrations appear at the levels of slabs, due to the relative movement between the wall and the slab. The stress concentration mainly depends on the diaphragm wall deflection which varies along the depth. The most critical stress concentration occurs at the connections between the wall and the deepest base slab, whilst the other slabs, e.g. Slab 1 or Slab 2, develop similar stress concentration as the base slab but in smaller magnitude.

For simplicity, only the computed results of the internal structural forces inside the base slab are shown in Figure 17, Figure 18, and Figure 19 for Long-term A & B & C, respectively. Compared with the short-term excavation-induced forces, internal structural forces inside the base slab changes significant during the long term (green curves), mainly caused by the dissipation of excess pore water pressure underneath the base slab. The comparison of Long-term B & C (Figure 18 & Figure 19) against Long-term A (Figure 17) indicates that the external thermal solicitations and seasonal geothermal operation do not have significant effect on the shear forces and bending moment, whereas some oscillations develop at normal forces due to the thermal solicitation from the station.

In general, the effect of thermal solicitations on the internal structural forces are negligible for both the wall and the slabs, except for some notable oscillations of normal forces in Long-term C. In particular, the maximum internal forces occur around the base slab, which can be considered as the most critical section for the design of geothermal deep foundation.

5 Conclusion

Geothermal diaphragm walls may act both as a renewable and clean energy source as well as load-bearing structural elements. Compared to geothermal piles, the mechanical behaviour of geothermal diaphragm walls has not yet been well-understood. This study conducted a thermo-hydro-mechanical finite element analysis to evaluate the effect of thermal solicitation due to geothermal operation on the long-term mechanical performance of diaphragm walls, with regard to both structural behaviour (wall movement, basement heave and internal structural forces) and geotechnical response (ground settlement). The main conclusions of this paper are listed as follows:

1) The wall displacement due to geothermal activation is likely to be in the same order of magnitude with those induced by consolidation only or only with external thermal solicitations; compared to the thermal effect, the hydro-mechanical coupled effect (e.g. lateral soil pressure and excess pore water pressure) overwhelmingly dominates the long-term wall displacement.

   If seasonal temperature change is considered but without geothermal operation, the thermal expansion of the slabs inside the station box may push against the retaining wall and thus induce slight horizontal movement.

   During geothermal operation inside the diaphragm walls, cyclically seasonal temperature variation may have an influence on the wall movement particularly near the ground surface at the connections between the diaphragm walls and the superstructure due to: i) the temperature gradient along the wall thickness in the lateral direction and ii) the differential vertical movement during seasonal variations. The differential wall movement induced by geothermal operation may potentially cause serviceability problems (e.g. cracks), particularly at the structural connections, for example, between the wall and the slabs.

2) Following seasonal geothermal operation mode assumed in this study, the temperature-induced ground settlement is unlikely to pose a potential risk to neighbouring buildings in stiff London clay. Notably, the ground settlement near the station is very sensitive to the stiffness degradation of the stiff clay due to the additional soil movement induced by the geothermal operation. For the design of geothermal retaining structure, it is desired to obtain the soil stiffness properties from the particular construction site rather than simply referring to past test data elsewhere.

3) Although the long-term basement heave is primarily governed by the dissipation of excess pore water pressure regardless of geothermal operation, it’s still necessary to assess structural performance at the connections between the wall and slabs for geothermal operation, as to evaluate the risk of cracks and other serviceability problems caused by thermo-induced additional stress concentration.

4) The changes of internal structural forces in the long term are mainly controlled by the dissipation of excess pore water pressure but less affected by the external thermal solicitations and geothermal operation. Although geothermal operation can cause some oscillations of structural forces along the wall and base slab, the magnitude may be negligible compared against the structural forces generated at the construction stage.

In summary, the geothermal operation may have an impact on the long-term mechanical performance of geothermal diaphragm wall in stiff clay in relation to potential serviceability issues (e.g. thermal-induced concrete cracks) but not critical safety problems. At present, the geothermal system of London Dean Street Station is not in operation but experiencing re-design, and therefore no relevant monitoring data is yet available to validate the long-term geothermal diaphragm wall behaviour, as stated by the Customer Experience Executive of Transport for London Customer Services. For future study, there is a high demand of field data in relation to long-term diaphragm wall behaviour during geothermal operation with particular emphasis on differential ground movement and serviceability issues (e.g. cracks) at connections between the wall and slabs. In addition, more detailed aspects will be considered in the further research, e.g. various thermal operation modes, more thermal loading situations and the arrangement of heat exchanger pipes in a 3D model.

6 Acknowledgements

This work was carried out under the framework of Transport and Urban Development COST Action GABI TU1405, European network for shallow geothermal energy applications in buildings and infrastructures. The first author, Quanwei Dai, is funded by the School of Engineering in University College Cork.

7 Appendix

The short-term model in this paper has been carefully validated with the monitoring data, nonetheless, it is still necessary to state the reliability of the long-term model in some extent. Thus, five more models derived from the numerical model of scenario Long-term C have been conducted to carry out the sensitivity analyses for the evaluation of three major concerns: 1) thermal properties of concrete elements; 2) various station temperature; 3) and stiffness degradation boundaries of clayey layers. All the analyses in the appendix are performed with regard to the comparison of horizontal wall movement between the additional model and the original Long-term C model.

7.1 Thermal properties of concrete slabs

As mentioned in Figure 7, the horizontal wall movement is significantly influenced by the thermal expansion of the concrete slabs. Rui (2014) pointed out that the thermal expansion coefficient of concrete material determines the thermal strain of the concrete elements and the displacements. In this study, a sensitivity analysis on this property is evaluated by comparing the effect of three different thermal expansion coefficients of concrete slabs on the wall behaviour, including zero thermal expansion coefficient, thermal expansion coefficient $\alpha = 1\times10^{-5}$ 1/K (original Long-term C model) and $\alpha = 4\times10^{-5}$ 1/K.

Figure 20 compares the horizontal wall movement with different concrete thermal expansion coefficients. Without the effect of thermal expansion from concrete slabs ($\alpha = 0$), the wall is generally pushed towards the excavation side as shown in Figure 20(b). Compared to the case with thermal expansion $\alpha = 1\times10^{-5}$ 1/K (original Long-term C model), the maximum difference between the case with $\alpha = 0$ and the original one with $\alpha = 1\times10^{-5}$ 1/K is 1.8 mm, appearing between Slab 1 and Slab 2, and the minimum difference is as small as 0.1 mm at the toe of the diaphragm wall. The effect of thermal volume expansion of the concrete slabs on the horizontal wall movement is relatively uniform along the wall at the station side, whilst the induced wall deflection difference between the two cases becomes less obvious at the lower part of the wall far below the base slab. On the contrary, Figure 20(c) presents the incremental horizontal wall movement by adopting a 4 times greater thermal expansion coefficient of the concrete slabs ($\alpha = 4\times10^{-5}$) than the original coefficient ($\alpha = 1\times10^{-5}$ 1/K). The bigger thermal expansion coefficient is, the greater the thermal expansion volume of the concrete slabs would be, and as such the wall is significantly pushed towards the soil side, with the maximum magnitude of 4.2 mm between Slab 1 and Base Slab. After 30 years of thermal operation, the differences between the two cases are becoming even smaller both near the toe of the wall and the part of wall between Slab 2 and Slab 1 within 0.3 mm. As discussed earlier, the horizontal wall deflection is contributed by hydro-mechanical effects (e.g. lateral soil pressure and excess pore water pressure), resisting forces of slabs and thermal effects (e.g. thermal expansion of the concrete wall and slabs). It is noted that the effect of thermal expansion of the concrete slabs on the horizontal wall movement is not constantly expanding with the thermal expansion coefficient but compensated by other aspects.

In summary, the thermal expansion force from the slabs inside the station pushes the retaining wall towards the soil side, and the larger thermal expansion coefficient of the concrete slabs is the greater wall movement would be. As soil consolidates with time, the other influencing factors (e.g. lateral soil pressure, propping force of the slabs) become more significant with time, whereas the effect of slab thermal expansion on horizontal wall movement relatively weakens.

7.2 Station temperature

For simplicity, all the thermal boundaries along the wall at the excavation side and the thermal boundaries of the slabs are represented by a uniform station temperature, assuming that the station temperature at the operation stage is kept constant by air ventilation system. In this study, a dedicated sensitivity analysis is conducted to evaluate the effect of station temperature on the D-wall behaviour including three scenarios: 4°C (lower bound as the air temperature in winter), 18°C (typical indoor temperature in a station as the original Long-term C model) and 23°C (upper bound as the air temperature in summer).

The temperature-induced horizontal wall movement in Long-term C is shown in Figure 21. The station temperature in Figure 21(a) is set constantly at 4°C, generating less thermal expansion for the concrete slabs and leading the wall to move significantly towards the excavation side, in comparison with the original model with the 18°C of station temperature. Unlike the original model, the horizontal wall movements near the ground surface reveals no obvious trend towards the soil side in winters, as a result of no temperature difference development along the wall thickness in winters (4°C near the soil side and 4°C near the station side). On the contrary, a higher constant station temperature (23°C) would push the part of the wall near the ground surface more towards the soil side than the original model, with regard to a 19°C temperature difference along the wall thickness direction in winters (4°C near the soil side and 23°C near the station side), as shown in Figure 21(b). In general, the station temperature variation in Figure 21(b) is only 5°C less than it in Figure 21(a) (14°C), as a result, the maximum horizontal wall movement difference obtained in 30 years is about 1.4 mm in Figure 21(b), much less than it in Figure 21(a) (3.9 mm). Besides, the bending lateral deflection of the wall near the ground surface in the model with 23°C of station temperature is about 0.9 mm, greater than that of 0.7 mm in the original model, as the temperature difference along the thickness of the wall is 5°C higher than the original model.

In summary, the change of temperature range for the thermal boundaries inside the station indicates that the higher the station temperature is, the more horizontal wall movement towards the soil side would be, which is dominated by the thermal expansion of the concrete slabs than the wall thermal bending effect. The temperature variation along the wall at the station side mainly contributes to the bending deflection of the wall near the ground surface.

7.3 High stiffness modulus of clayey layers

To better understand the wall displacement, an additional model with remarkably higher stiffness modulus for clayey layers is analysed in this section. The soil properties of the clay layers for both the higher stiffness model parameters and original parameters in HSS models are listed in Table 6. The performance of HSS models with both the original model parameters and higher stiffness are compared against experimental data from other sites available in literature, respectively, as shown in Figure 22: the HSS soil models in original model match with the experimental data, while the results from the additional model shows higher stiffness than the experimental curves, as expected.

Figure 23 shows the short-term model validation between the original model and higher stiffness bound HSS model. Although the validation near the excavation surface is slightly improved, there still exists obvious wall deflection at the toe of the wall. As the shear stiffness at the higher strain range is low, the wall displacement due to excavation can still be considerable. In addition, as base slab heaves after soil excavation, the wall below the base slab has to move towards the excavation side according to Terzaghi (1943)'s theory of rigid body movement below a foundation. Figure 24 shows the incremental horizontal wall movement in Long-term C with higher stiffness bound of HSS soil models. The deflection for the part of wall between Slab 2 and Slab 1 in this model is very similar to the original model, while the wall movements towards the excavation side above Slab 2 and below Base Slab in the long term are reduced by about 1.3 mm.

In summary, the short-term model validation can be improved and the long-term horizontal wall movements can be reduced by significantly increasing the HSS soil stiffness modulus. Nevertheless, there is no evidence for such high stiff clayey layers on site in practice as the green curves plotted in Figure 22.

8 References

ADAM, D. & MARKIEWICZ, R. 2009. Energy from earth-coupled structures, foundations, tunnels and sewers. *Geotechnique,* 59**,** 229-236.

AMIS, T., ROBINSON, C. & WONG, S. 2010. Intergrating geothermal loops into the diaphragm walls of the Knightsbridge Palace Hotel project. *In Proc. 11th DFI/EFFC Int. Conf. Geotechnical Challenges in Urban Regeneration.* London.

BARLA, M., DI DONNA, A. & SANTI, A. 2018. Energy and mechanical aspects on the thermal activation of diaphragm walls for heating and cooling. *Renewable Energy*.

BOURNE-WEBB, P., AMATYA, B., SOGA, K., AMIS, T., DAVIDSON, C. & PAYNE, P. 2009. Energy pile test at Lambeth College, London: geotechnical and thermodynamic aspects of pile response to heat cycles. *Geotechnique,* 59**,** 237-248.

BOURNE-WEBB, P., BURLON, S., JAVED, S., KURTEN, S. & LOVERIDGE, F. 2016. Analysis and design methods for energy geostructures. *Renewable & Sustainable Energy Reviews,* 65**,** 402-419.

BRANDL, H. 1998. Energy piles and diaphragm walls for heat transfer from and into the ground. *Deep Foundations on Bored and Auger Piles - Bap Iii*, 37-60.

BRANDL, H. 2006. Energy foundations and other thermo-active ground structures. *Geotechnique,* 56**,** 81-122.

BRINKGREVE, R. B. J., KUMARSWAMY, S., SWOLFS, W. M. & FORIA, F. 2018. *PLAXIS 2D Reference Manual Version 2018,* Delft, PLAXIS.

BURLAND, J. B. & WROTH, C. P. 1975. Settlement of buildings and associated damage. *Proceedings, British Geotechnical Society Conference on Settlement of Structures, Cambridge.* Cambridge: Pentech Press.

CABARKAPA, Z., MILLIGAN, G. W. E., MENKITI, C. O., MURPHY, J. & POTTS, D. M. 2003. Design and performance of a large diameter shaft in Dublin Boulder Clay. *Bga International Conference on Foundations: Innovations, Observations, Design and Practice*, 175-185.

CHAN, D., MADABHUSHI, S., NICHOLSON, D., CHAPMAN, T. & SOLERA, S. 2018. *Technical Paper: Twenty-one Years of Heave Monitoring in London Clay at Horseferry Road Basement* [Online]. Ground Engineering. Available: https://www.geplus.co.uk/technical-papers/technical-paper-twenty-one-years-of-heave-monitoring-in-london-clay-at-horseferry-road-basement/10035934.article?search=https%3a%2f%2fwww.geplus.co.uk%2fsearcharticles%3fqsearch%3d1%26keywords%3dheave+monitoring+in+london [Accessed 04/12/2018 2018].

CHAN, D. Y. K. & MADABHUSHI, S. P. G. 2017. Designing urban deep basements in South East England for future ground movement - Progress and opportunities for experimental simulation of long-term heave. *International Symposium for Next Generation Infrastructure.* London.

COLETTO, A. & STERPI, D. 2016. Structural and geotechnical effects of thermal loads in energy walls. *Vi Italian Conference of Researchers in Geotechnical Engineering, Cnrig2016 - Geotechnical Engineering in Multidisciplinary Research: From Microscale to Regional Scale,* 158, 224-229.

DI DONNA, A., CECINATO, F., LOVERIDGE, F. & BARLA, M. 2017. Energy performance of diaphragm walls used as heat exchangers. *Proceedings of the Institution of Civil Engineers-Geotechnical Engineering,* 170, 232-245.

DONG, S., LI, X., MINH TANG, A., MICHEL PEREIRA, J., TRI NGUYEN, V., CHE, P. & XIONG, Z. 2018. Thermo-mechanical behaviour of energy diaphragm wall: physical and numerical modelling. *Applied Thermal Engineering*.

GABA, A., SIMPSON, B., POWRIE, W. & BEADMAN, D. 2003. *CIRIA C580 Embedded rataining walls - guidance for economic design,* London, CIRIA.

GASHTI, E., MALASKA, M. & KUJALA, K. 2014. Evaluation of thermo-mechanical behaviour of composite energy piles during heating/cooling operations. *Engineering Structures,* 75, 363-373.

GASPARRE, A. 2005. *Advanced Laboratory Characterisation of London Clay.* PhD PhD thesis, Imperial College London.

HIGHT, D. W., ELLISON, R. A. & PAGE, D. P. 2004. *Engineering in the Lambeth Group,* London, CIRIA.

HOUSTON, S. L., HOUSTON, W. N. & WILLIAMS, N. D. 1985. Thermo‐Mechanical Behavior of Seafloor Sediments. 111, 1249-1263.

HSIEH, P. G., OU, C. Y. & HSIEH, W. H. 2016. Efficiency of excavations with buttress walls in reducing the deflection of the diaphragm wall. *Acta Geotechnica,* 11, 1087-1102.

JEONG, S., LIM, H., LEE, J. K. & KIM, J. 2014. Thermally induced mechanical response of energy piles in axially loaded pile groups. *Applied Thermal Engineering,* 71, 608-615.

KNELLWOLF, C., PERON, H. & LALOUI, L. 2011. Geotechnical Analysis of Heat Exchanger Piles. *Journal of Geotechnical and Geoenvironmental Engineering,* 137, 890-902.

LALOUI, L., NUTH, M. & VULLIET, L. 2006. Experimental and numerical investigations of the behaviour of a heat exchanger pile. *International Journal for Numerical and Analytical Methods in Geomechanics,* 30, 763-781.

LIM, A., OU, C. Y. & HSIEH, P. G. 2018. Investigation of the integrated retaining system to limit deformations induced by deep excavation. *Acta Geotechnica,* 13, 973-995.

LINGNAU, B. E., GRAHAM, J. & TANAKA, N. 1995. Isothermal modeling of sand–bentonite mixtures at elevated temperatures. *Canadian Geotechnical Journal,* 32, 78-88.

MILIZIANO, S. 1992. *Influenza della temperatura sul comportamento meccanico delle terre coesive.* Tesi di Dottorato in Ingegneria Geotecnica, Università di Roma "La Sapienza".

MIMOUNI, T. & LALOUI, L. 2015. Behaviour of a group of energy piles. *Canadian Geotechnical Journal,* 52, 1913-1929.

NISHA, J. J. & MUTTHARAM, M. 2017. Deep Excavation Supported by Diaphragm Wall: A Case Study. *Indian Geotechnical Journal,* 47, 373-383.

NOAA. 2018. *London weather averages* [Online]. National Centers for Environmental Information. Available: https://www.ncdc.noaa.gov/ [Accessed 01/11/2018 2018].

OU, C. Y. & HSIEH, P. G. 2011. A simplified method for predicting ground settlement profiles induced by excavation in soft clay. *Computers and Geotechnics,* 38**,** 987-997.

OU, C. Y. & LAI, C. H. 1994. Finite-Element Analysis of Deep Excavation in Layered Sandy and Clayey Soil Deposits. *Canadian Geotechnical Journal,* 31**,** 204-214.

OUYANG, Y. 2014. *Geotechnical behaviour of energy piles.* PhD PhD Thesis, University of Cambridge.

RAMMAL, D. 2017. *Thermal-mechanical behaviour of geothermal structures: numerical modelling and recommendations.* PhD PhD Thesis, University of Lille 1 Sciences et Technologies.

RAMMAL, D., HROUEH, H., BURLON, S. & SURYATRIYASTUTI, M. E. Numerical study of the performance of energy diaphragm walls. *In:* WUTTKE, B. S., ed. Eneegy Geotechnics, 2016 London. Taylor & Francis Group.

RAMMAL, D., MROUEH, H. & BURLON, S. 2018. Impact of thermal solicitations on the design of energy piles. *Renewable & Sustainable Energy Reviews,* 92**,** 111-120.

RUI, Y. 2014. *Thermo-hydro-mechanical coupling analysis of a thermo-active diaphragm wall.* PhD PhD Thesis, University of Cambridge.

RUI, Y. & YIN, M. 2018. Thermo-hydro-mechanical coupling analysis of a thermo-active diaphragm wall. *Canadian Geotechnical Journal,* 55**,** 720-735.

SCHWAMB, T. 2014. *Performance Monitoring and Numerical Modelling of a Deep Circular Excavation.* PhD PhD Thesis, University of Cambridge.

STERPI, D., ANGELOTTI, A., CORTI, D. & RAMUS, M. Numerical analysis of theat transfer in thermo-active diaphragm walls. *In:* HICKS, B., ROHE, ed. Numerical Methods in Geotechnical Engineering, 2014 London. Taylor & Francis Group.

STERPI, D., COLETTO, A. & MAURI, L. 2017. Investigation on the behaviour of a thermo-active diaphragm wall by thermo-mechanical analyses. *Geomechanics for Energy and the Environment,* 9**,** 1-20.

SUN, M., XIA, C. C. & ZHANG, G. Z. 2013. Heat transfer model and design method for geothermal heat exchange tubes in diaphragm walls. *Energy and Buildings,* 61**,** 250-259.

SURYATRIYASTUTI, M. E., MROUEH, H. & BURLON, S. 2012. Understanding the temperature-induced mechanical behaviour of energy pile foundations. *Renewable & Sustainable Energy Reviews,* 16**,** 3344-3354.

TERZAGHI, K. 1943. *Theoretical Soil Mechanics,* New York, Wiley.

WONGSAROJ, J. 2005. *Three-dimensional finite element analysis of short and long-term ground response to open-face tunnelling in stiff clay.* PhD Thesis, University of Cambridge.

XIA, C. C., SUN, M., ZHANG, G. Z., XIAO, S. G. & ZOU, Y. C. 2012. Experimental study on geothermal heat exchangers buried in diaphragm walls. *Energy and Buildings,* 52**,** 50-55.

ZDRAVKOVIC, L., POTTS, D. M. & JOHN, H. D. S. 2005. Modelling of a 3D excavation in finite element analysis. *Géotechnique,* 55**,** 497-513.

NOTATATIONS

C	Cohesion
C_s	Specific heat capacity
E	Stiffness
E_{50}^{ref}	Secant stiffness in standard drained triaxial test
E_{oed}^{ref}	Tangent stiffness for primary oedometer loading
E_{ur}^{ref}	Unloading / reloading stiffness
EA	Normal stiffness of props
D_e	External diameter of props
GHE	Ground heat exchanger
G_0^{ref}	Reference shear modulus at very small strains
Gs	Secant stiffness shear modulus
HM	Hydro-mechanical analysis
HSS	Hardening soil model with small-strain stiffness
k	Permeability coefficient
K_o	Lateral pressure ratio
L	the distance between the edge of the station and the very settled ground
LMC	Upper Mottled Clay
m	Power for stress-level dependency of stiffness
M	Bending moment
MC	Mohr-Coulomb model
N	Normal force

p^{ref}	Reference stress for stiffness
Q	Shear force
R_f	Failure ratio q_f / q_a (deault $R_f = 0.9$)
TH	Thermo-mechanical analysis
THM	Thermo-hydro-mechanical analysis
UMC	Upper Mottled Clay
2D	Two-dimensional
3D	Three-dimensional
Δ	Relative settlement between the edge of the station and the very settled ground
Δ/L	Settlement assessment ratio
γ	Material weight
$\gamma_{0.7}$	Threshold shear stain at which $G_s = 0.72G_0$
ν	Poisson’s ratio
λ_s	Thermal conductivity
ρ_s	Soil density
ϕ	Friction angle
ψ	Tension cut-off and tensile strength
α	Thermal expansion coefficient

List of Figures

Figure 10 – Incremental ground settlement

(a) Long-term A
(b) Long-term B
(c) Long-term C

Figure 11 – Heave development with square-root of time

Figure 12 – Stress development with square-root of time

(a) Total stress
(b) Pore water pressure
(c) Effective stress

Figure 13 – Incremental vertical base slab movement

(a) Long-term A
(b) Long-term B
(c) Long-term C

Figure 14 – Internal structural forces inside the wall in Long-term A

(a) Normal force
(b) Shear force
(c) Bending moment

Figure 15 – Internal structural forces inside the wall in Long-term B

(a) Normal force
(b) Shear force
(c) Bending moment

Figure 16 – Internal structural forces inside the wall in Long-term C

(a) Normal force
(b) Shear force
(c) Bending moment

Figure 17 – Internal structural forces inside the base slab in Long-term A

(a) Normal force
(b) Shear force
(c) Bending moment

Figure 18 – Internal structural forces inside the base slab in Long-term B

(a) Normal force
(b) Shear force
(c) Bending moment

Figure 19 – Internal structural forces inside the base slab in Long-term C

(a) Normal force
(b) Shear force
(c) Bending moment

Figure 20 – Incremental horizontal wall movement in Long-term C with various thermal expansion coefficients of concrete slabs

(a) Thermal expansion coefficient equal to 1×10^{-5} 1/K (Original model)
(b) Thermal expansion coefficient equal to 0 1/K
(c) Thermal expansion coefficient equal to 4×10^{-5} 1/K

Figure 21 – Incremental horizontal wall movement in Long-term C with various station temperature

(a) Station temperature at 4°C
(b) Station temperature at 23°C

Figure 22 – HSS model calibration of clayey layers

(a) London Clay A3
(b) London Clay A2
(c) Lambeth Group UMC
(d) Lambeth Group LMC

Figure 23 – Short-term model validation results with high bound HSS models

(a) After Prop 2 installed
(b) After Prop 3 installed
(c) After Slab 2 installed
(d) After Base Slab installed

Figure 24 – Incremental horizontal wall movement in Long-term C with higher stiffness bound of HSS soil models

List of Tables

Figure 1


Tottenham Court Road Oversite Development
Crossrail
TCR East OSD
Sites A & B
Centre Point
Soho Square
TCR West OSD
Sites C & D
Royal Mail Depot
Tottenham Court Rd
Oxford Street
Soho Street
Charing Cross Road
Oxford Street
Dean Street
A
B
C
D

Figure 2

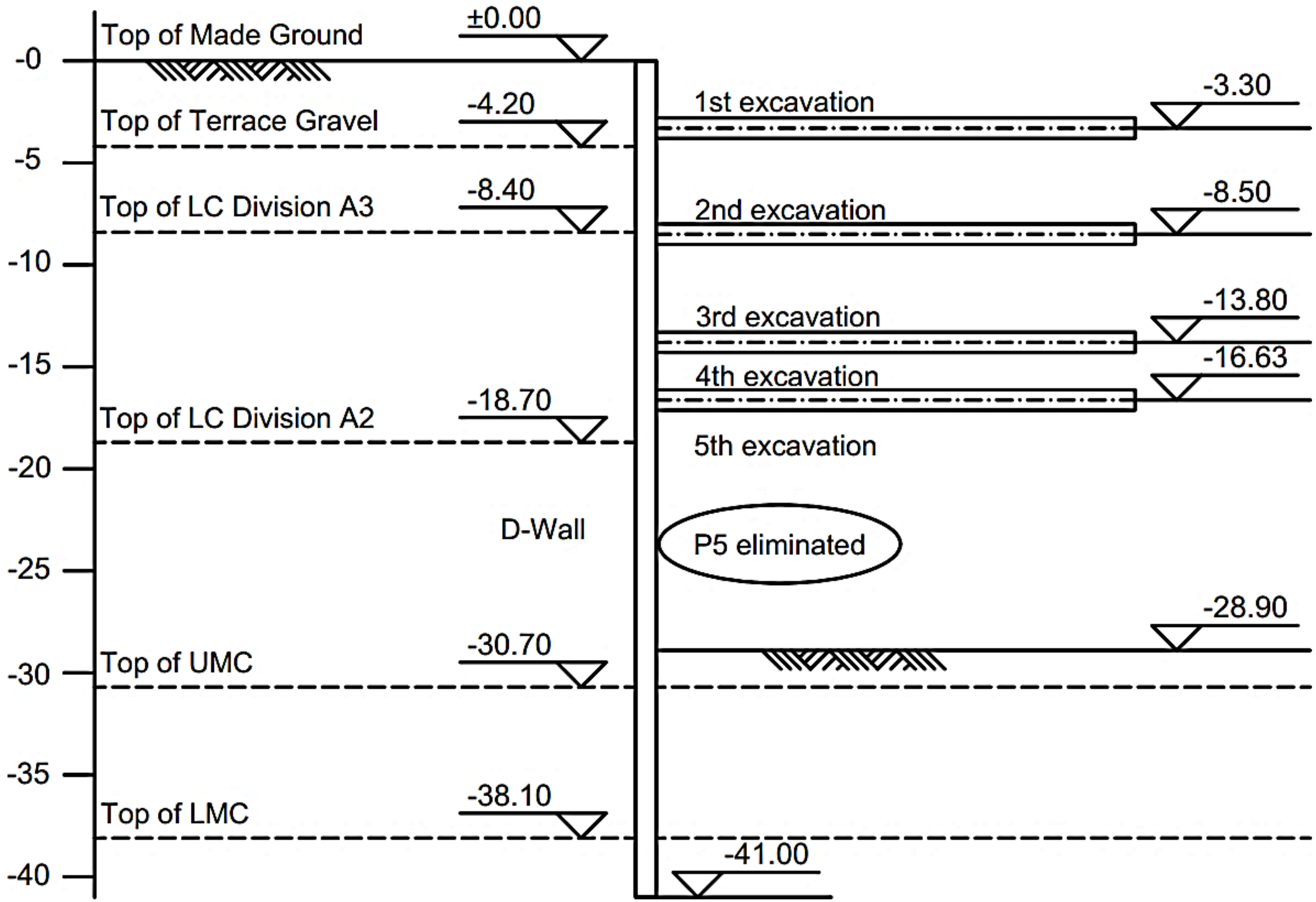
Top of Made Ground
±0.00
-0
Top of Terrace Gravel
-4.20
-5
Top of LC Division A3
-8.40
-10
-15
Top of LC Division A2
-18.70
-20
D-Wall
-25
Top of UMC
-30.70
-30
-35
Top of LMC
-38.10
-40
1st excavation
-3.30
2nd excavation
-8.50
3rd excavation
-13.80
4th excavation
-16.63
5th excavation
P5 eliminated
-28.90
-41.00

Figure 3

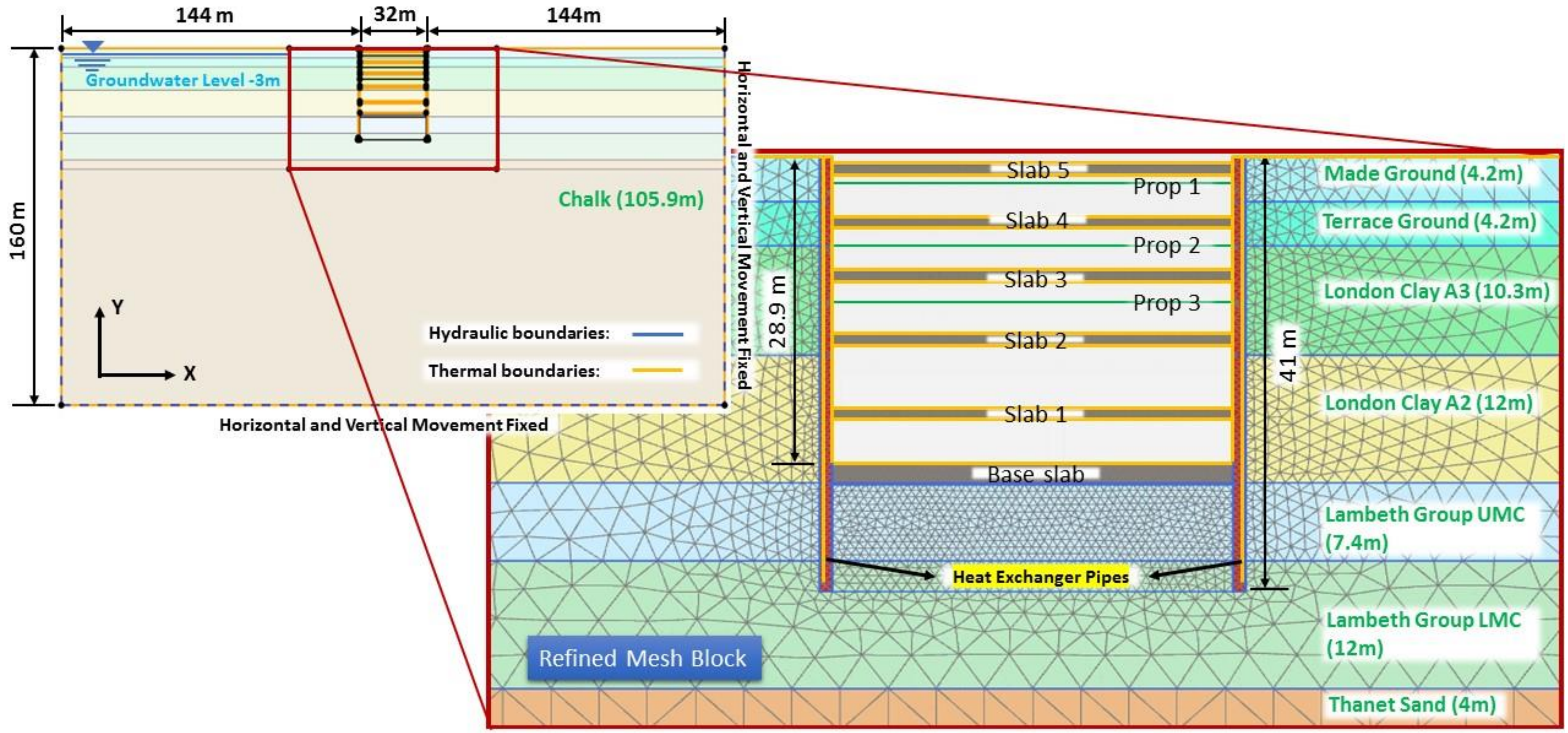
144 m
32m
144m
160 m
Groundwater Level -3m
Chalk (105.9m)
Y
X
Hydraulic boundaries:
Thermal boundaries:
Horizontal and Vertical Movement Fixed
Horizontal and Vertical Movement Fixed
Slab 5
Prop 1
Slab 4
Prop 2
Slab 3
Prop 3
Slab 2
Slab 1
Base slab
28.9 m
41 m
Made Ground (4.2m)
Terrace Ground (4.2m)
London Clay A3 (10.3m)
London Clay A2 (12m)
Lambeth Group UMC (7.4m)
Heat Exchanger Pipes
Lambeth Group LMC (12m)
Refined Mesh Block
Thanet Sand (4m)

Figure 4a

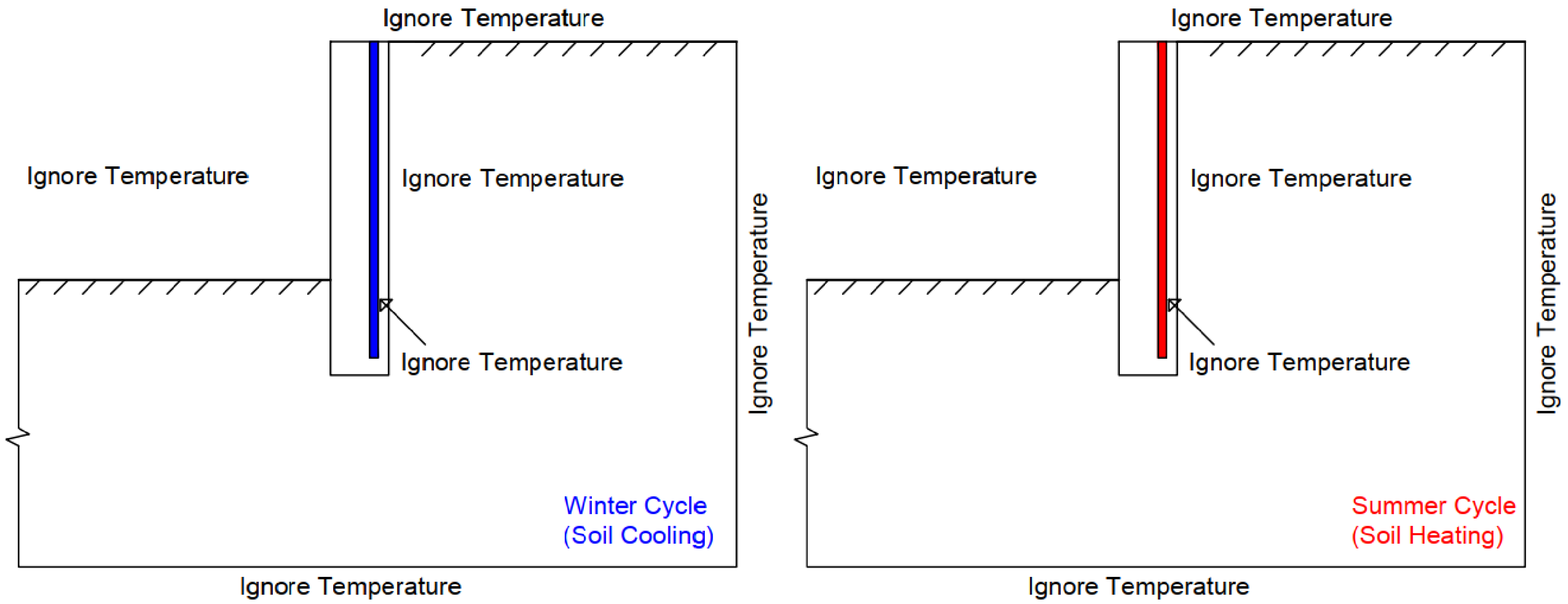
Ignore Temperature
Ignore Temperature
Ignore Temperature
Ignore Temperature
Ignore Temperature
Ignore Temperature
Winter Cycle
(Soil Cooling)
Ignore Temperature
Ignore Temperature
Ignore Temperature
Ignore Temperature
Ignore Temperature
Ignore Temperature
Summer Cycle
(Soil Heating)

Figure 4b

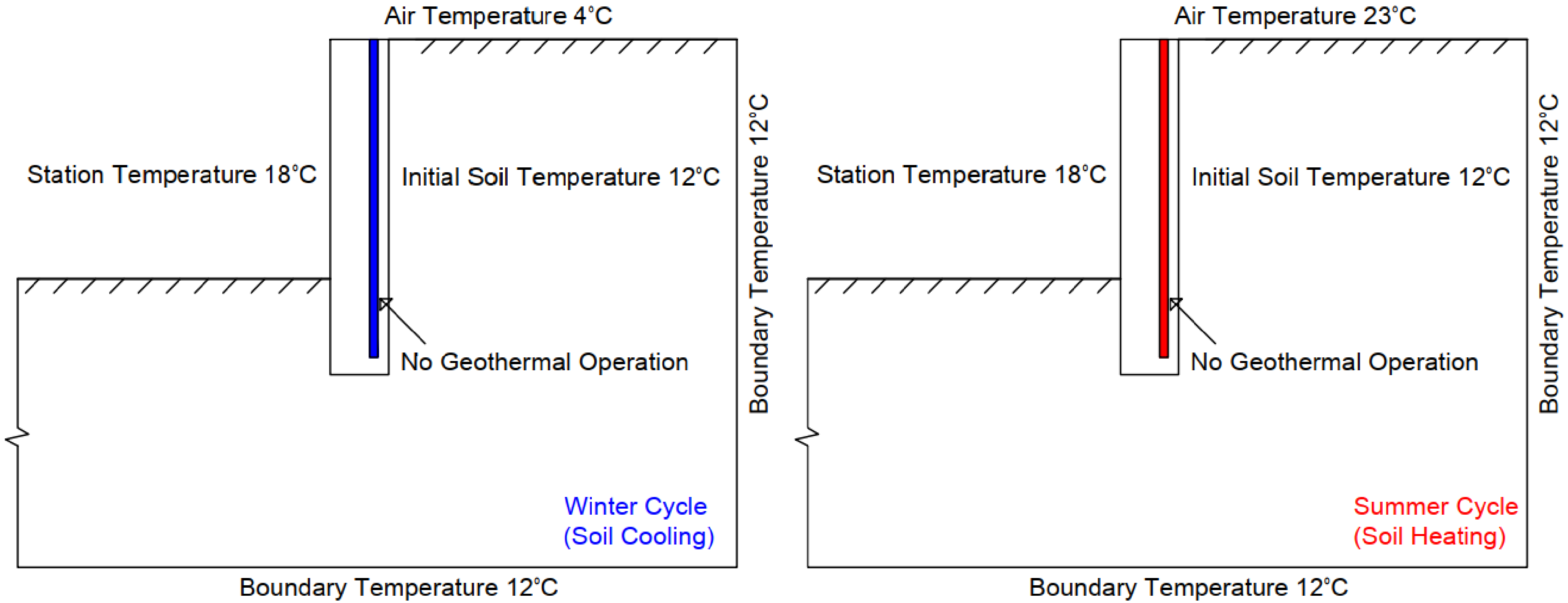
Air Temperature 4°C
Station Temperature 18°C
Initial Soil Temperature 12°C
Boundary Temperature 12°C
No Geothermal Operation
Winter Cycle
(Soil Cooling)
Boundary Temperature 12°C
Air Temperature 23°C
Station Temperature 18°C
Initial Soil Temperature 12°C
Boundary Temperature 12°C
No Geothermal Operation
Summer Cycle
(Soil Heating)
Boundary Temperature 12°C

Figure 4c

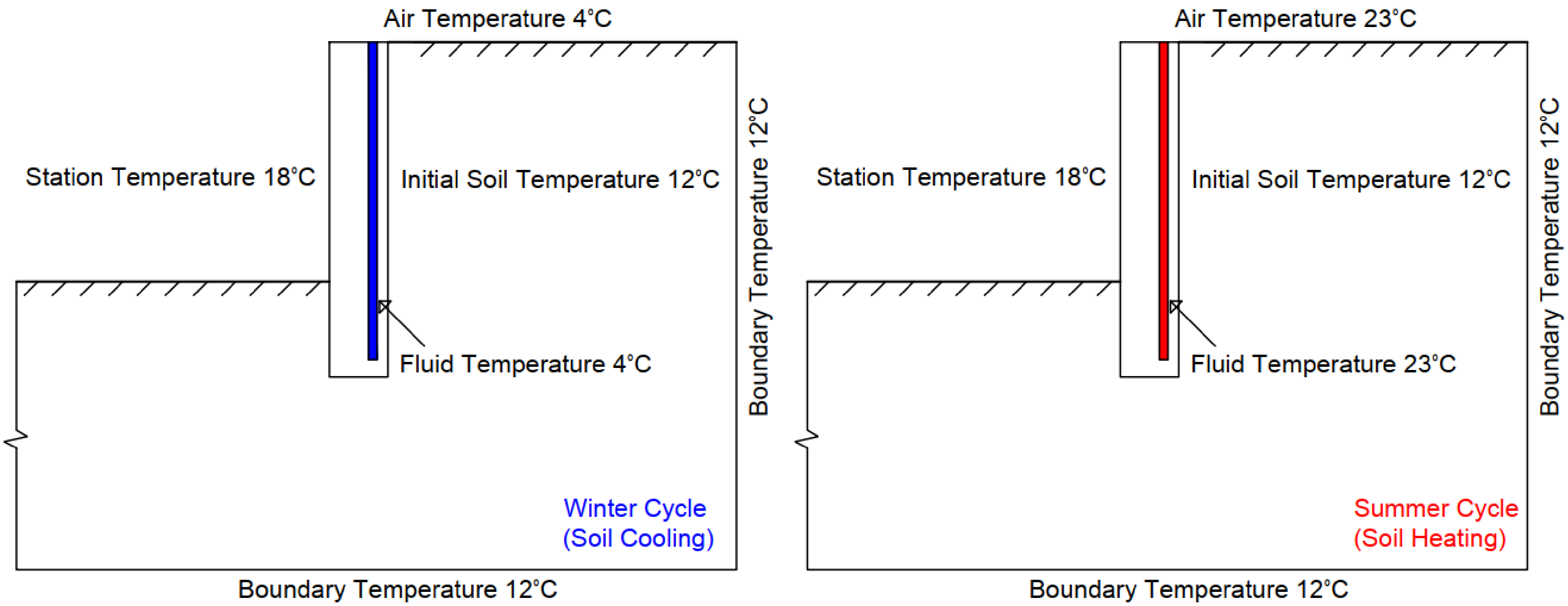
Air Temperature 4°C
Station Temperature 18°C
Initial Soil Temperature 12°C
Boundary Temperature 12°C
Fluid Temperature 4°C
Winter Cycle
(Soil Cooling)
Boundary Temperature 12°C
Air Temperature 23°C
Station Temperature 18°C
Initial Soil Temperature 12°C
Boundary Temperature 12°C
Fluid Temperature 23°C
Summer Cycle
(Soil Heating)
Boundary Temperature 12°C

Figure 5

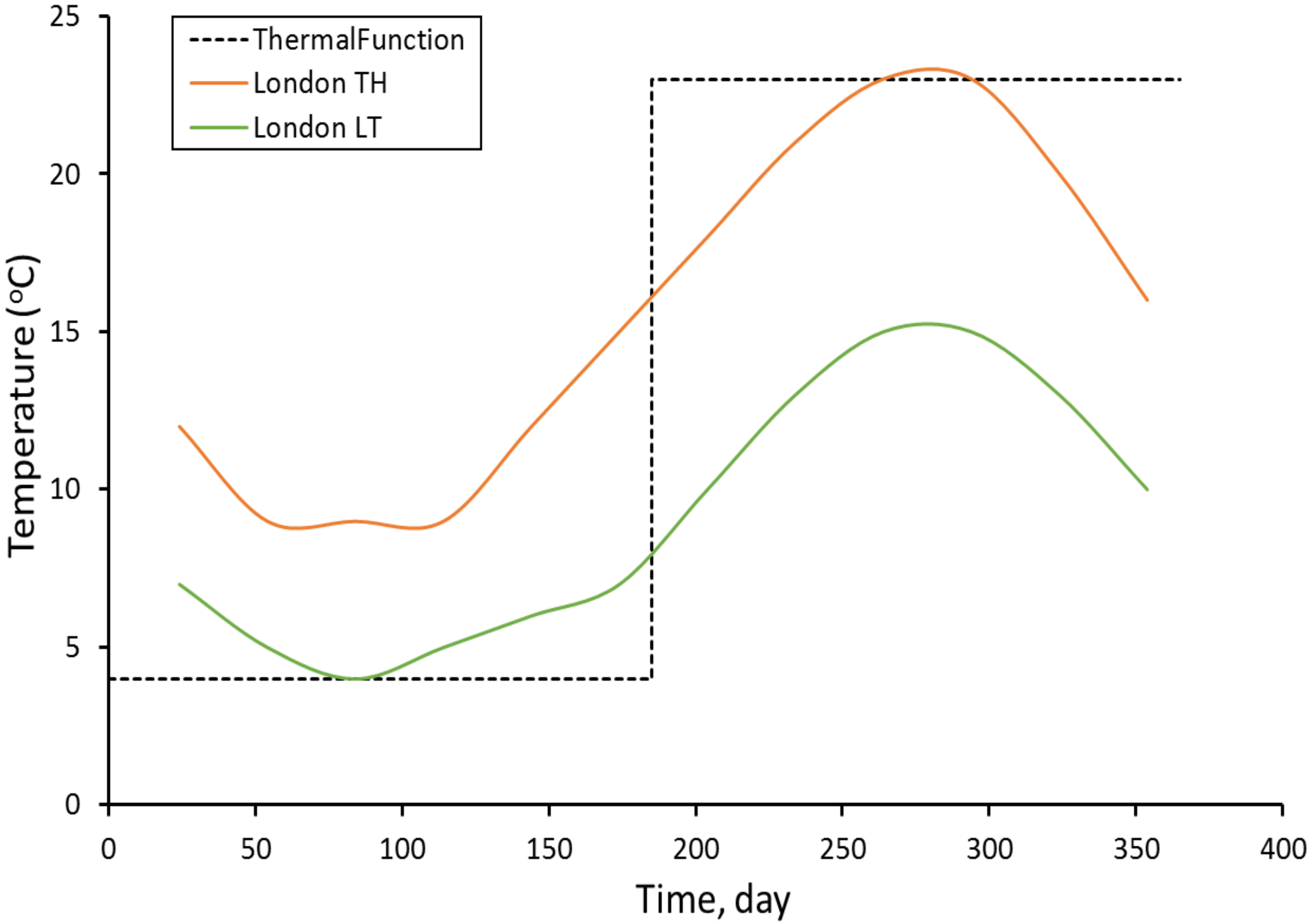
ThermalFunction
London TH
London LT
Temperature (°C)
Time, day
0
5
10
15
20
25
0
50
100
150
200
250
300
350
400

Figure 6a&b

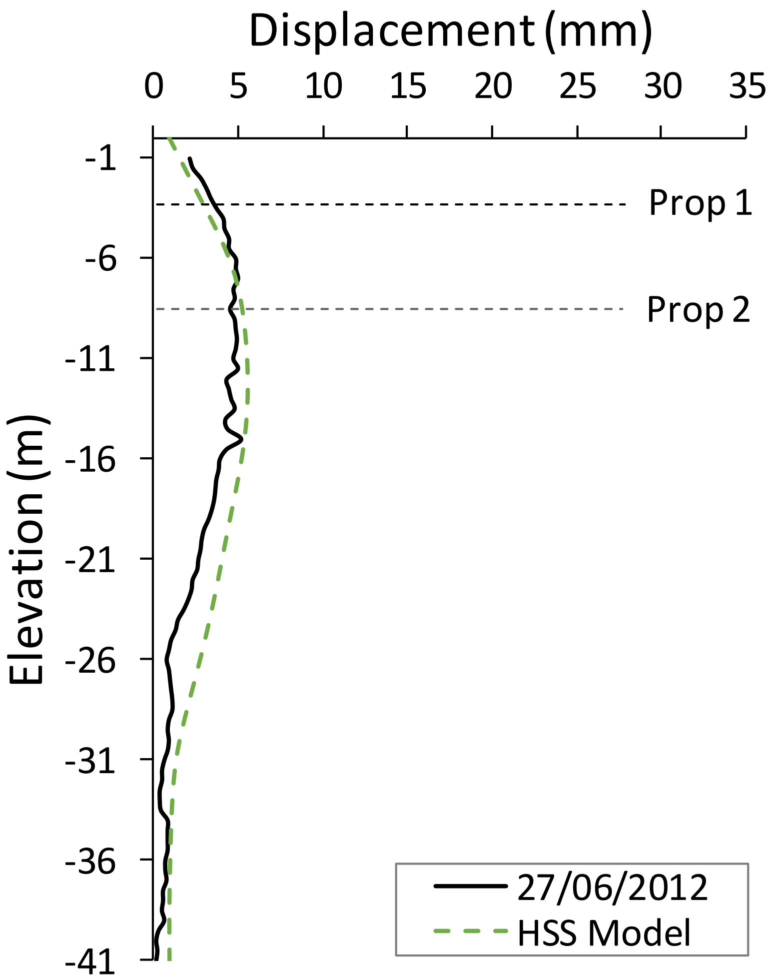
Displacement (mm)
0
5
10
15
20
25
30
35
Elevation (m)
-1
-6
-11
-16
-21
-26
-31
-36
-41
Prop 1
Prop 2
27/06/2012
HSS Model

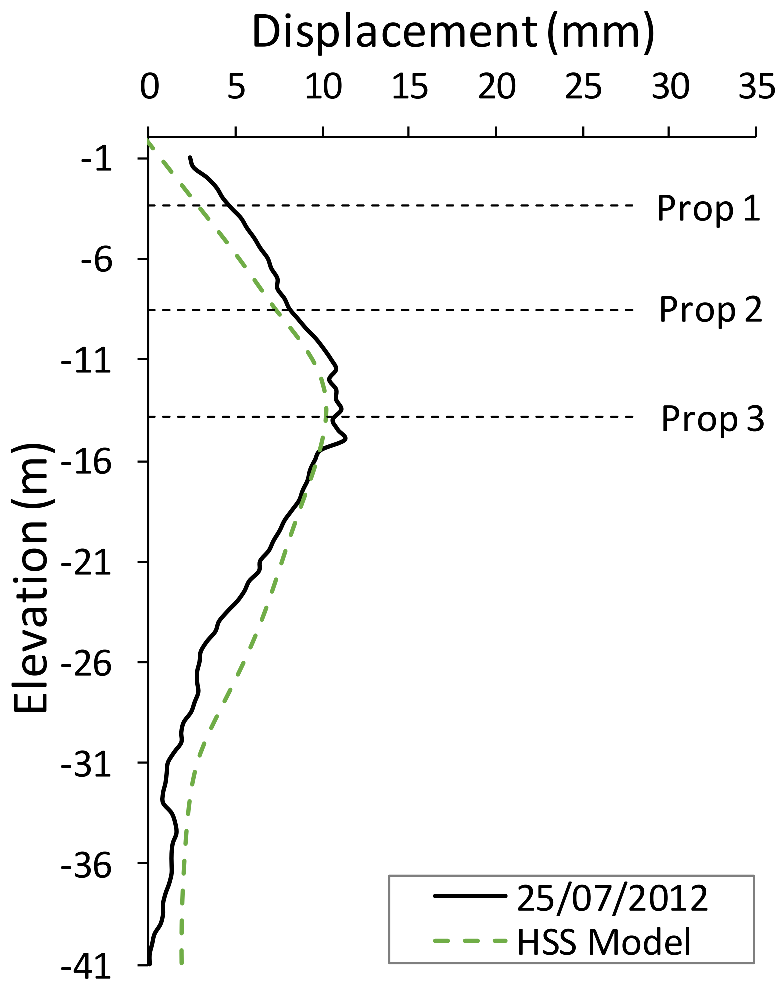
Displacement (mm)
0
5
10
15
20
25
30
35
Elevation (m)
-1
-6
-11
-16
-21
-26
-31
-36
-41
Prop 1
Prop 2
Prop 3
25/07/2012
HSS Model

Figure 6c&d

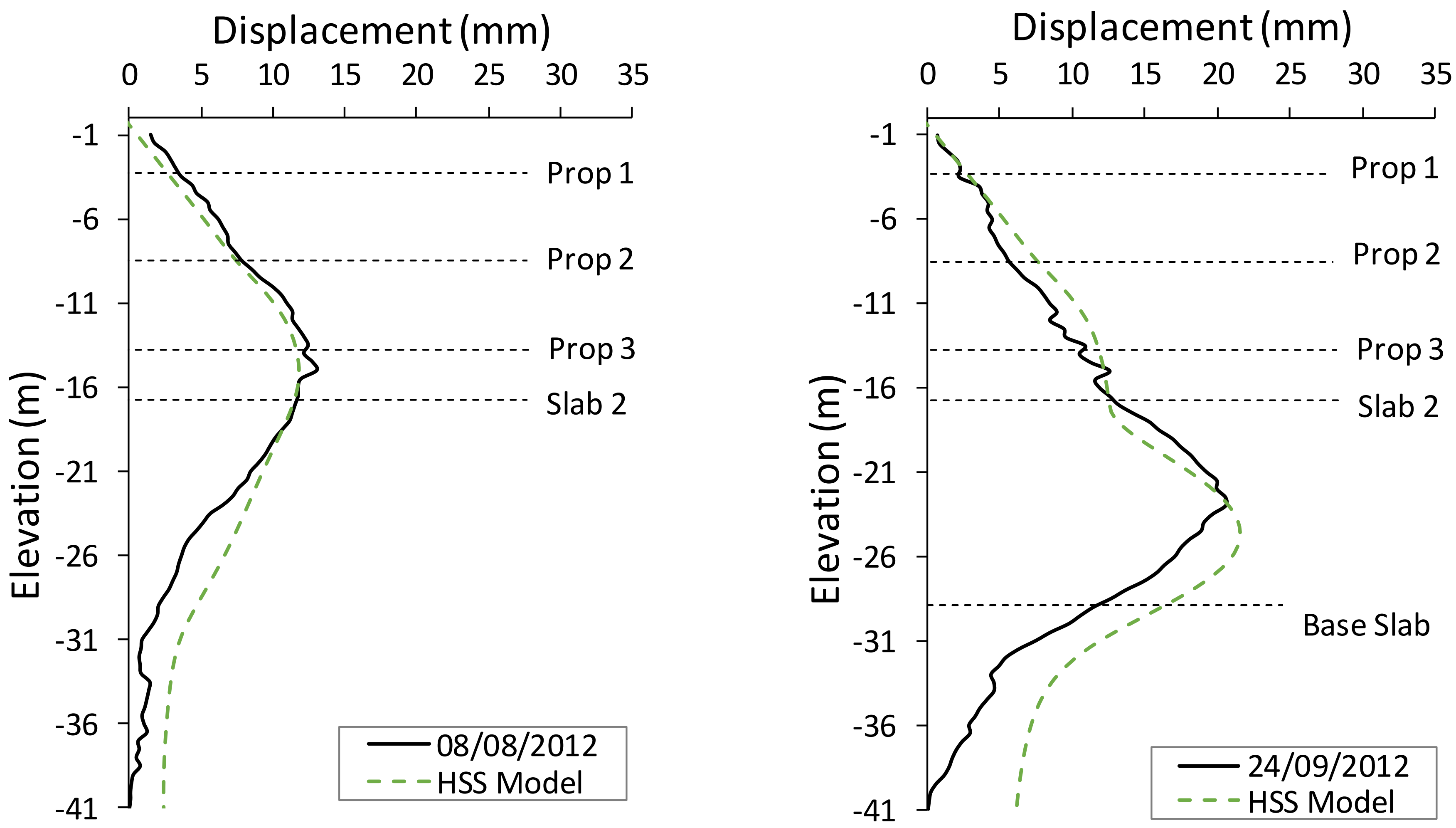
Displacement (mm)
0
5
10
15
20
25
30
35
-1
-6
-11
-16
-21
-26
-31
-36
-41
Elevation (m)
Prop 1
Prop 2
Prop 3
Slab 2
08/08/2012
HSS Model
Displacement (mm)
0
5
10
15
20
25
30
35
-1
-6
-11
-16
-21
-26
-31
-36
-41
Elevation (m)
Prop 1
Prop 2
Prop 3
Slab 2
Base Slab
24/09/2012
HSS Model

Figue 7a

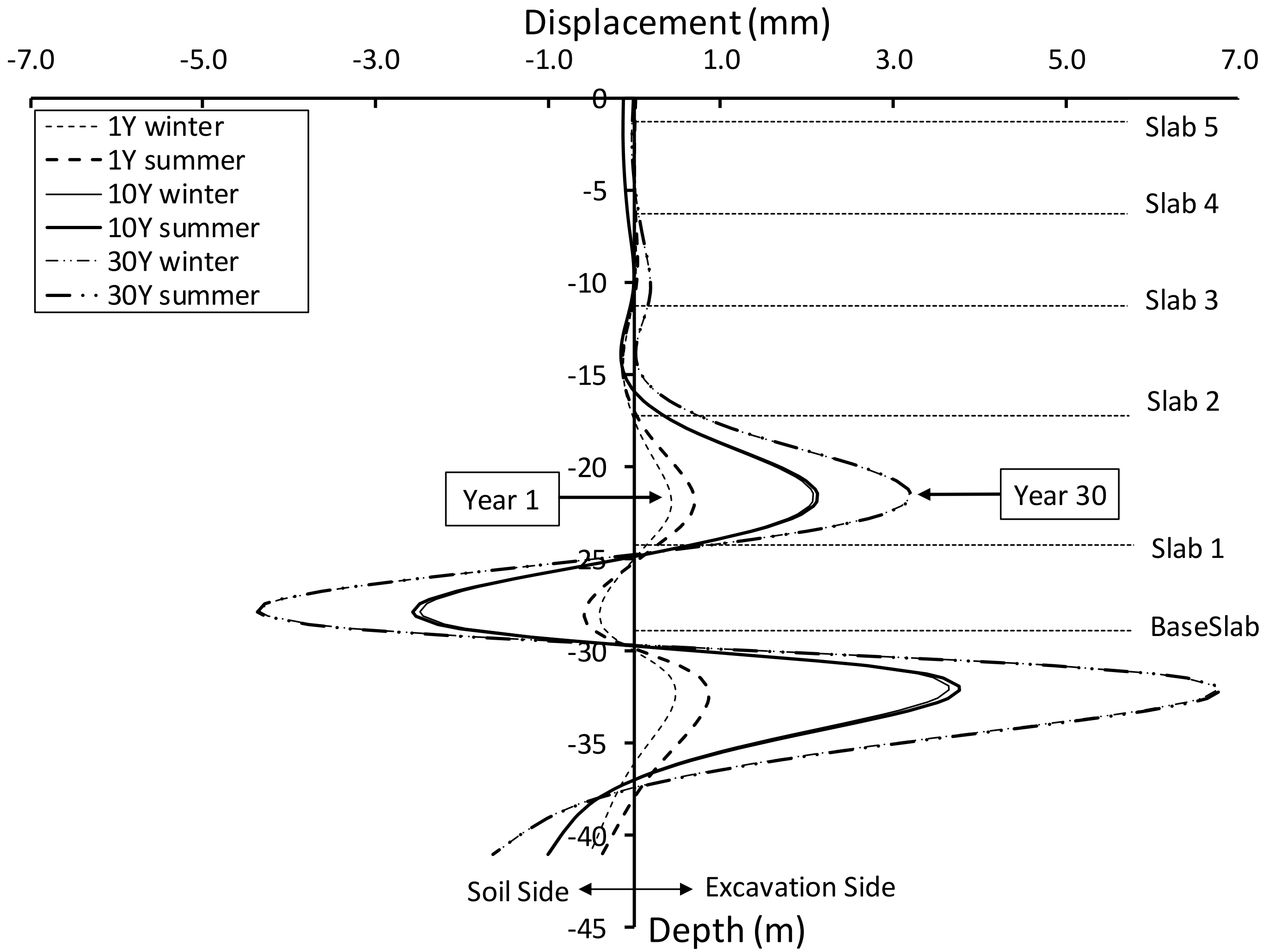
Displacement (mm)
-7.0
-5.0
-3.0
-1.0
1.0
3.0
5.0
7.0
0
-5
-10
-15
-20
-25
-30
-35
-40
-45
Depth (m)
1Y winter
1Y summer
10Y winter
10Y summer
30Y winter
30Y summer
Slab 5
Slab 4
Slab 3
Slab 2
Slab 1
BaseSlab
Year 1
Year 30
Soil Side
Excavation Side

Figure 7b

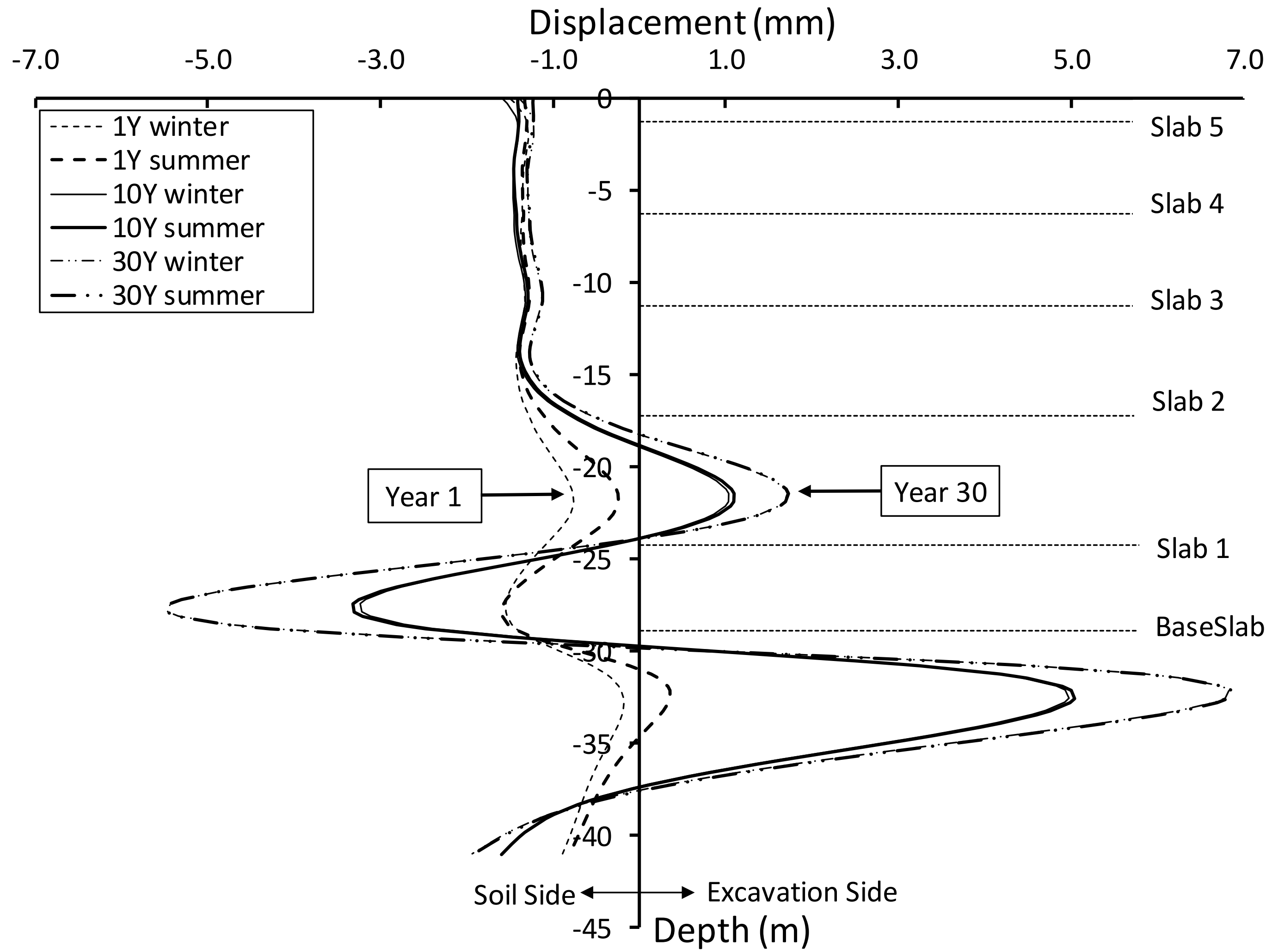
Displacement (mm)
-7.0
-5.0
-3.0
-1.0
1.0
3.0
5.0
7.0
0
-5
-10
-15
-20
-25
-30
-35
-40
-45
1Y winter
1Y summer
10Y winter
10Y summer
30Y winter
30Y summer
Slab 5
Slab 4
Slab 3
Slab 2
Slab 1
BaseSlab
Year 1
Year 30
Soil Side
Excavation Side
Depth (m)

Figure 7c

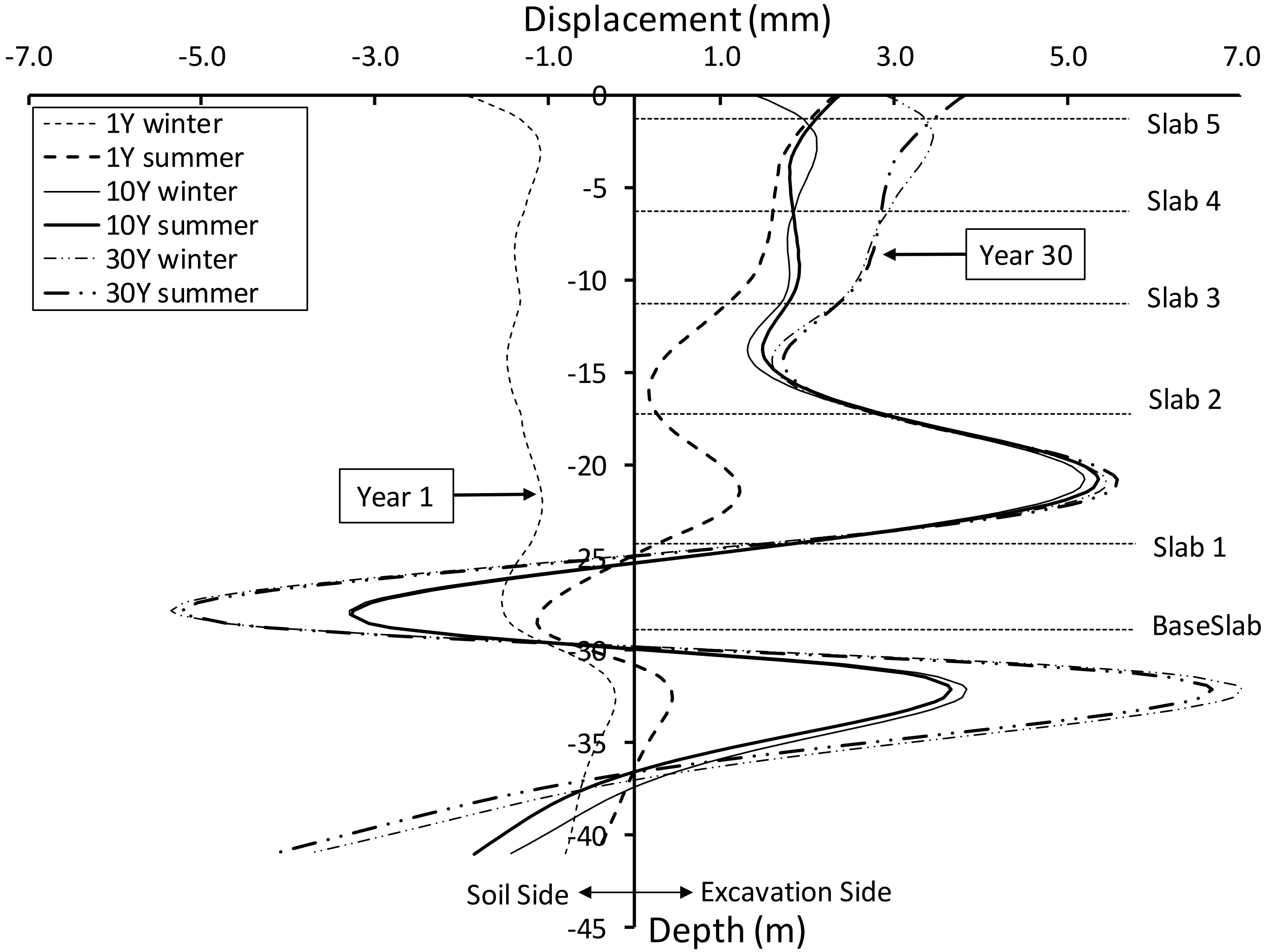

Displacement (mm)
-7.0
-5.0
-3.0
-1.0
1.0
3.0
5.0
7.0
0
-5
-10
-15
-20
-25
-30
-35
-40
-45
1Y winter
1Y summer
10Y winter
10Y summer
30Y winter
30Y summer
Slab 5
Slab 4
Year 30
Slab 3
Slab 2
Year 1
Slab 1
BaseSlab
Soil Side
Excavation Side
Depth (m)

Figure 8

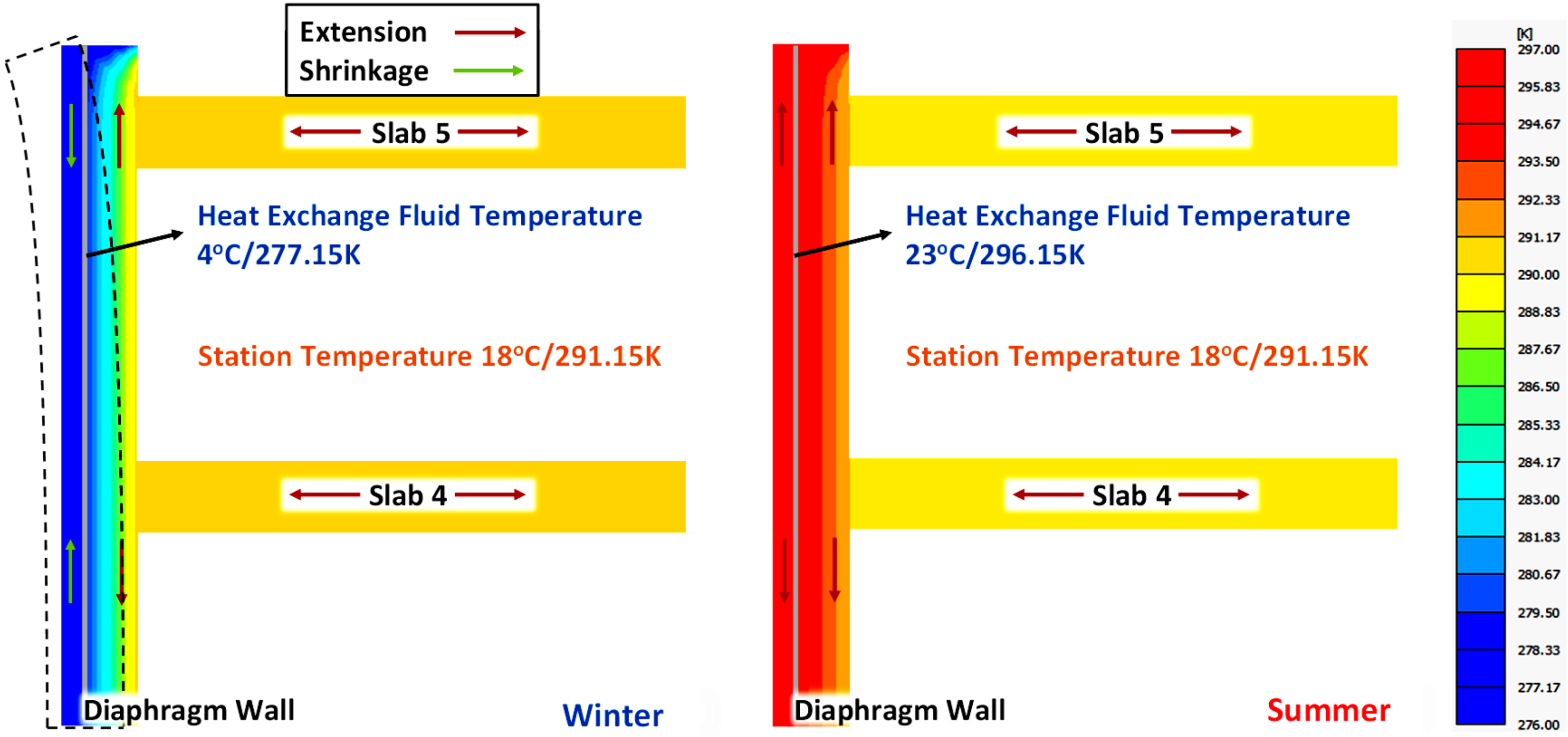
Extension
Shrinkage
Slab 5
Heat Exchange Fluid Temperature
4°C/277.15K
Station Temperature 18°C/291.15K
Slab 4
Diaphragm Wall
Winter
Slab 5
Heat Exchange Fluid Temperature
23°C/296.15K
Station Temperature 18°C/291.15K
Slab 4
Diaphragm Wall
Summer
[K]
297.00
295.83
294.67
293.50
292.33
291.17
290.00
288.83
287.67
286.50
285.33
284.17
283.00
281.83
280.67
279.50
278.33
277.17
276.00

Figure 9a

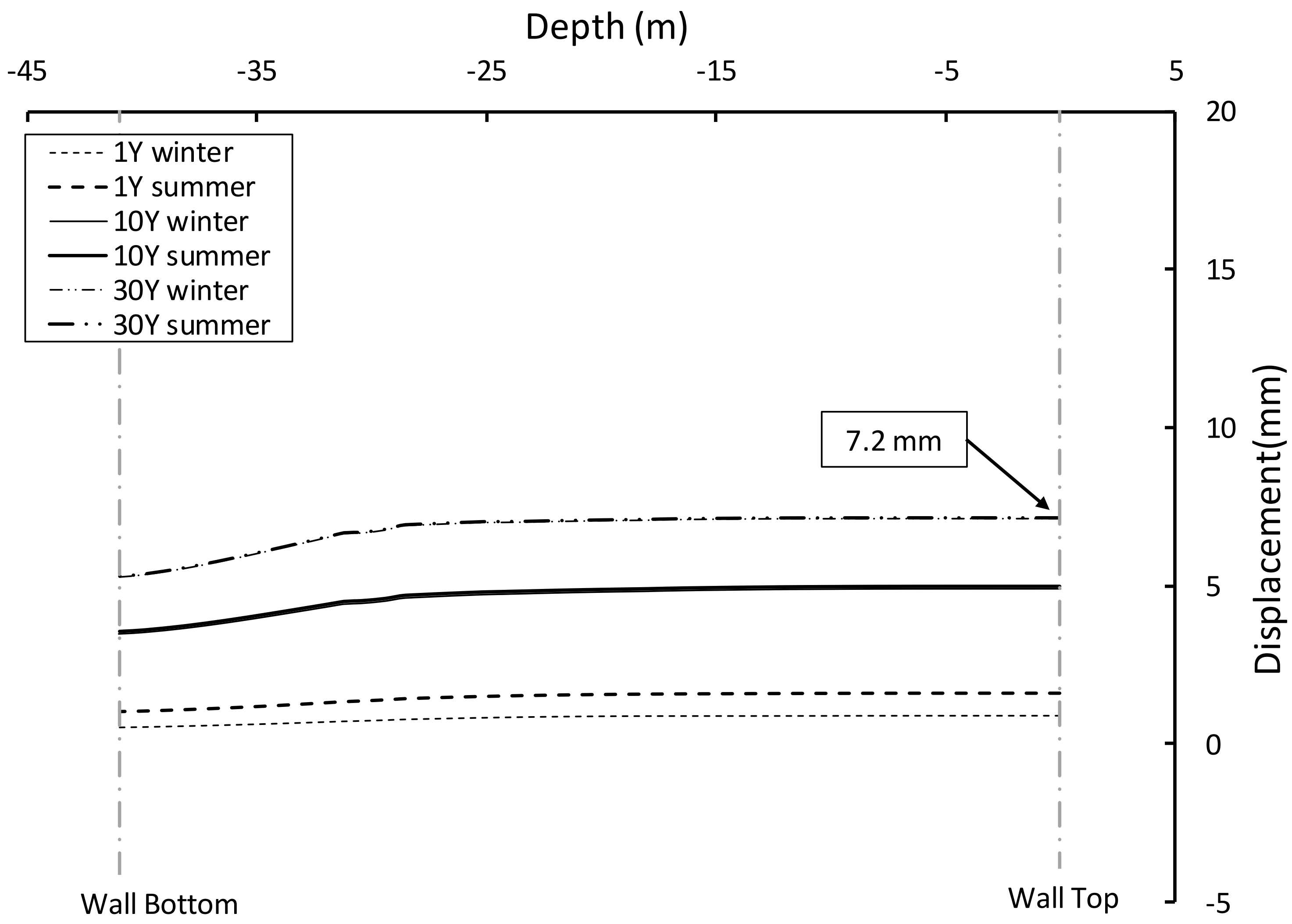
Depth (m)
-45
-35
-25
-15
-5
5
20
15
10
5
0
-5
Displacement(mm)
1Y winter
1Y summer
10Y winter
10Y summer
30Y winter
30Y summer
7.2 mm
Wall Bottom
Wall Top

Figure 9b

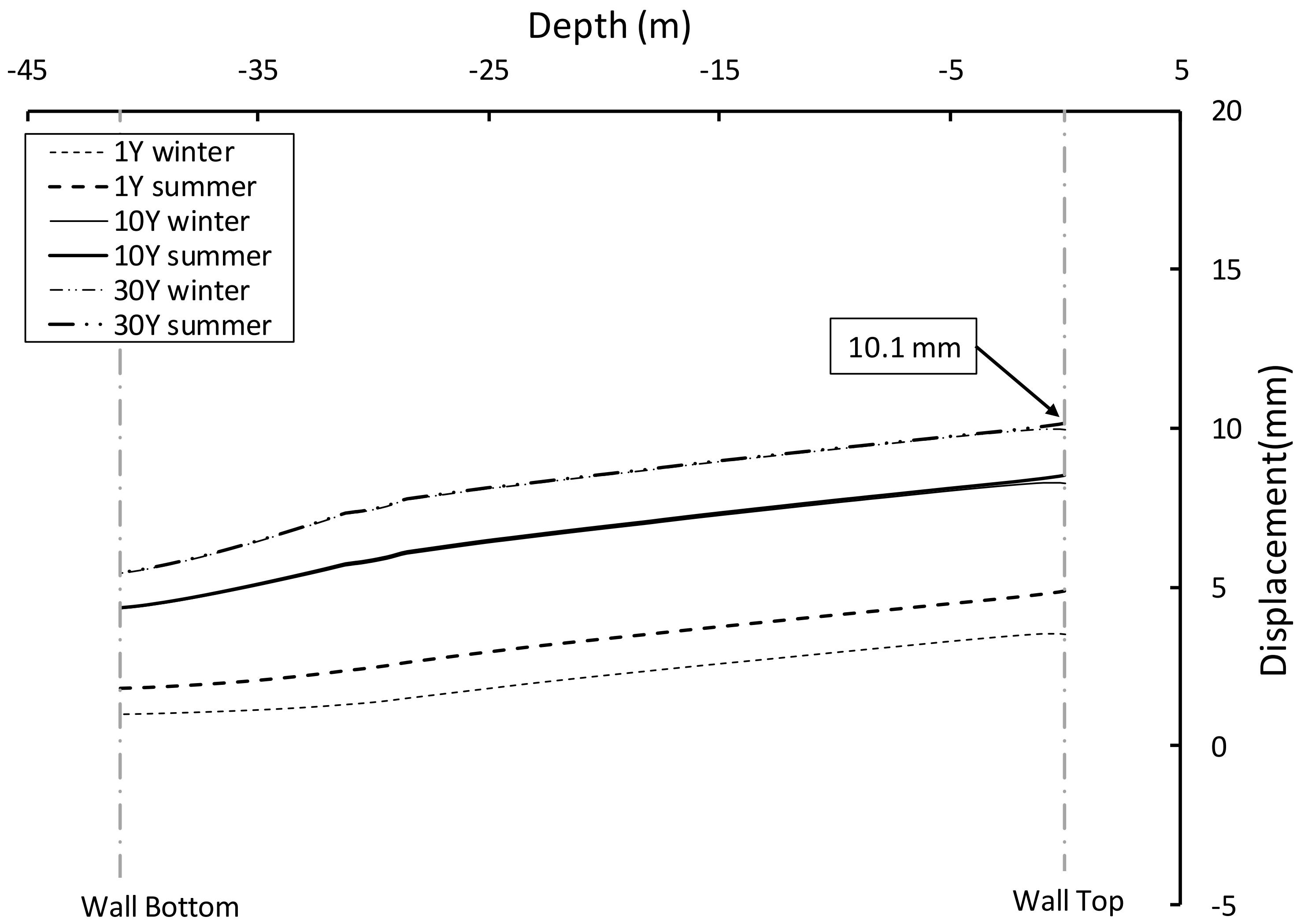
Depth (m)
-45
-35
-25
-15
-5
5
20
15
10
5
0
-5
Displacement(mm)
1Y winter
1Y summer
10Y winter
10Y summer
30Y winter
30Y summer
10.1 mm
Wall Bottom
Wall Top

Figure 9c

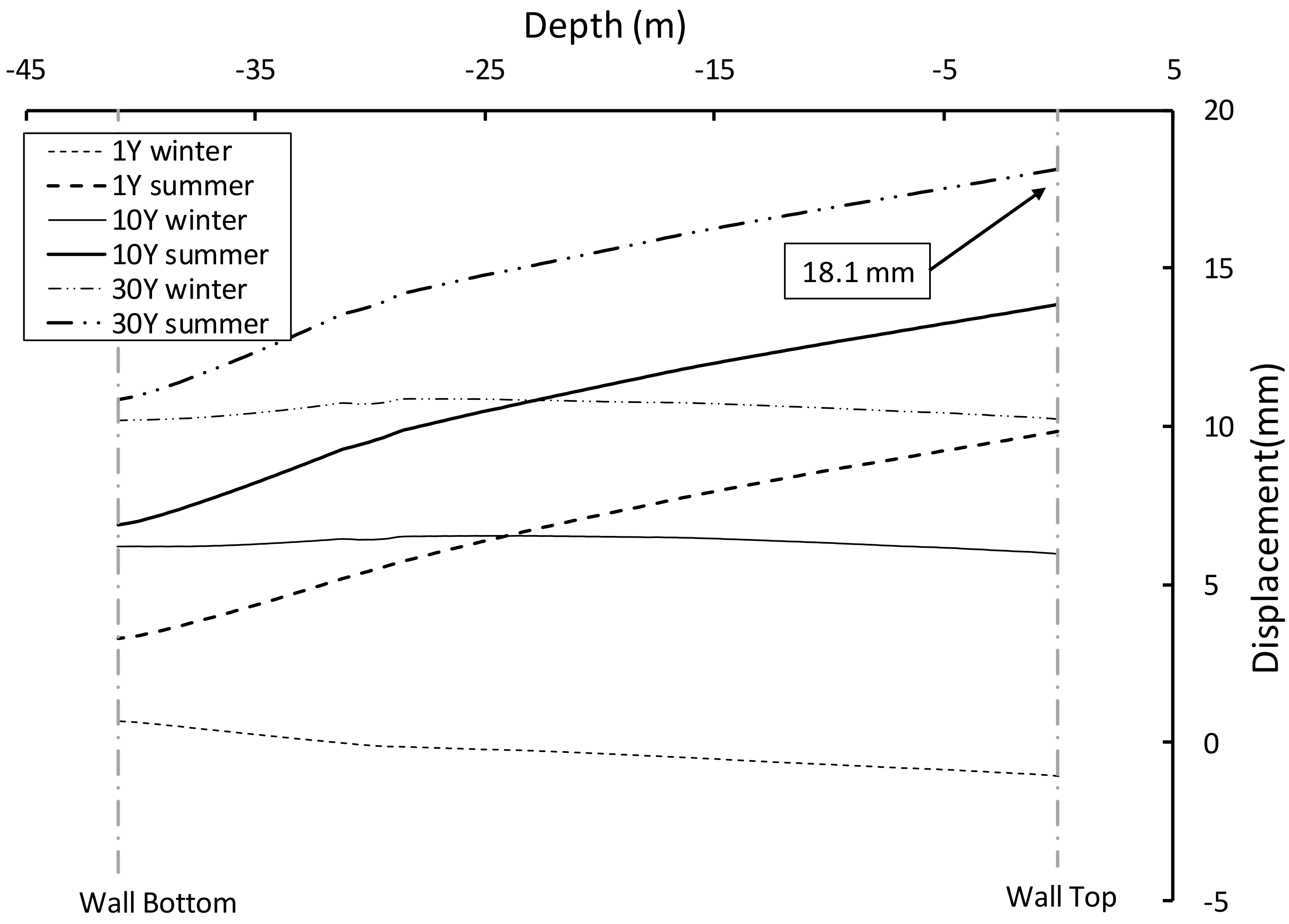
Depth (m)
-45
-35
-25
-15
-5
5
20
15
10
5
0
-5
Displacement(mm)
1Y winter
1Y summer
10Y winter
10Y summer
30Y winter
30Y summer
18.1 mm
Wall Bottom
Wall Top

Figure 10a

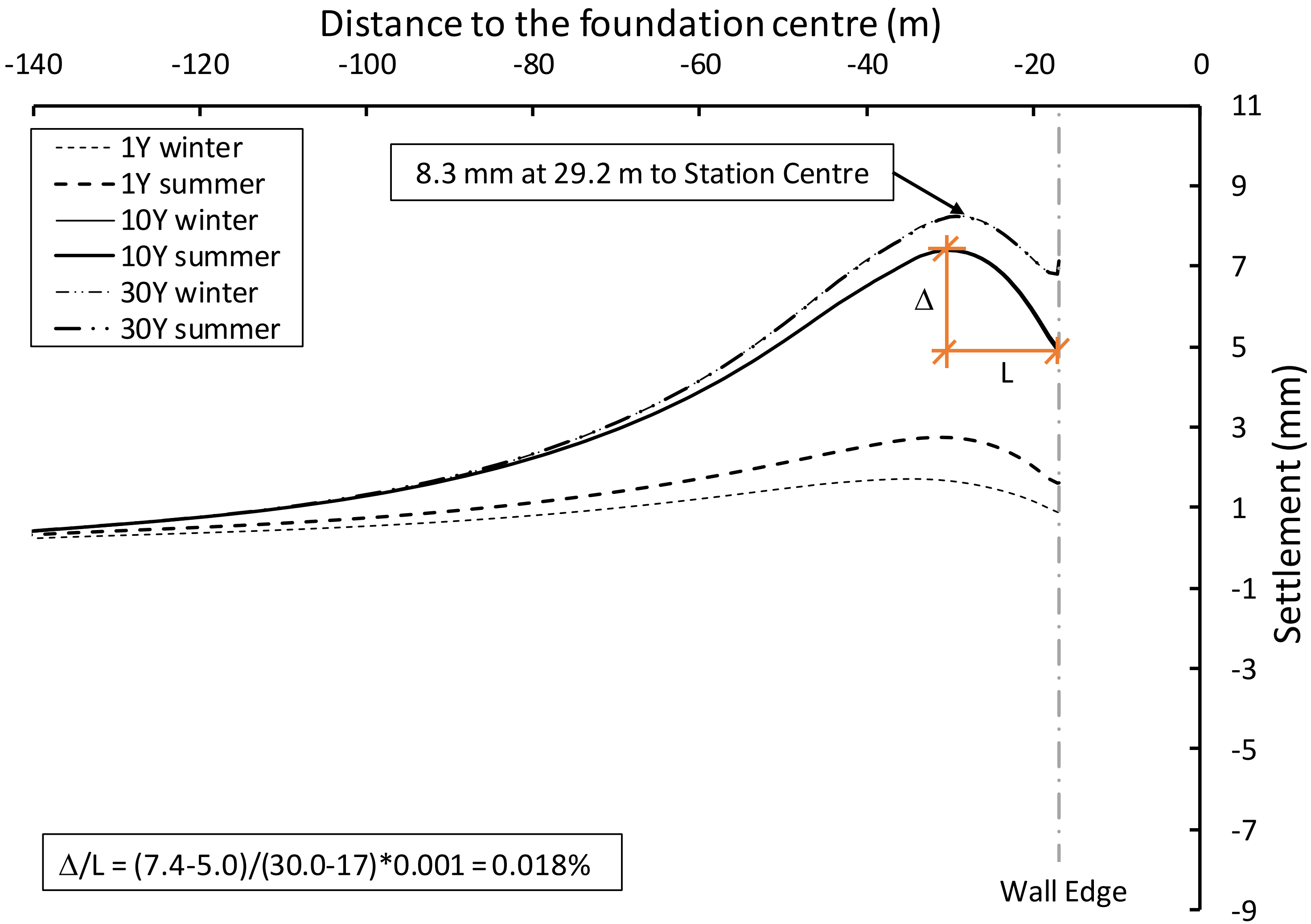
Distance to the foundation centre (m)
-140
-120
-100
-80
-60
-40
-20
0
11
9
7
5
3
1
-1
-3
-5
-7
-9
Settlement (mm)
1Y winter
1Y summer
10Y winter
10Y summer
30Y winter
30Y summer
8.3 mm at 29.2 m to Station Centre
Δ
L
Δ/L = (7.4-5.0)/(30.0-17)*0.001 = 0.018%
Wall Edge

Figure 10b

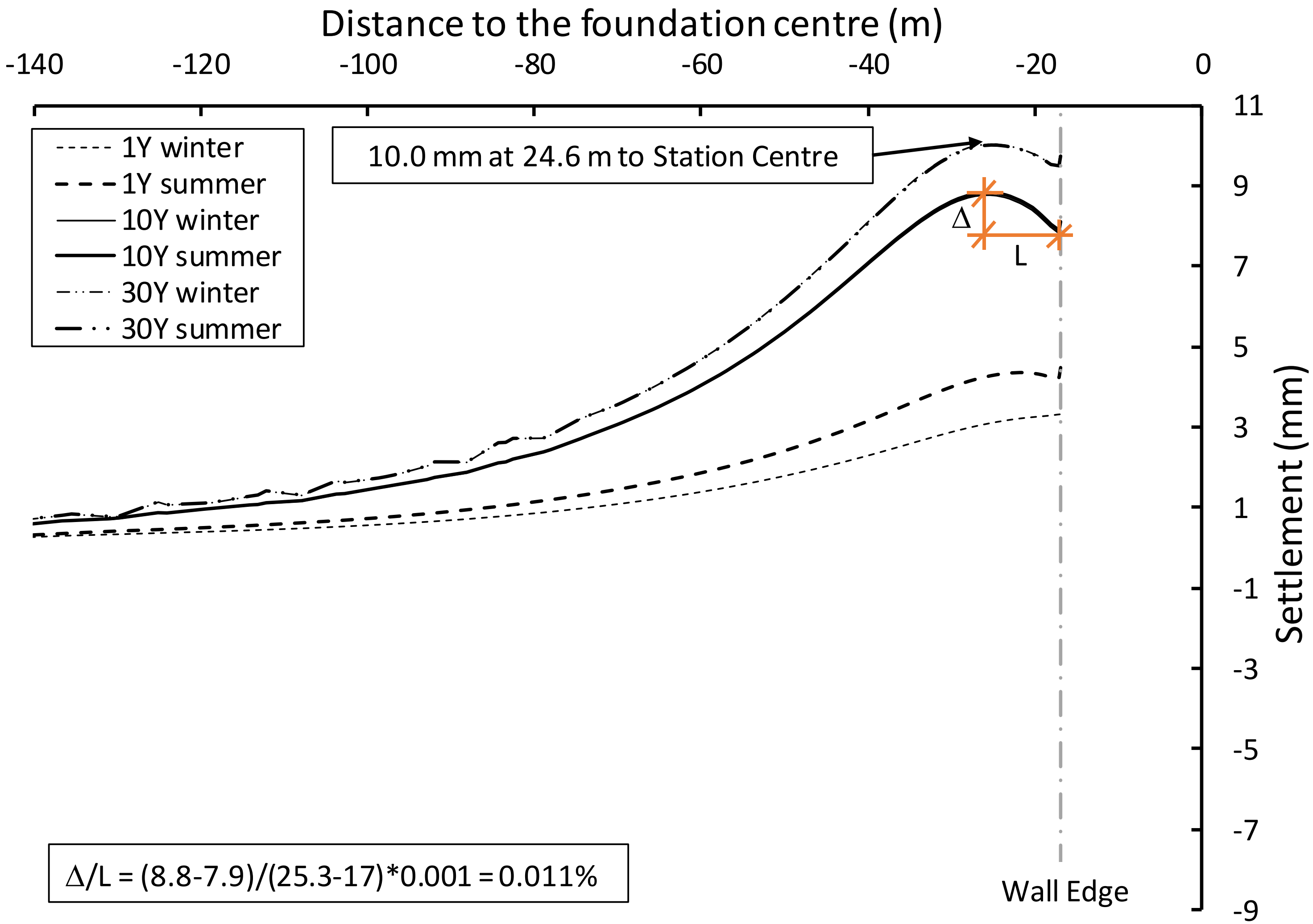
Distance to the foundation centre (m)
-140
-120
-100
-80
-60
-40
-20
0
11
9
7
5
3
1
-1
-3
-5
-7
-9
Settlement (mm)
1Y winter
1Y summer
10Y winter
10Y summer
30Y winter
30Y summer
10.0 mm at 24.6 m to Station Centre
Δ
L
Wall Edge
Δ/L = (8.8-7.9)/(25.3-17)*0.001 = 0.011%

Figure 10c

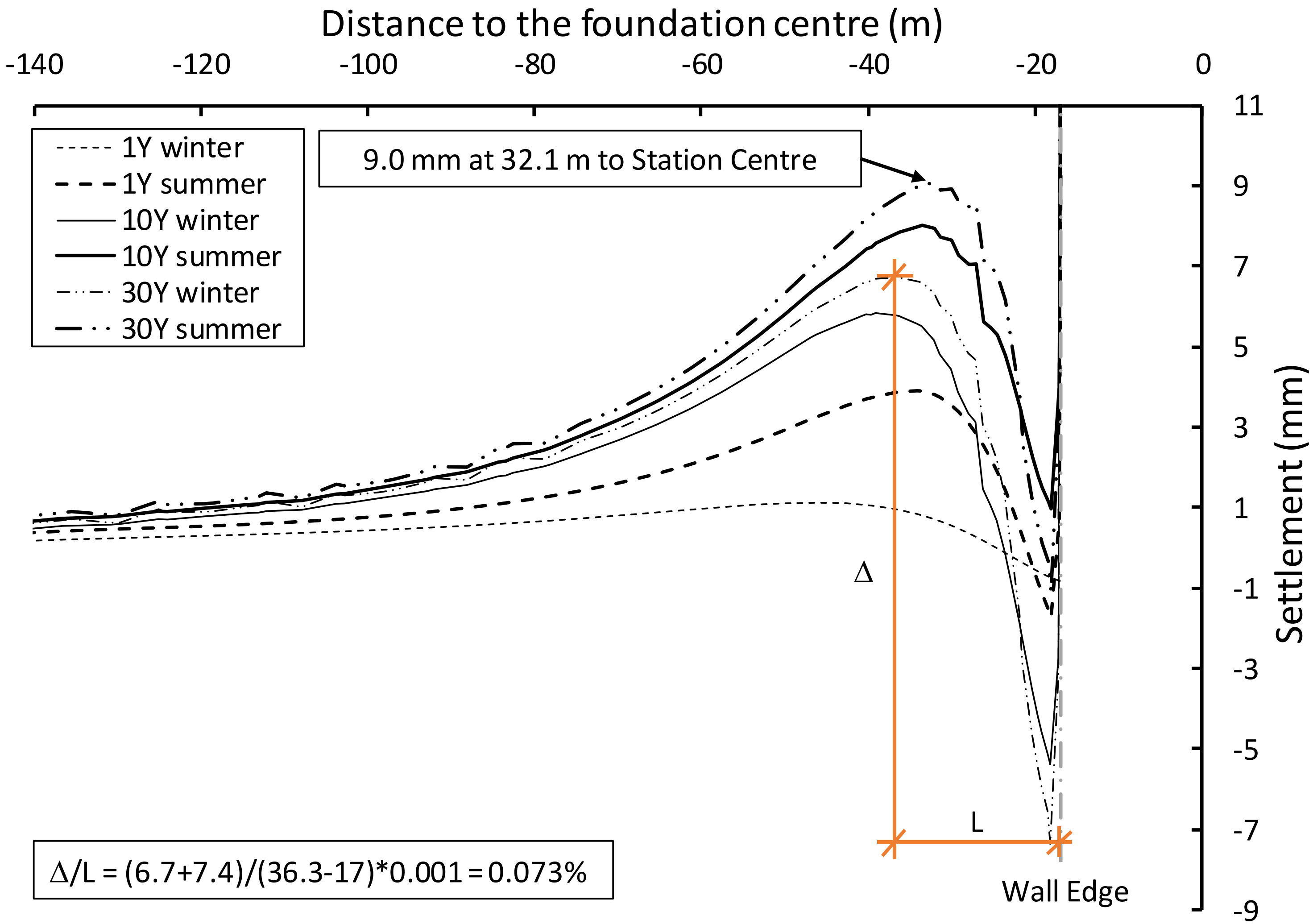
Distance to the foundation centre (m)
-140
-120
-100
-80
-60
-40
-20
0
11
9
7
5
3
1
-1
-3
-5
-7
-9
Settlement (mm)
1Y winter
1Y summer
10Y winter
10Y summer
30Y winter
30Y summer
9.0 mm at 32.1 m to Station Centre
Δ
L
Wall Edge
Δ/L = (6.7+7.4)/(36.3-17)*0.001 = 0.073%

Figure 11

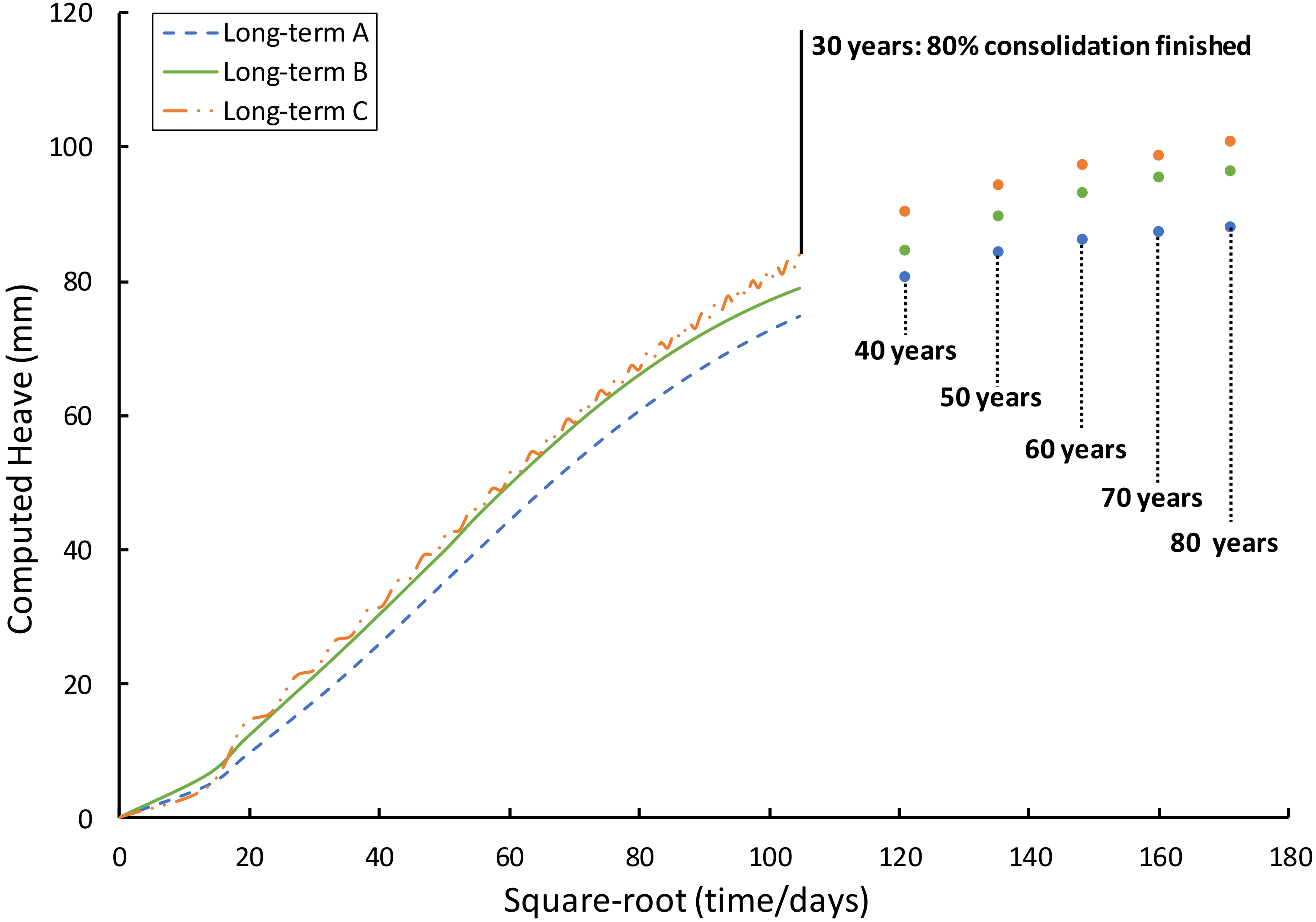

120
100
80
60
40
20
0
Computed Heave (mm)
Long-term A
Long-term B
Long-term C
30 years: 80% consolidation finished
40 years
50 years
60 years
70 years
80 years
0
20
40
60
80
100
120
140
160
180
Square-root (time/days)

Figure 12a

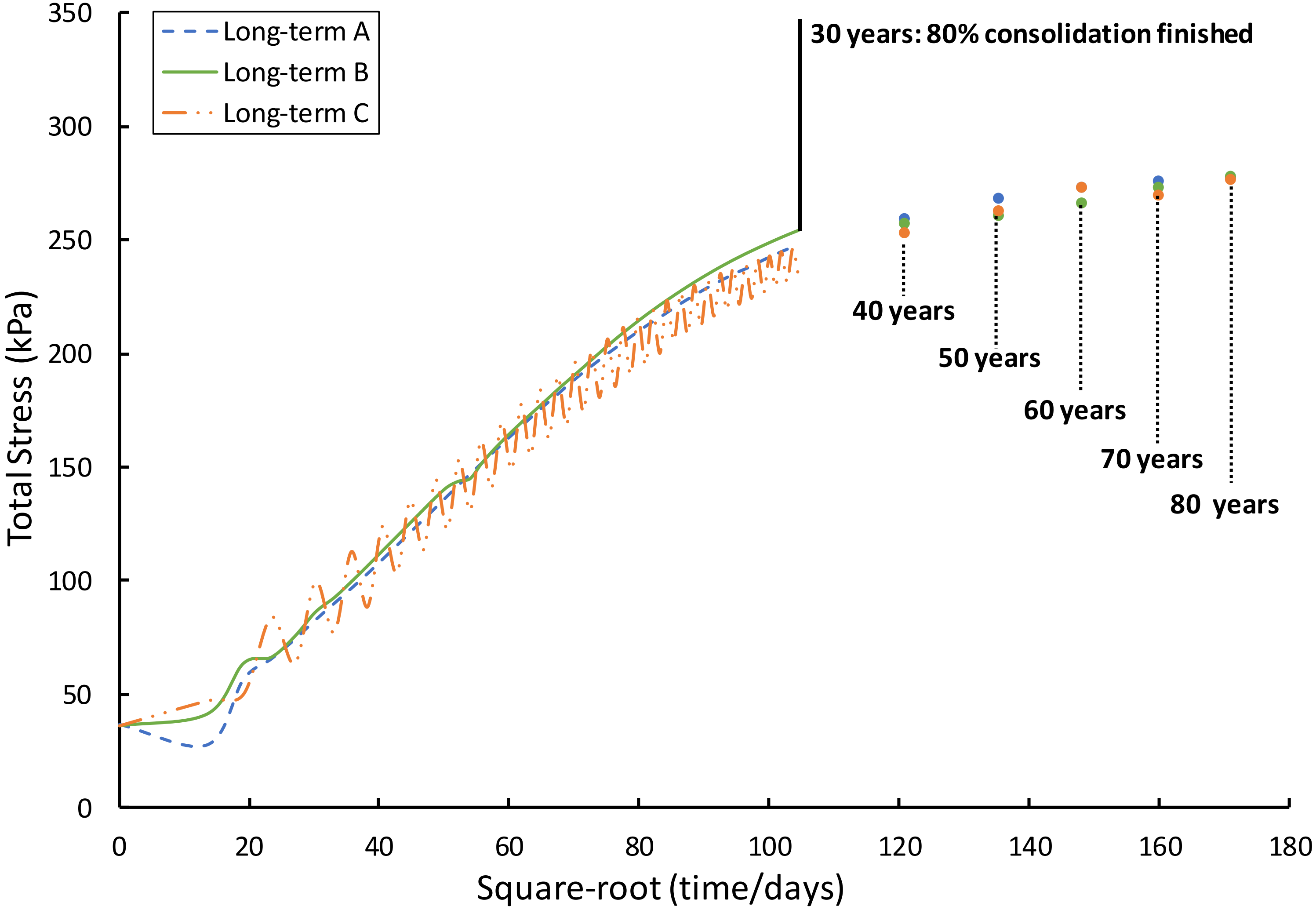

Long-term A
Long-term B
Long-term C
30 years: 80% consolidation finished
40 years
50 years
60 years
70 years
80 years
Total Stress (kPa)
Square-root (time/days)
0
50
100
150
200
250
300
350
0
20
40
60
80
100
120
140
160
180

Figure 12b

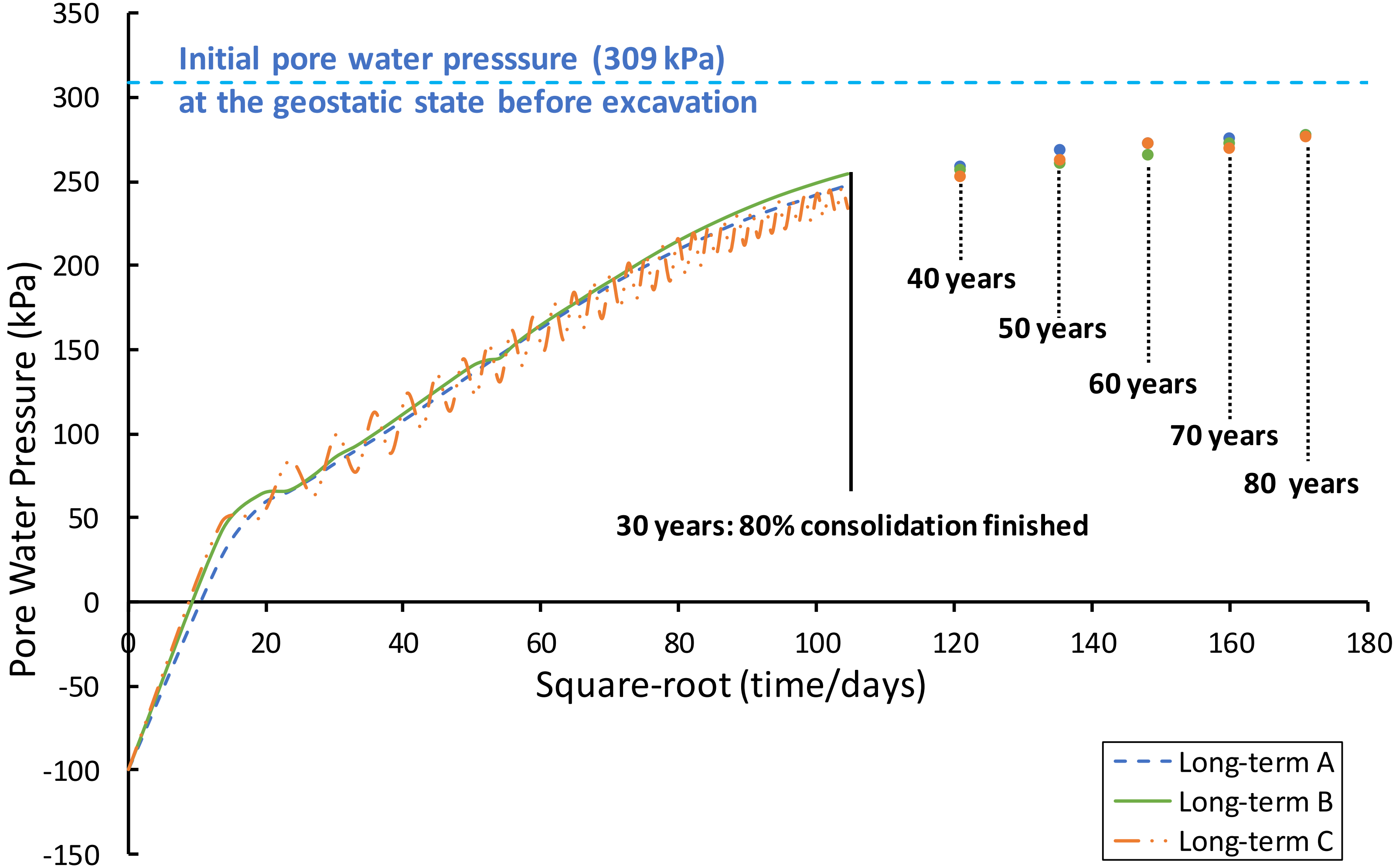
Initial pore water presssure (309 kPa)
at the geostatic state before excavation
40 years
50 years
60 years
70 years
80 years
30 years: 80% consolidation finished
Pore Water Pressure (kPa)
Square-root (time/days)
350
300
250
200
150
100
50
0
-50
-100
-150
0
20
40
60
80
100
120
140
160
180
Long-term A
Long-term B
Long-term C

Figure 12c

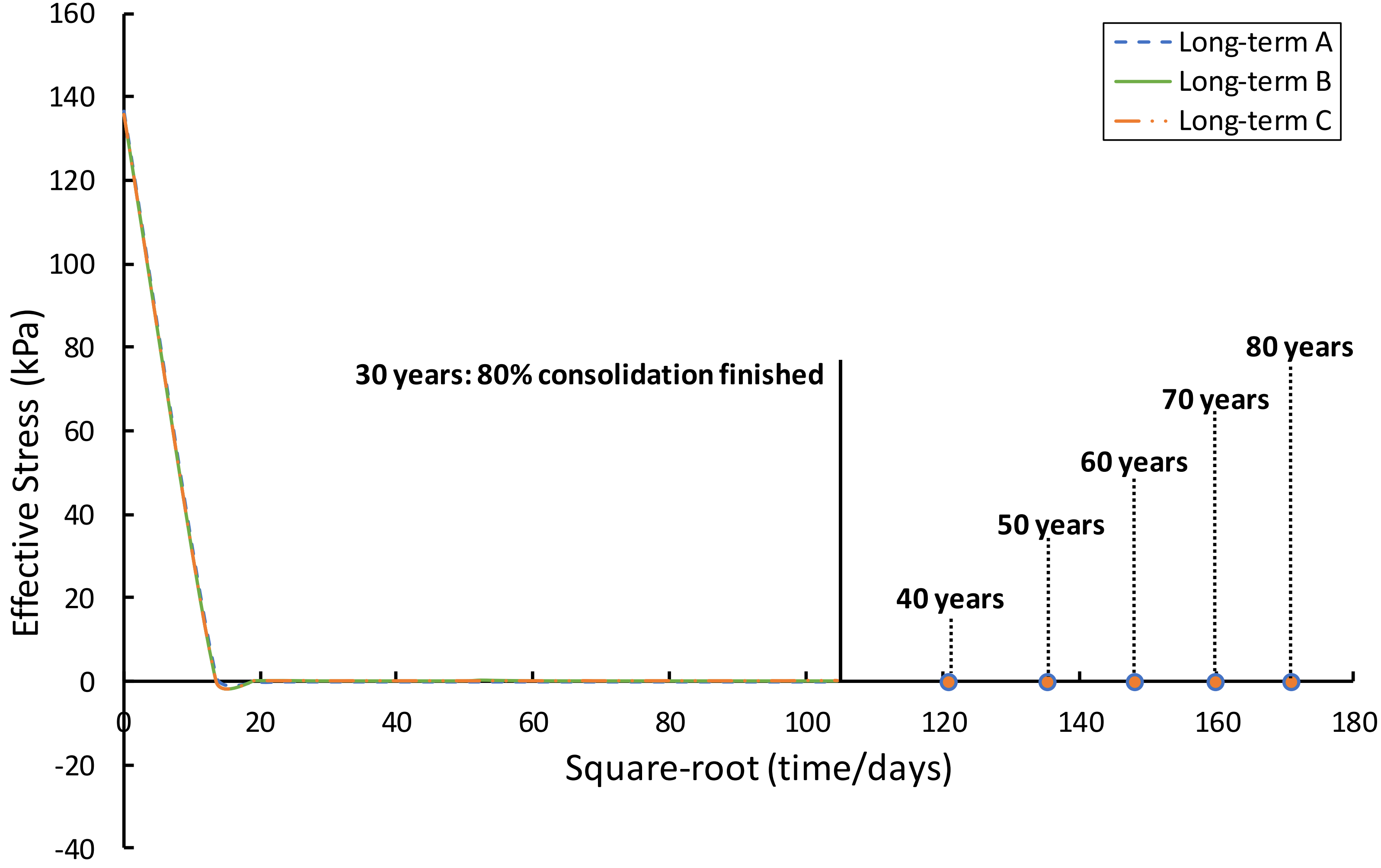
Long-term A
Long-term B
Long-term C
30 years: 80% consolidation finished
40 years
50 years
60 years
70 years
80 years
Effective Stress (kPa)
Square-root (time/days)
160
140
120
100
80
60
40
20
0
-20
-40
0
20
40
60
80
100
120
140
160
180

Figure 13a

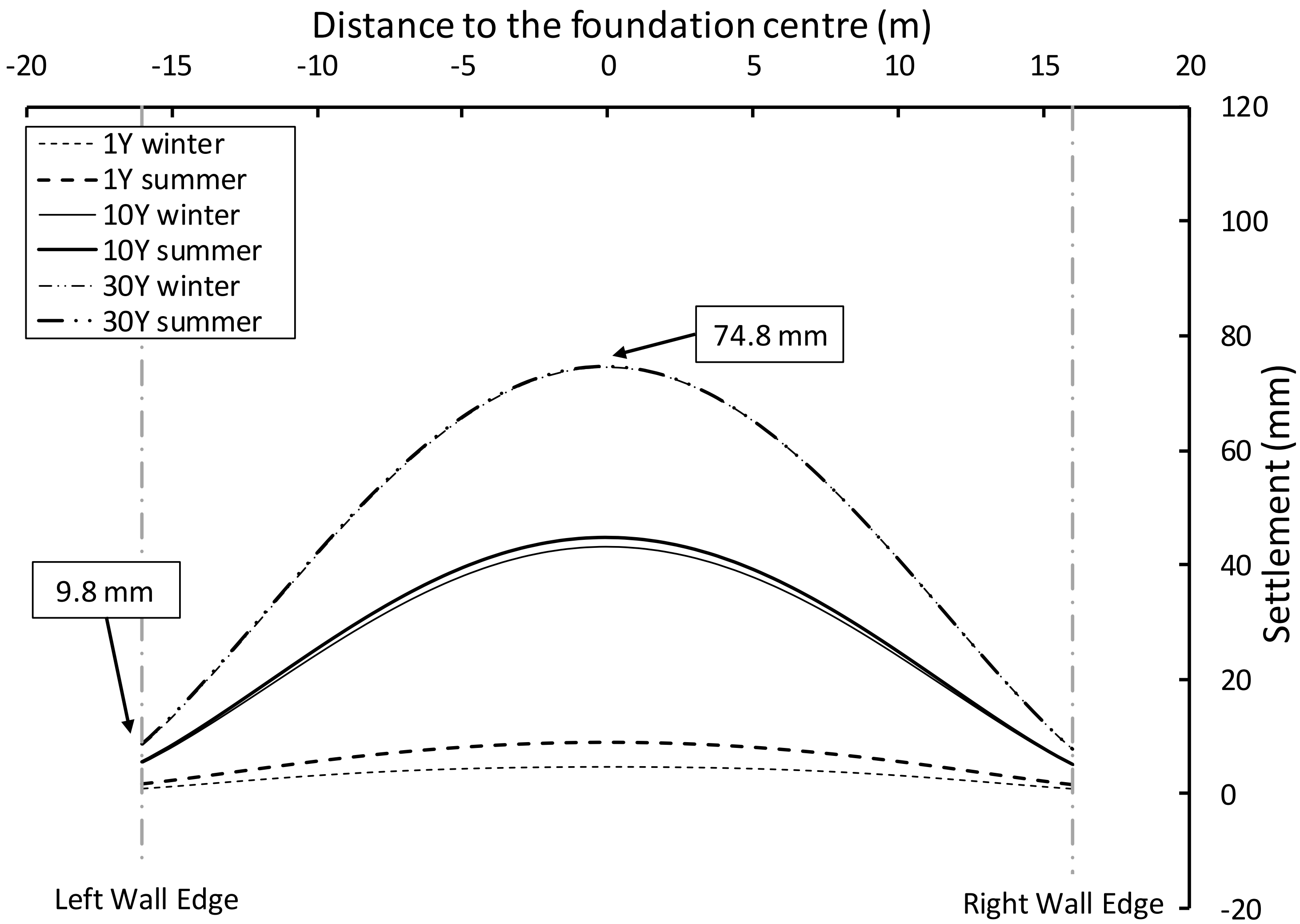
Distance to the foundation centre (m)
-20
-15
-10
-5
0
5
10
15
20
120
100
80
60
40
20
0
-20
Settlement (mm)
1Y winter
1Y summer
10Y winter
10Y summer
30Y winter
30Y summer
74.8 mm
9.8 mm
Left Wall Edge
Right Wall Edge

Figure 13b

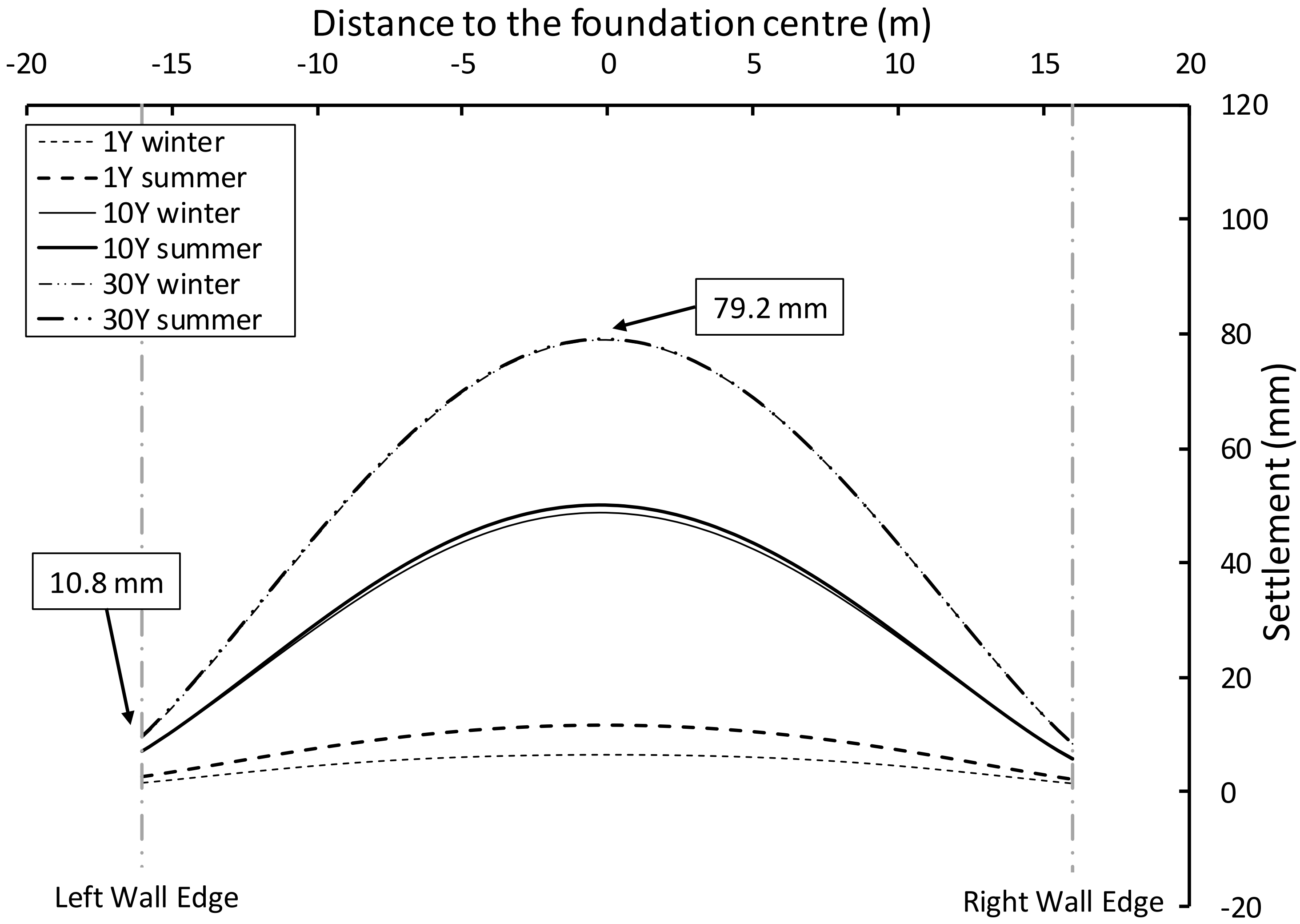
Distance to the foundation centre (m)
-20
-15
-10
-5
0
5
10
15
20
120
100
80
60
40
20
0
-20
Settlement (mm)
1Y winter
1Y summer
10Y winter
10Y summer
30Y winter
30Y summer
79.2 mm
10.8 mm
Left Wall Edge
Right Wall Edge

Figure 13c

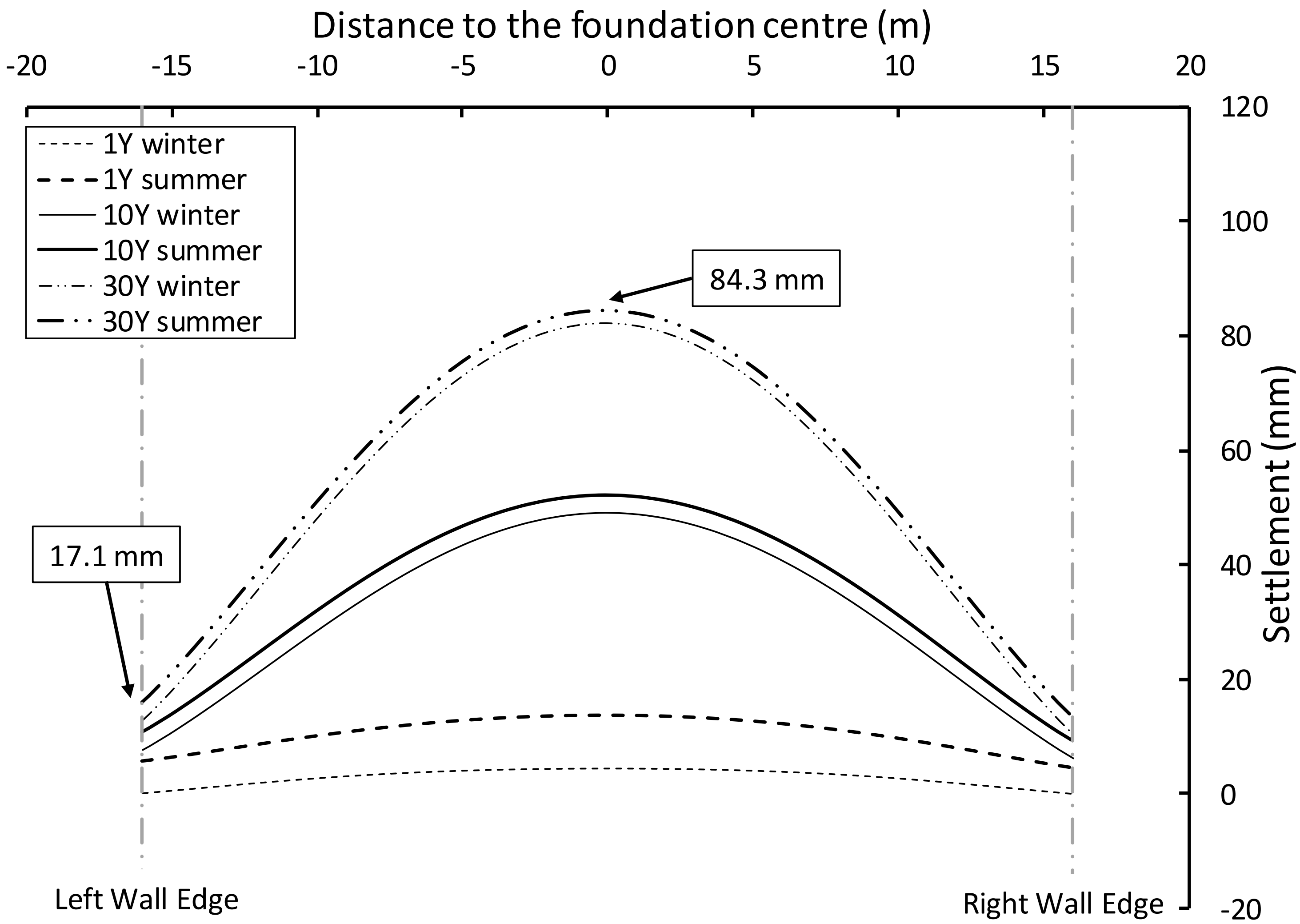
Distance to the foundation centre (m)
-20
-15
-10
-5
0
5
10
15
20
120
100
80
60
40
20
0
-20
Settlement (mm)
1Y winter
1Y summer
10Y winter
10Y summer
30Y winter
30Y summer
84.3 mm
17.1 mm
Left Wall Edge
Right Wall Edge

Figure 14

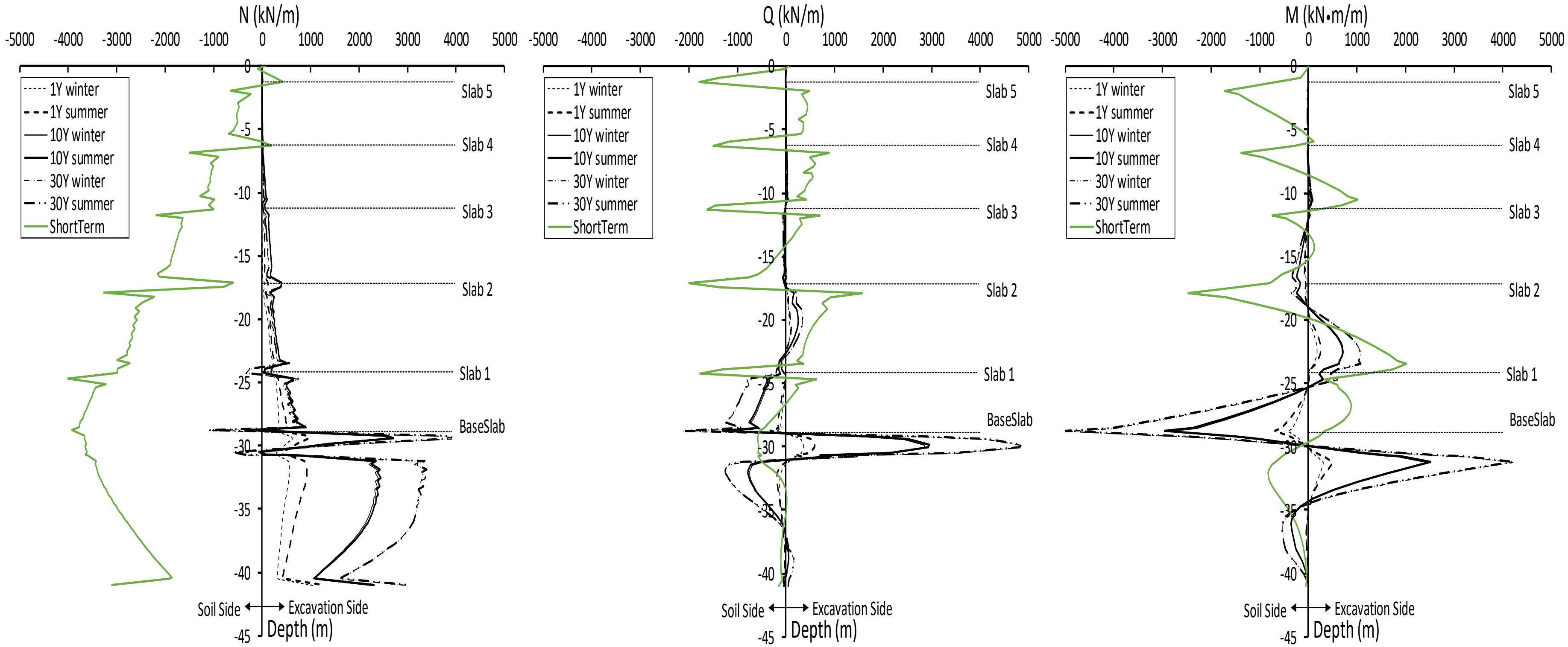
N (kN/m)
Q (kN/m)
M (kN•m/m)
-5000
-4000
-3000
-2000
-1000
0
1000
2000
3000
4000
5000
1Y winter
1Y summer
10Y winter
10Y summer
30Y winter
30Y summer
ShortTerm
Slab 5
Slab 4
Slab 3
Slab 2
Slab 1
BaseSlab
-5
-10
-15
-20
-25
-30
-35
-40
-45
Soil Side
Excavation Side
Depth (m)

Figure 15

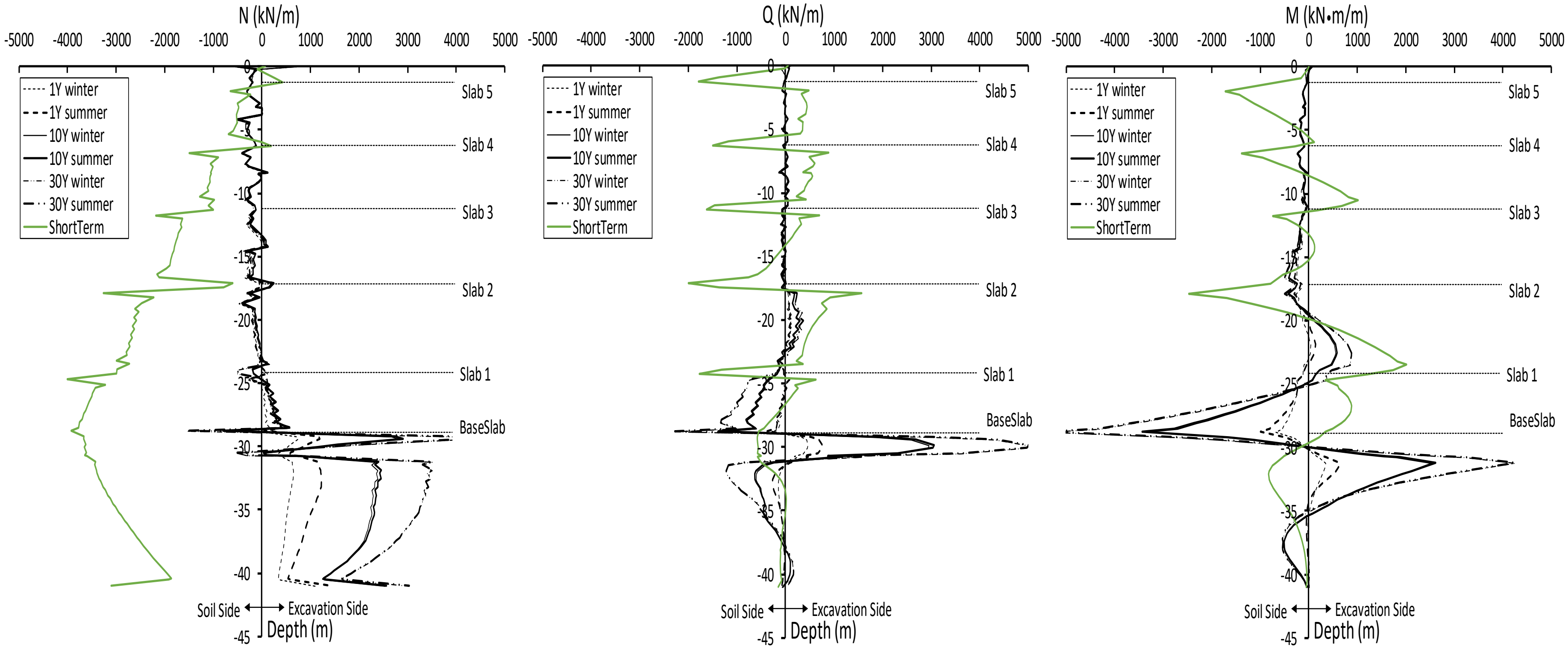
N (kN/m)
Q (kN/m)
M (kN•m/m)
-5000 -4000 -3000 -2000 -1000 0 1000 2000 3000 4000 5000
1Y winter
1Y summer
10Y winter
10Y summer
30Y winter
30Y summer
ShortTerm
Slab 5
Slab 4
Slab 3
Slab 2
Slab 1
BaseSlab
0 -5 -10 -15 -20 -25 -30 -35 -40 -45
Soil Side
Excavation Side
Depth (m)

Figure 16

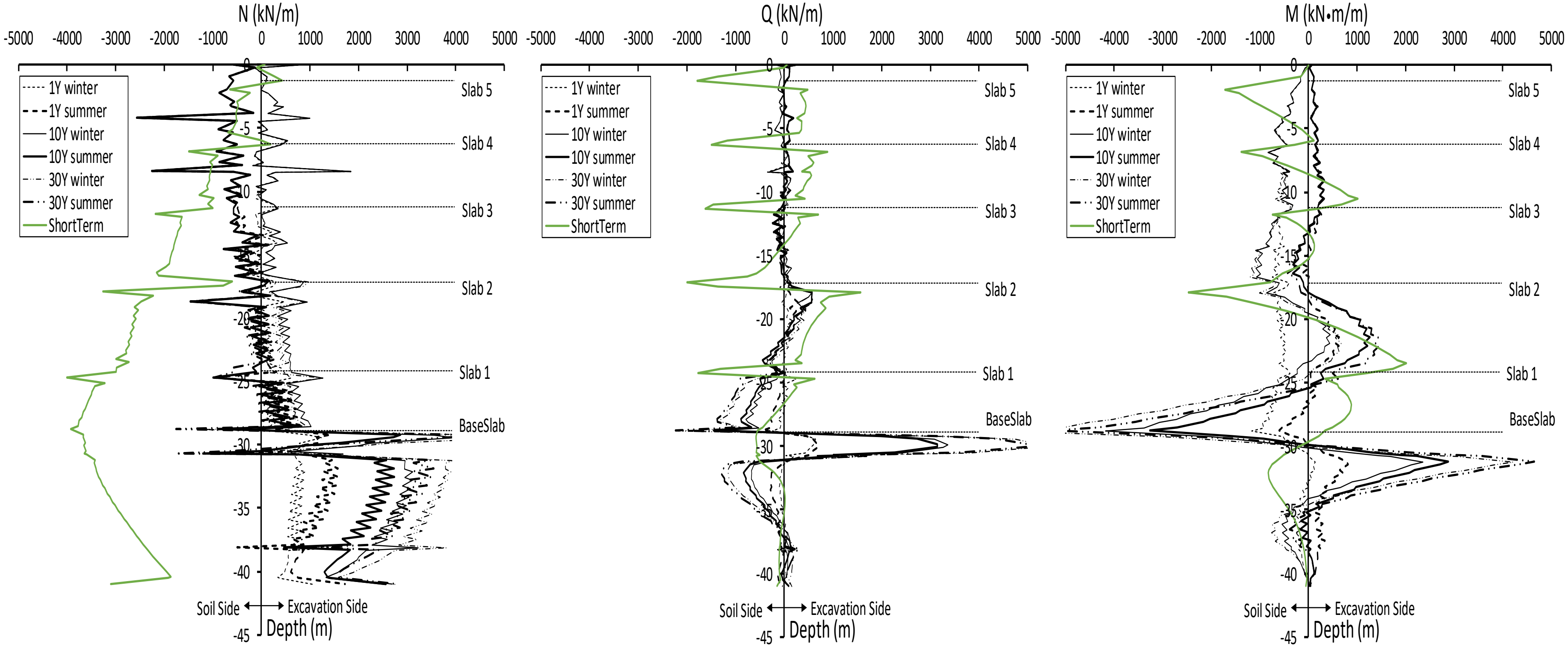

N (kN/m)
Q (kN/m)
M (kN•m/m)
-5000 -4000 -3000 -2000 -1000 0 1000 2000 3000 4000 5000
1Y winter
1Y summer
10Y winter
10Y summer
30Y winter
30Y summer
ShortTerm
Slab 5
Slab 4
Slab 3
Slab 2
Slab 1
BaseSlab
0
-5
-10
-15
-20
-25
-30
-35
-40
-45
Soil Side
Excavation Side
Depth (m)

Figure 17

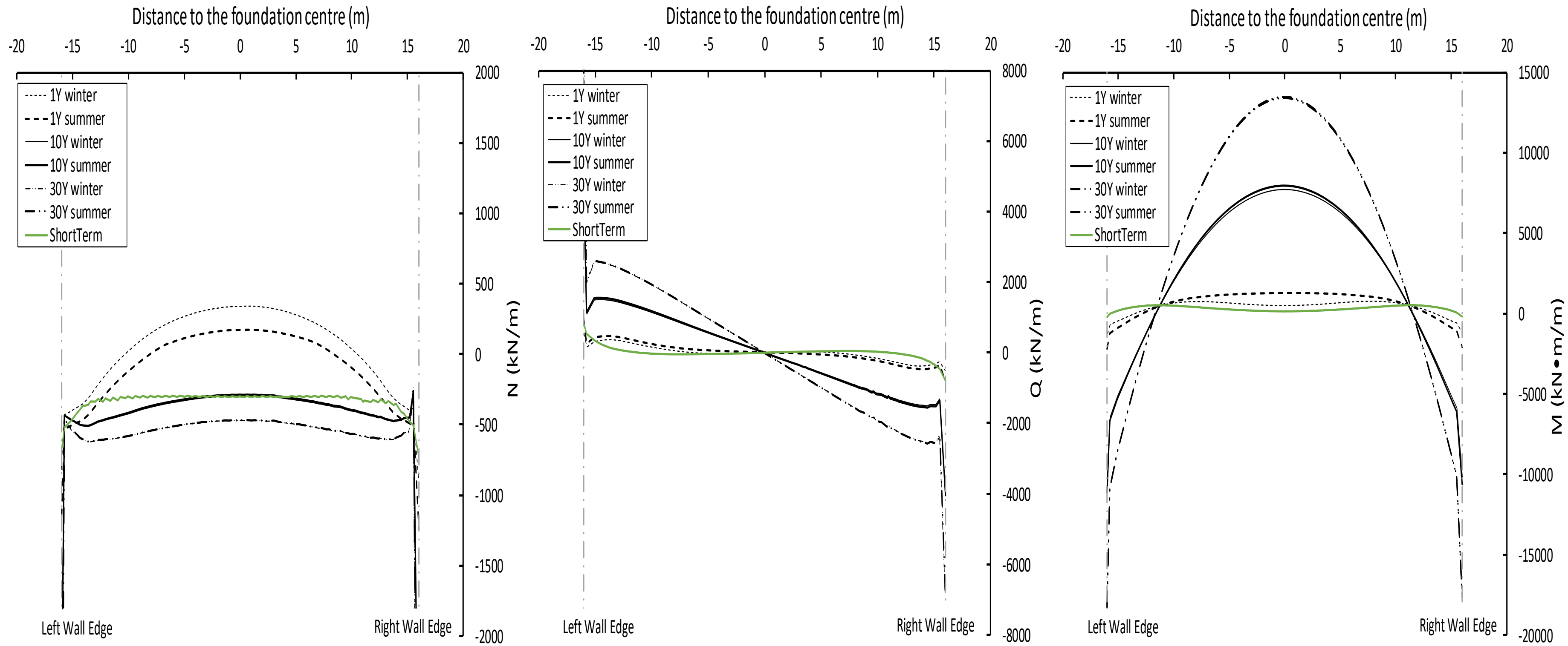
Distance to the foundation centre (m)
-20
-15
-10
-5
0
5
10
15
20
1Y winter
1Y summer
10Y winter
10Y summer
30Y winter
30Y summer
ShortTerm
2000
1500
1000
500
0
-500
-1000
-1500
-2000
N (kN/m)
Left Wall Edge
Right Wall Edge
8000
6000
4000
2000
0
-2000
-4000
-6000
-8000
Q (kN/m)
15000
10000
5000
0
-5000
-10000
-15000
-20000
M (kN•m/m)

Figure 18

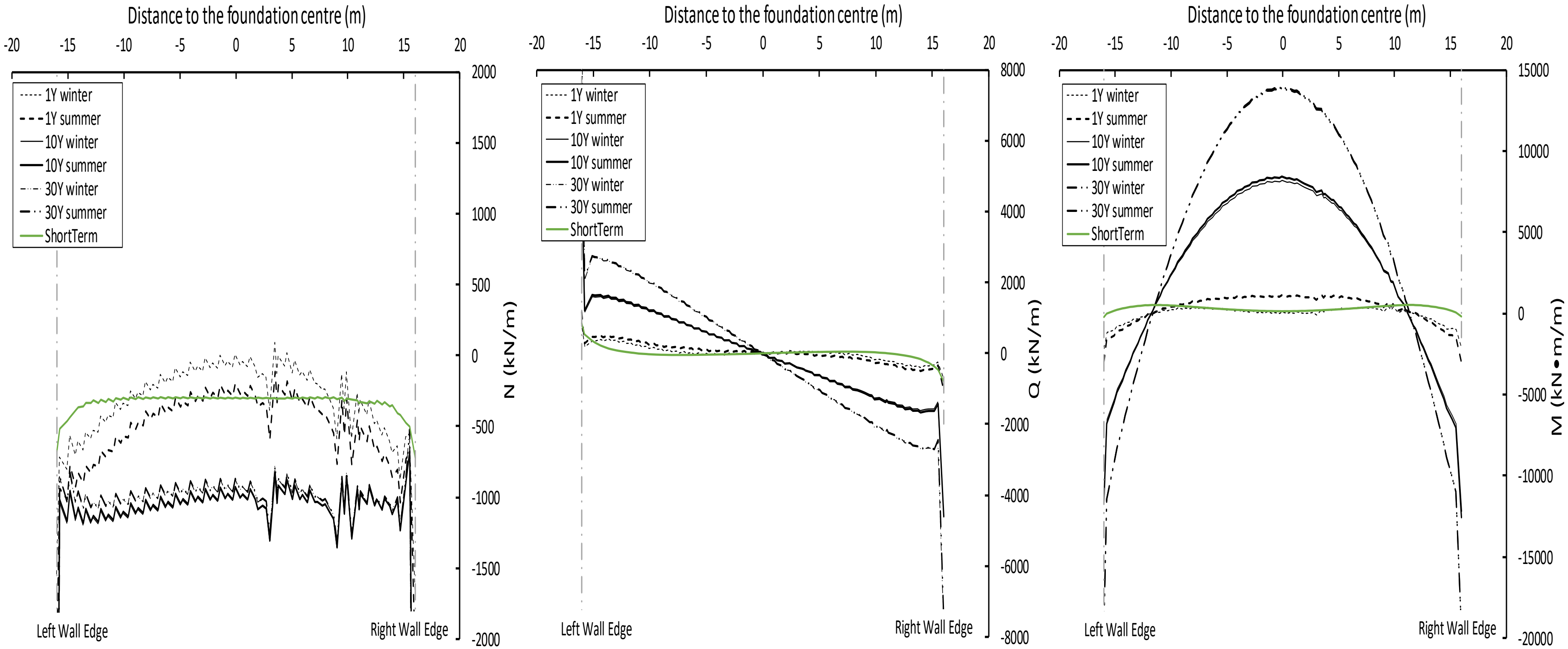
Distance to the foundation centre (m)
-20 -15 -10 -5 0 5 10 15 20
1Y winter
1Y summer
10Y winter
10Y summer
30Y winter
30Y summer
ShortTerm
2000 1500 1000 500 0 -500 -1000 -1500 -2000
N (kN/m)
Left Wall Edge
Right Wall Edge
Distance to the foundation centre (m)
-20 -15 -10 -5 0 5 10 15 20
1Y winter
1Y summer
10Y winter
10Y summer
30Y winter
30Y summer
ShortTerm
8000 6000 4000 2000 0 -2000 -4000 -6000 -8000
Q (kN/m)
Left Wall Edge
Right Wall Edge
Distance to the foundation centre (m)
-20 -15 -10 -5 0 5 10 15 20
1Y winter
1Y summer
10Y winter
10Y summer
30Y winter
30Y summer
ShortTerm
15000 10000 5000 0 -5000 -10000 -15000 -20000
M (kN•m/m)
Left Wall Edge
Right Wall Edge

Figure 19

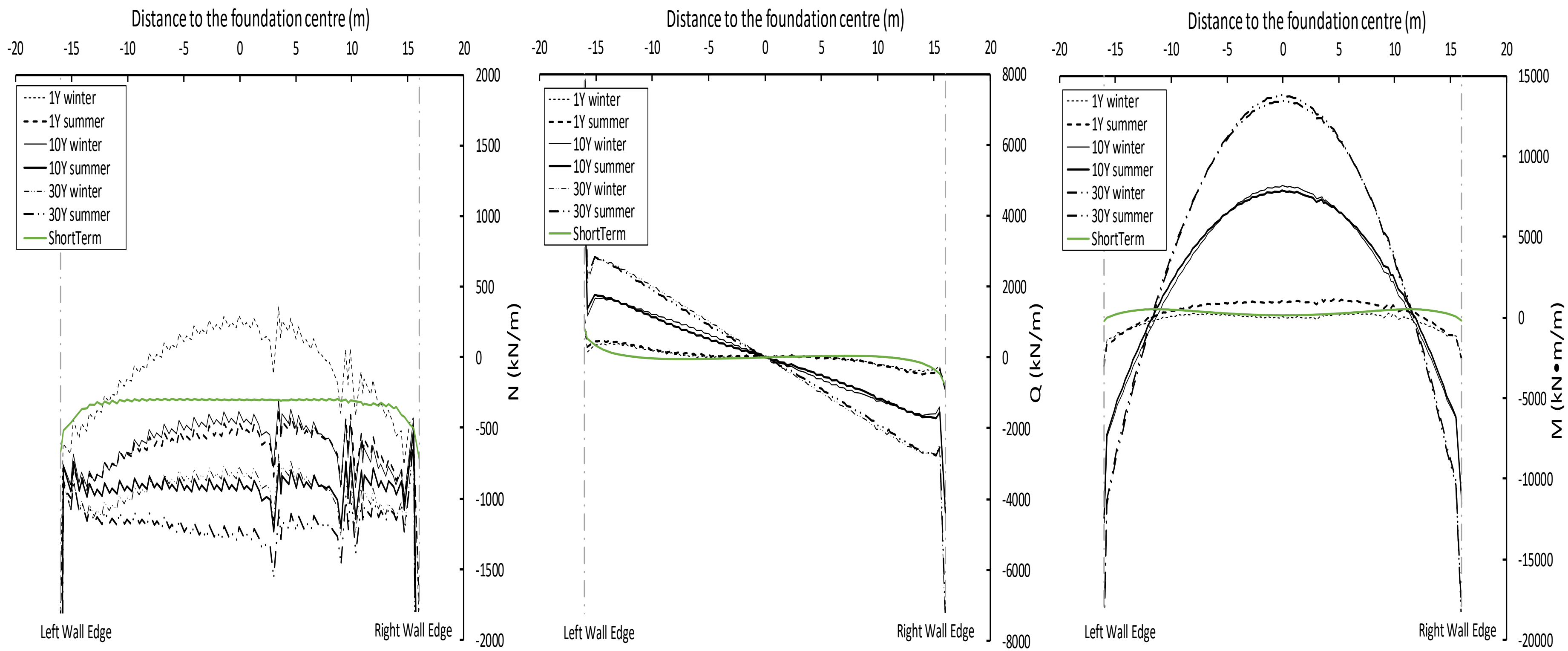
Distance to the foundation centre (m)
-20
-15
-10
-5
0
5
10
15
20
1Y winter
1Y summer
10Y winter
10Y summer
30Y winter
30Y summer
ShortTerm
2000
1500
1000
500
0
-500
-1000
-1500
-2000
N (kN/m)
Left Wall Edge
Right Wall Edge
Distance to the foundation centre (m)
8000
6000
4000
2000
0
-2000
-4000
-6000
-8000
Q (kN/m)
Distance to the foundation centre (m)
15000
10000
5000
0
-5000
-10000
-15000
-20000
M (kN•m/m)

Figure 20a

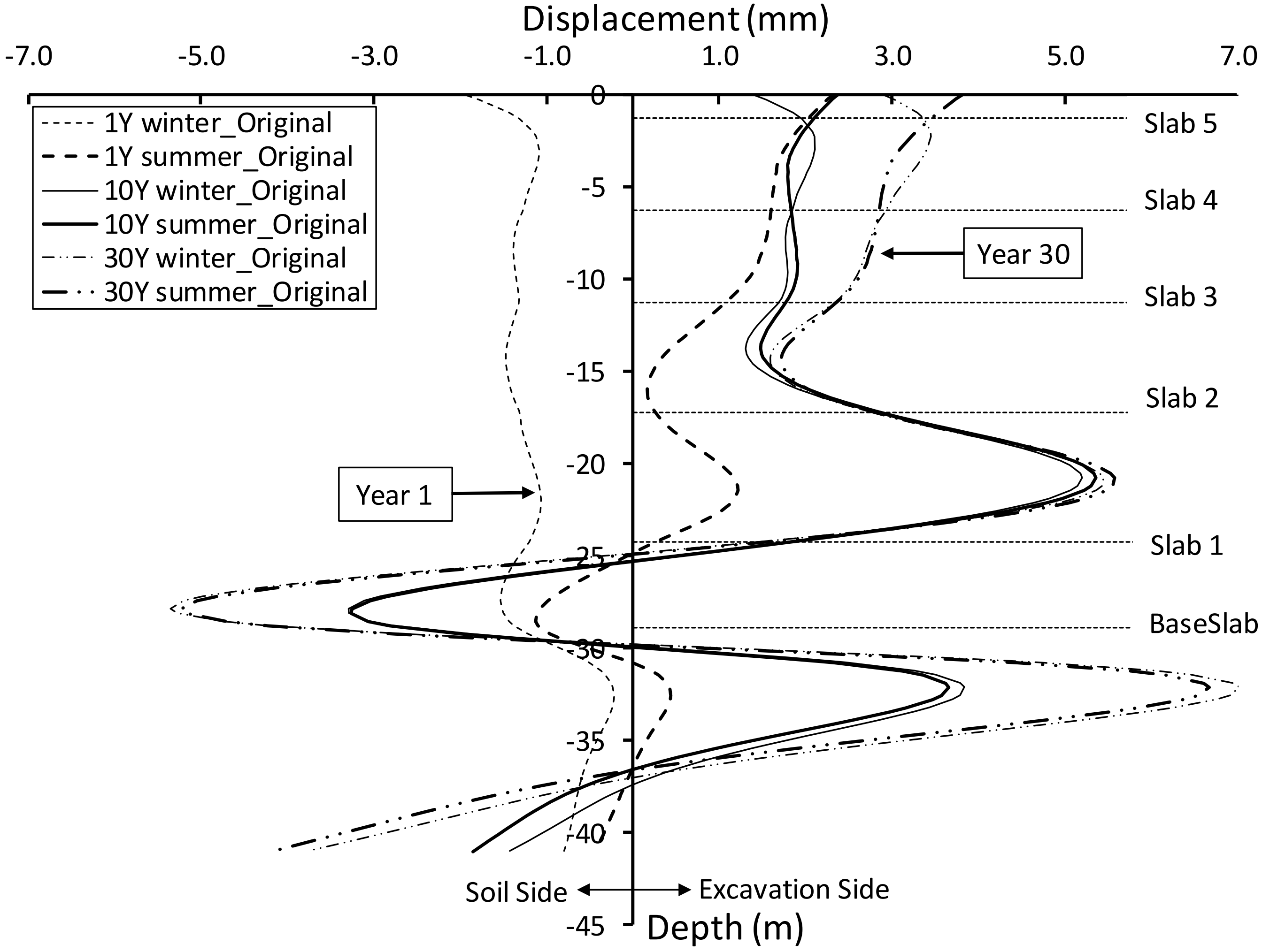

Displacement (mm)
-7.0
-5.0
-3.0
-1.0
1.0
3.0
5.0
7.0
0
-5
-10
-15
-20
-25
-30
-35
-40
-45
Depth (m)
1Y winter_Original
1Y summer_Original
10Y winter_Original
10Y summer_Original
30Y winter_Original
30Y summer_Original
Slab 5
Slab 4
Year 30
Slab 3
Slab 2
Year 1
Slab 1
BaseSlab
Soil Side
Excavation Side

Figure 20b

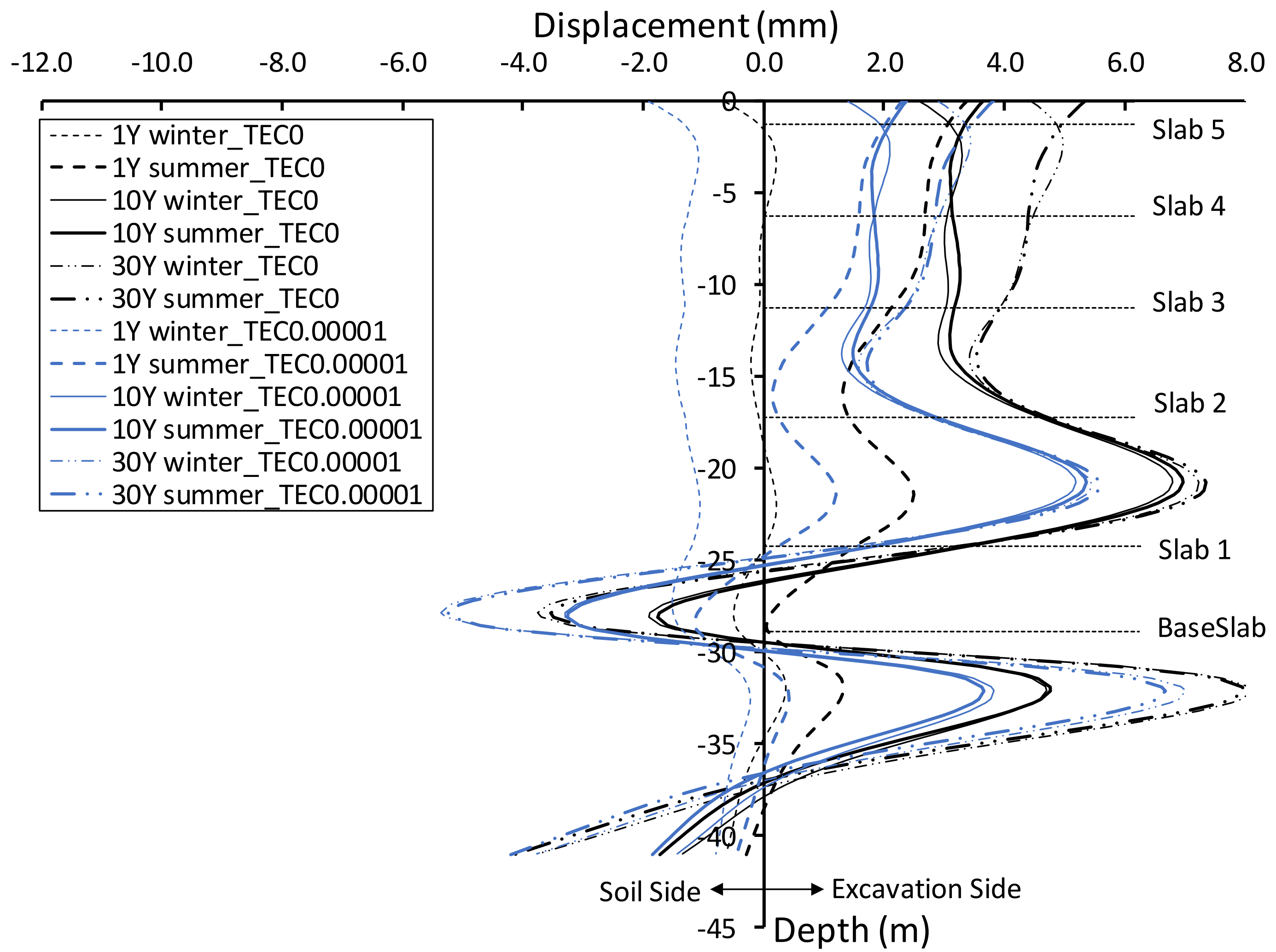
Displacement (mm)
-12.0
-10.0
-8.0
-6.0
-4.0
-2.0
0.0
2.0
4.0
6.0
8.0
0
-5
-10
-15
-20
-25
-30
-35
-40
-45
Depth (m)
1Y winter_TEC0
1Y summer_TEC0
10Y winter_TEC0
10Y summer_TEC0
30Y winter_TEC0
30Y summer_TEC0
1Y winter_TEC0.00001
1Y summer_TEC0.00001
10Y winter_TEC0.00001
10Y summer_TEC0.00001
30Y winter_TEC0.00001
30Y summer_TEC0.00001
Slab 5
Slab 4
Slab 3
Slab 2
Slab 1
BaseSlab
Soil Side
Excavation Side

Figure 20c

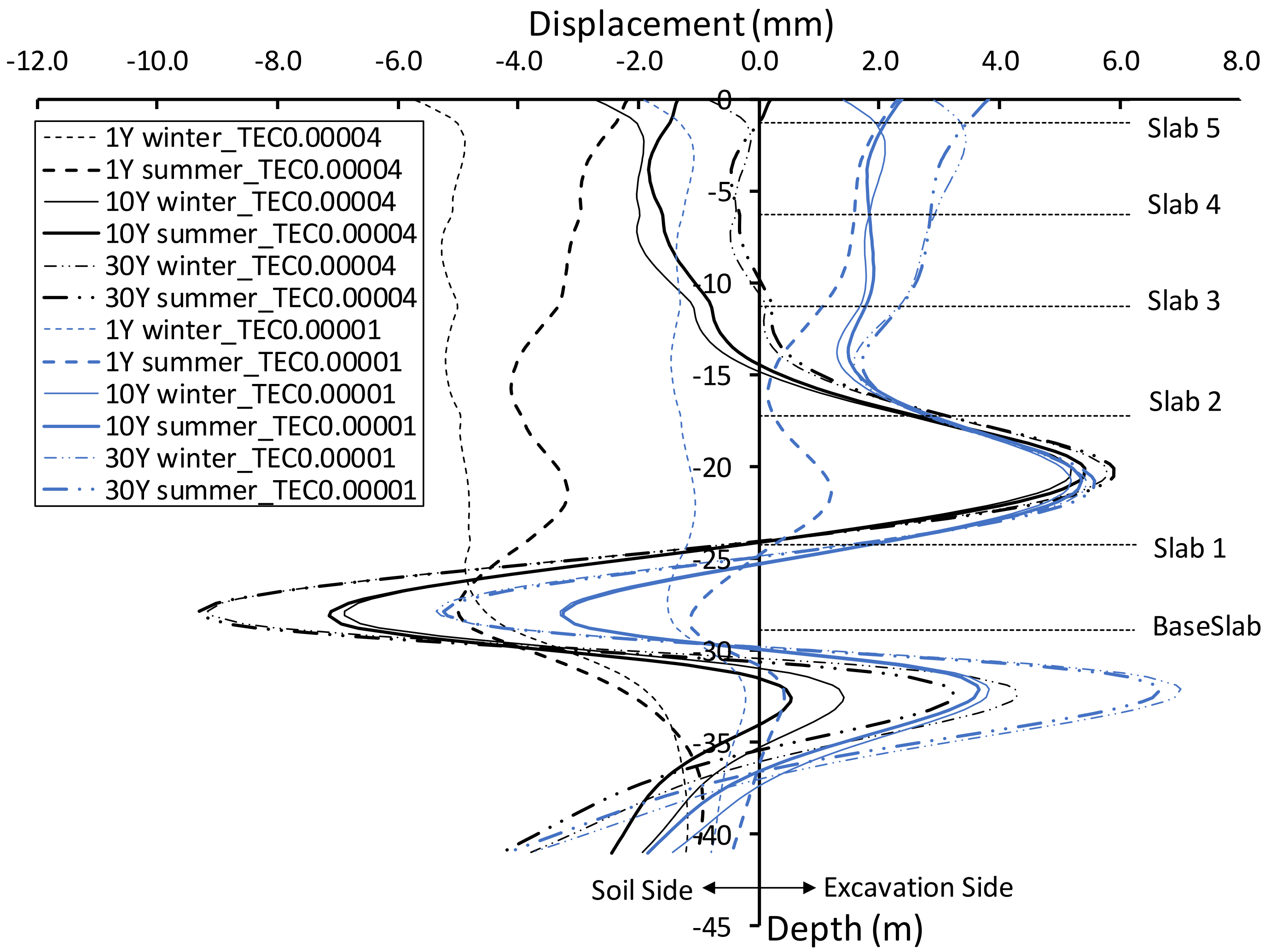
Displacement (mm)
-12.0
-10.0
-8.0
-6.0
-4.0
-2.0
0.0
2.0
4.0
6.0
8.0
0
-5
-10
-15
-20
-25
-30
-35
-40
-45
Depth (m)
1Y winter_TEC0.00004
1Y summer_TEC0.00004
10Y winter_TEC0.00004
10Y summer_TEC0.00004
30Y winter_TEC0.00004
30Y summer_TEC0.00004
1Y winter_TEC0.00001
1Y summer_TEC0.00001
10Y winter_TEC0.00001
10Y summer_TEC0.00001
30Y winter_TEC0.00001
30Y summer_TEC0.00001
Slab 5
Slab 4
Slab 3
Slab 2
Slab 1
BaseSlab
Soil Side
Excavation Side

Figure 21a

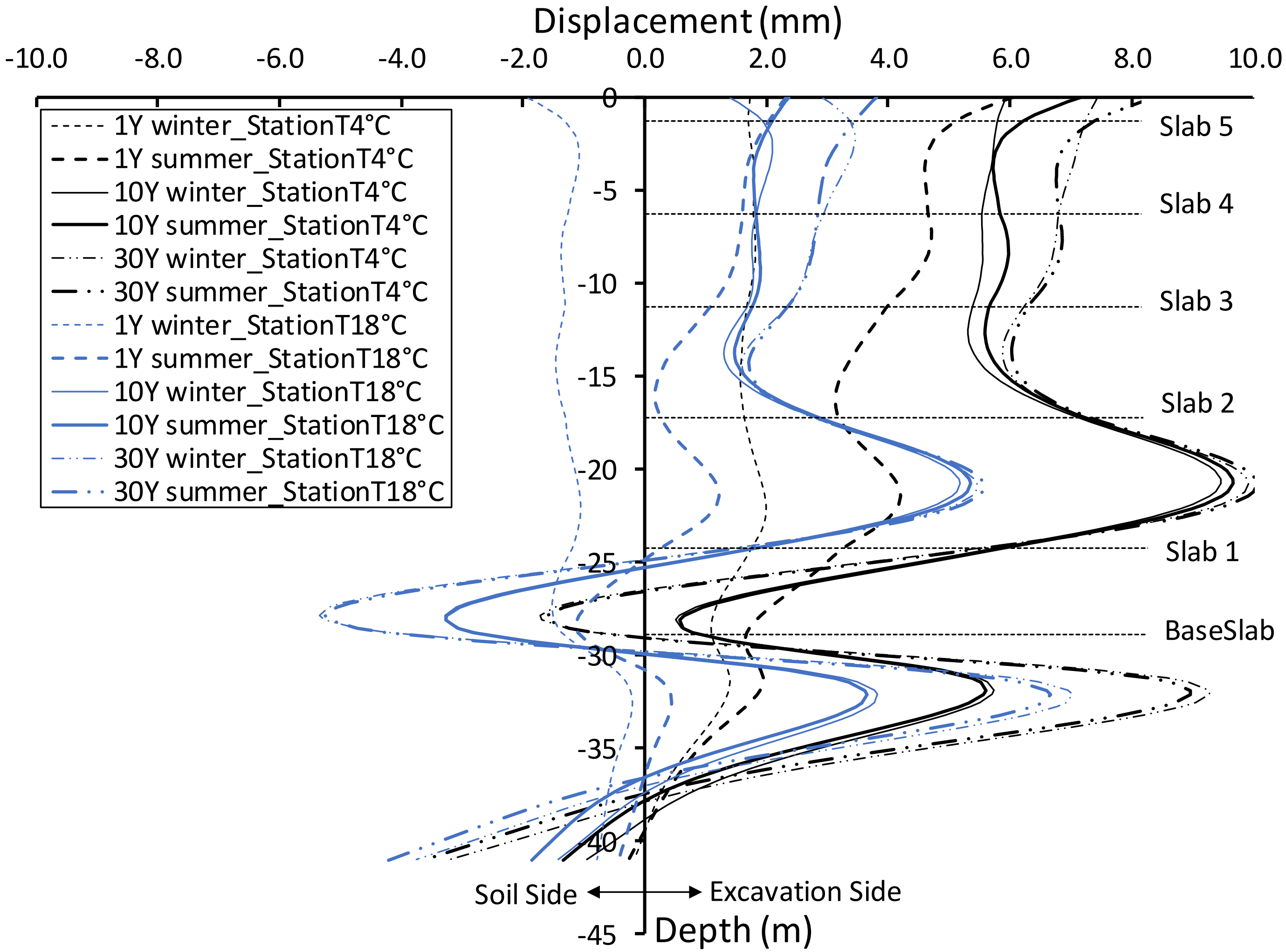
Displacement (mm)
-10.0
-8.0
-6.0
-4.0
-2.0
0.0
2.0
4.0
6.0
8.0
10.0
0
-5
-10
-15
-20
-25
-30
-35
-40
-45
Depth (m)
1Y winter_StationT4°C
1Y summer_StationT4°C
10Y winter_StationT4°C
10Y summer_StationT4°C
30Y winter_StationT4°C
30Y summer_StationT4°C
1Y winter_StationT18°C
1Y summer_StationT18°C
10Y winter_StationT18°C
10Y summer_StationT18°C
30Y winter_StationT18°C
30Y summer_StationT18°C
Slab 5
Slab 4
Slab 3
Slab 2
Slab 1
BaseSlab
Soil Side
Excavation Side

Figure 21b

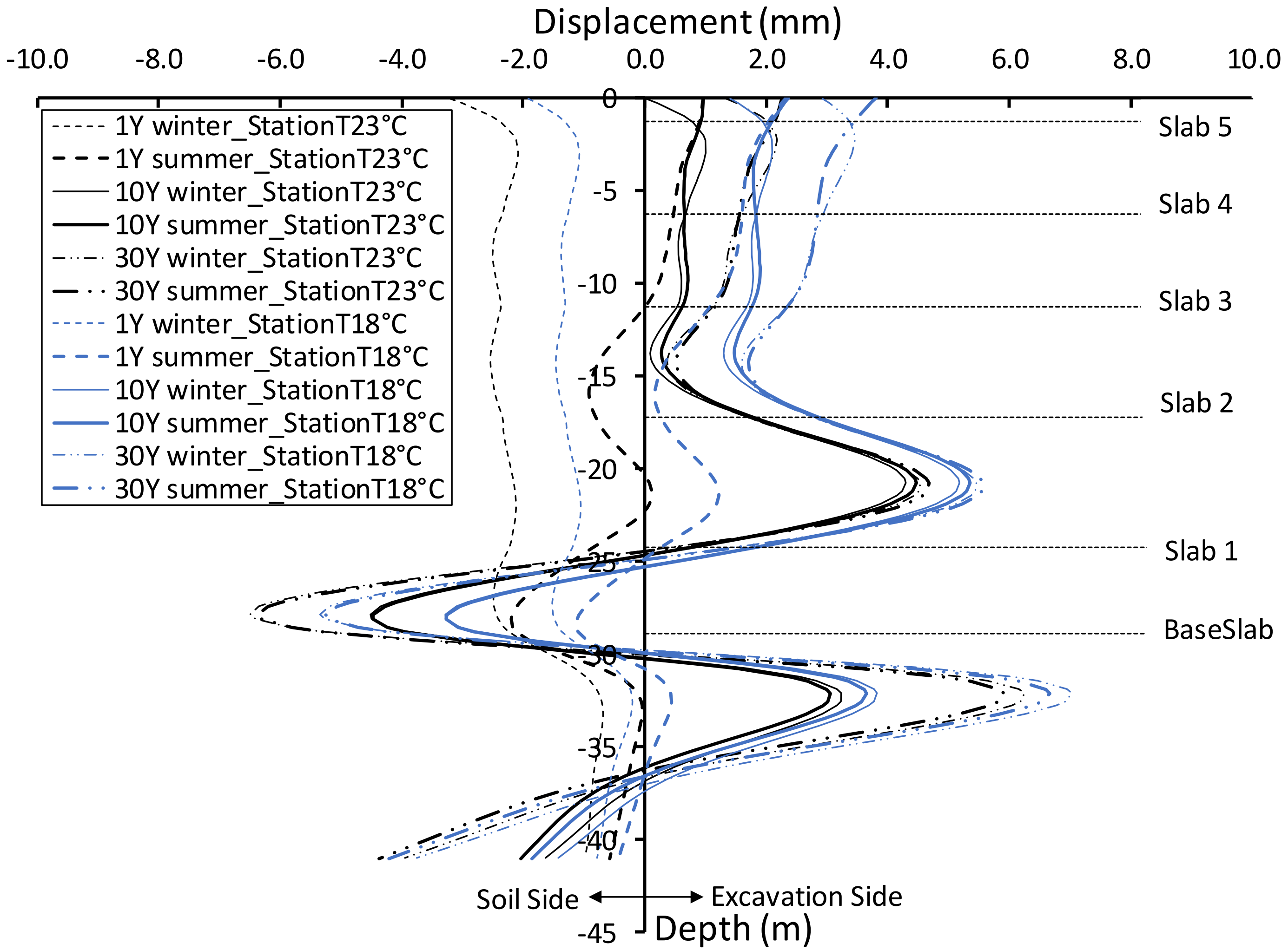
Displacement (mm)
-10.0
-8.0
-6.0
-4.0
-2.0
0.0
2.0
4.0
6.0
8.0
10.0
0
-5
-10
-15
-20
-25
-30
-35
-40
-45
Depth (m)
1Y winter_StationT23°C
1Y summer_StationT23°C
10Y winter_StationT23°C
10Y summer_StationT23°C
30Y winter_StationT23°C
30Y summer_StationT23°C
1Y winter_StationT18°C
1Y summer_StationT18°C
10Y winter_StationT18°C
10Y summer_StationT18°C
30Y winter_StationT18°C
30Y summer_StationT18°C
Slab 5
Slab 4
Slab 3
Slab 2
Slab 1
BaseSlab
Soil Side
Excavation Side

Figure 22a

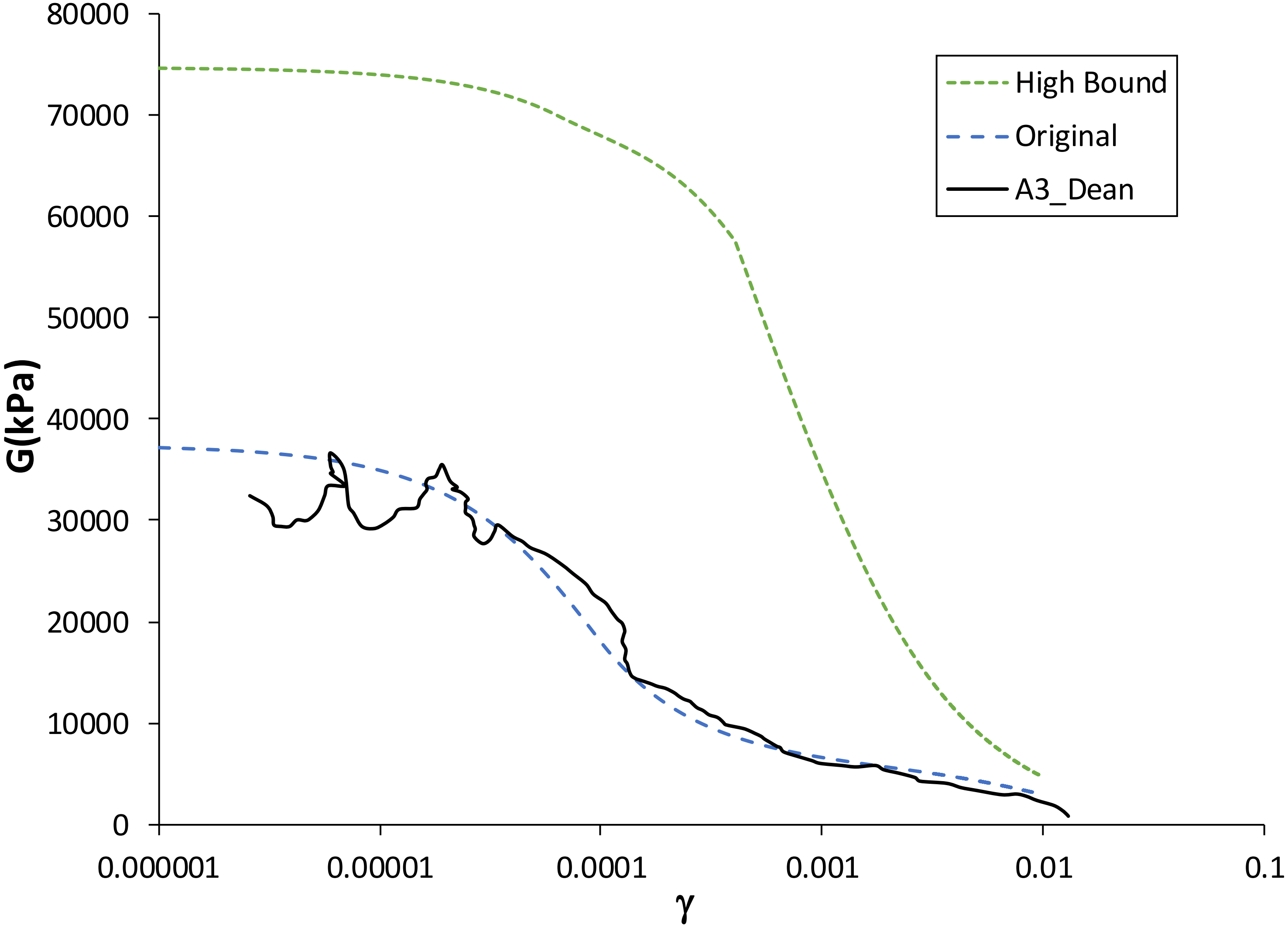
80000
70000
60000
50000
40000
30000
20000
10000
0
G(kPa)
0.000001
0.00001
0.0001
0.001
0.01
0.1
γ
High Bound
Original
A3_Dean

Figure 22b

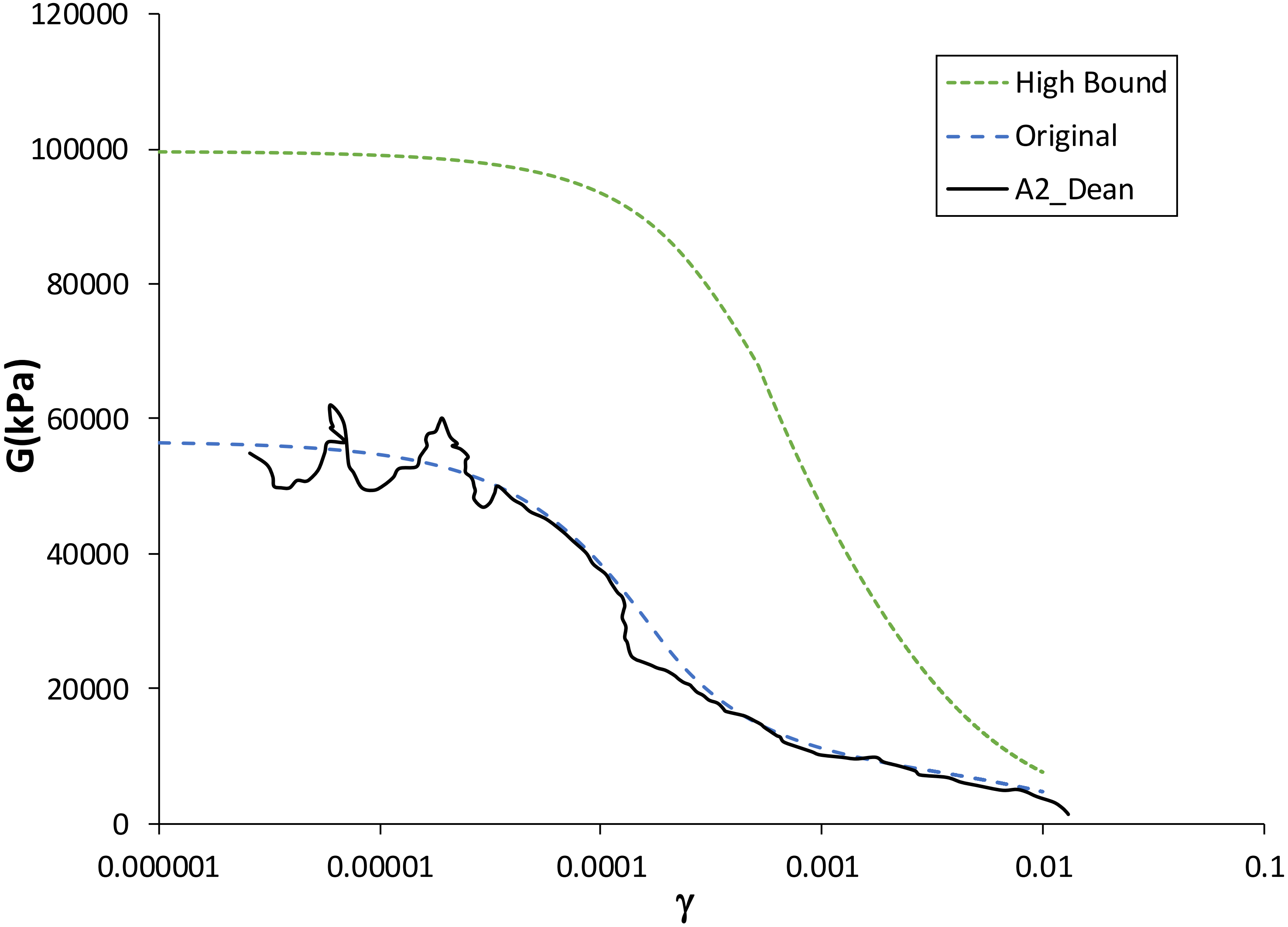
120000
100000
80000
60000
40000
20000
0
G(kPa)
0.000001
0.00001
0.0001
0.001
0.01
0.1
γ
High Bound
Original
A2_Dean

Figure 22c

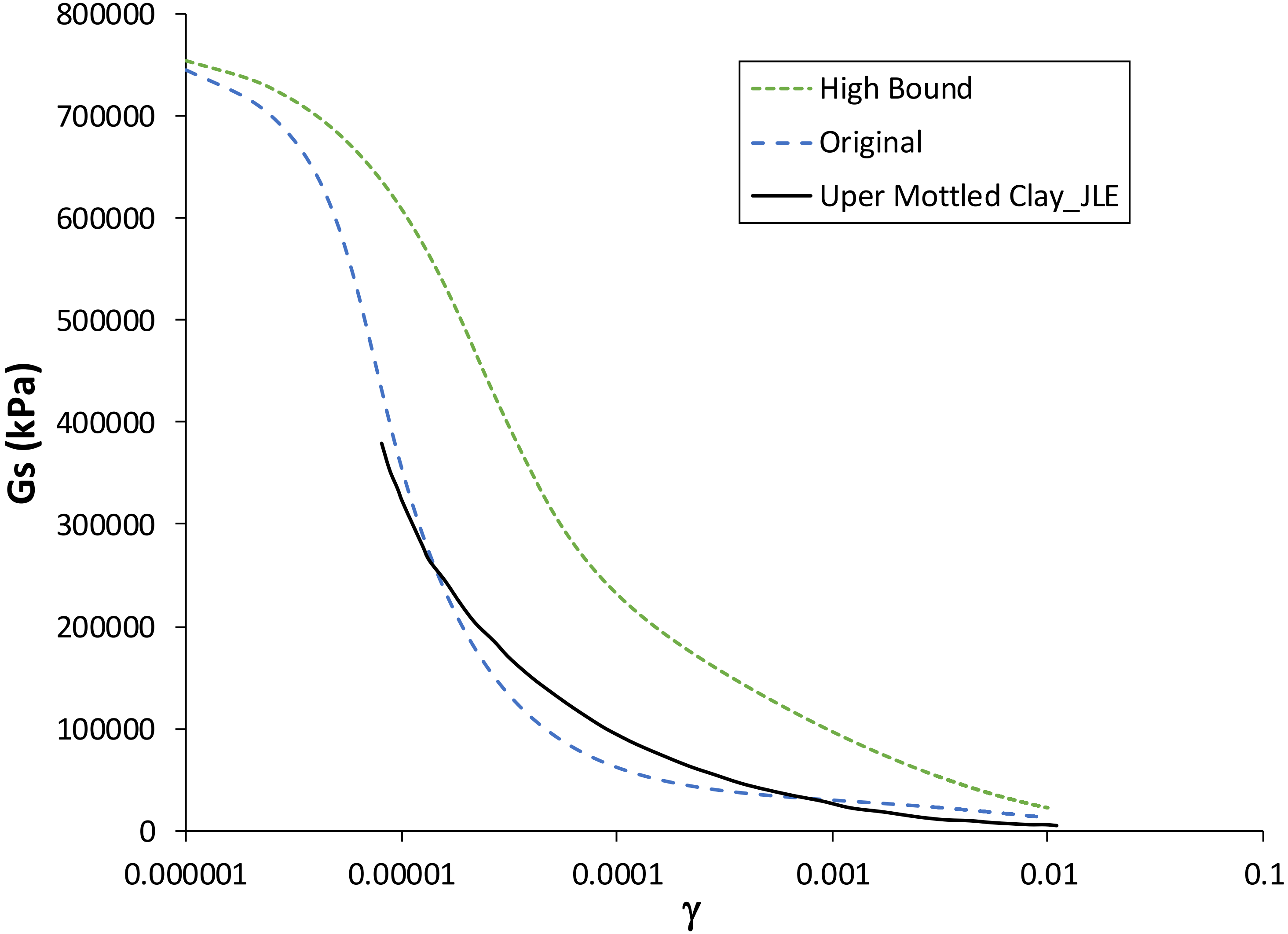

800000
700000
600000
500000
400000
300000
200000
100000
0
Gs (kPa)
0.000001
0.00001
0.0001
0.001
0.01
0.1
γ
High Bound
Original
Uper Mottled Clay_JLE

Figure 22d

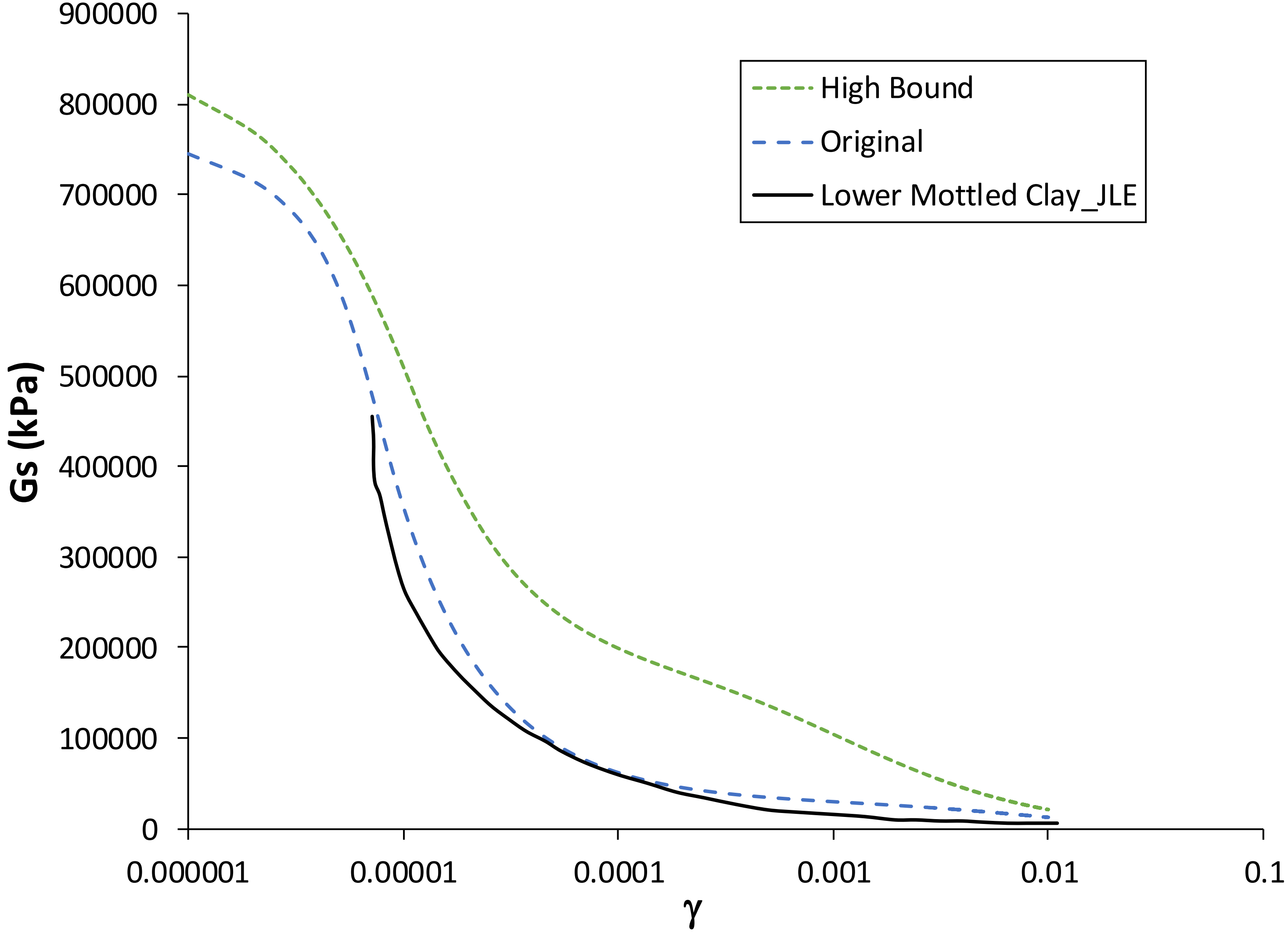
900000
800000
700000
600000
500000
400000
300000
200000
100000
0
Gs (kPa)
0.000001
0.00001
0.0001
0.001
0.01
0.1
γ
High Bound
Original
Lower Mottled Clay_JLE

Figure 23a&b

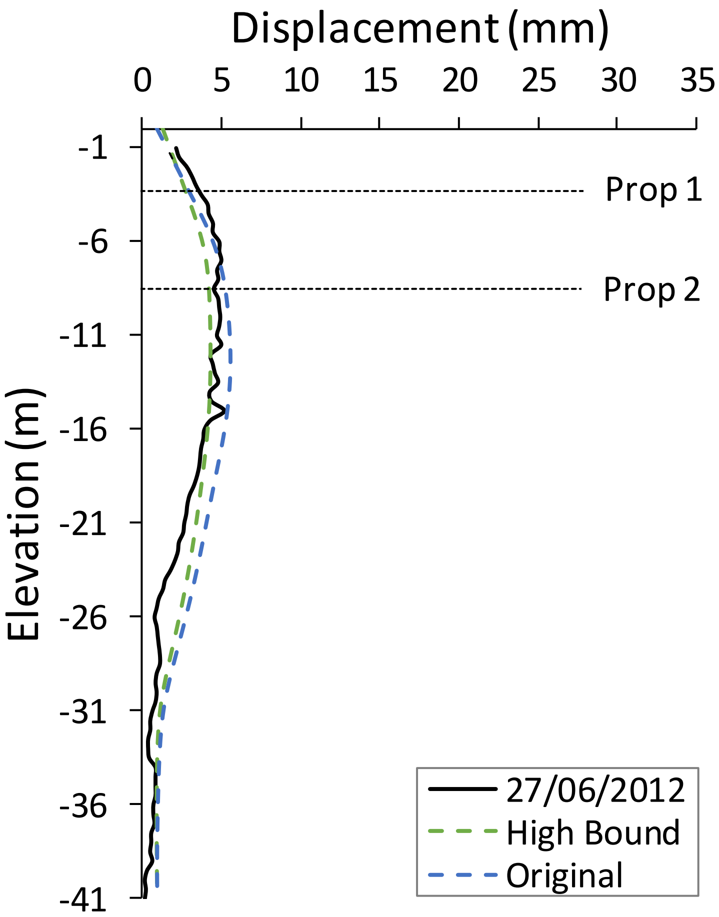
Displacement (mm)
0
5
10
15
20
25
30
35
-1
-6
-11
-16
-21
-26
-31
-36
-41
Elevation (m)
Prop 1
Prop 2
27/06/2012
High Bound
Original

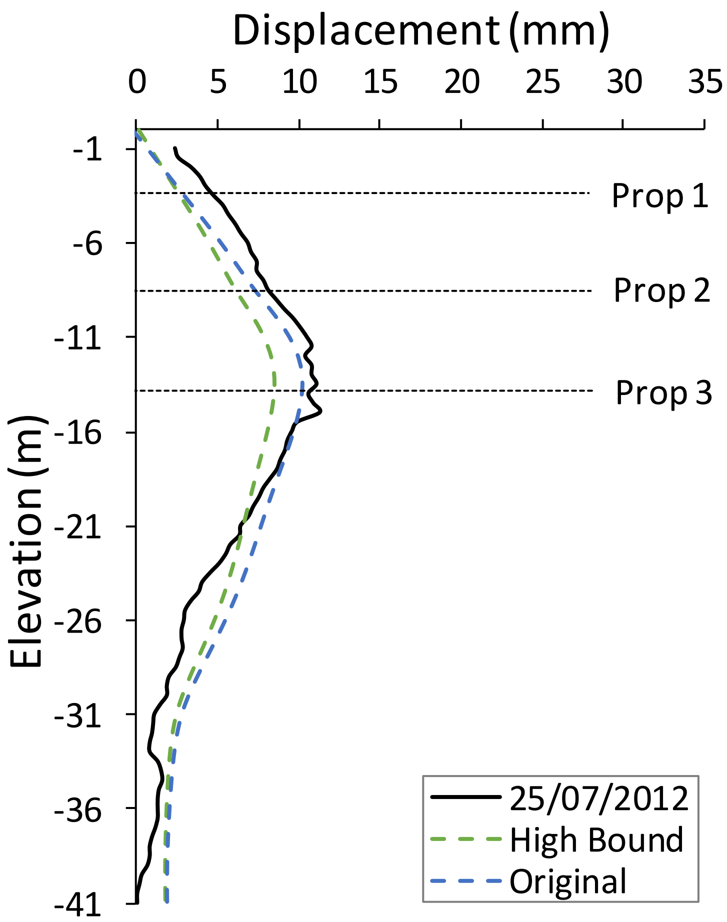
Displacement (mm)
0
5
10
15
20
25
30
35
-1
-6
-11
-16
-21
-26
-31
-36
-41
Elevation (m)
Prop 1
Prop 2
Prop 3
25/07/2012
High Bound
Original

Figure 23c&d

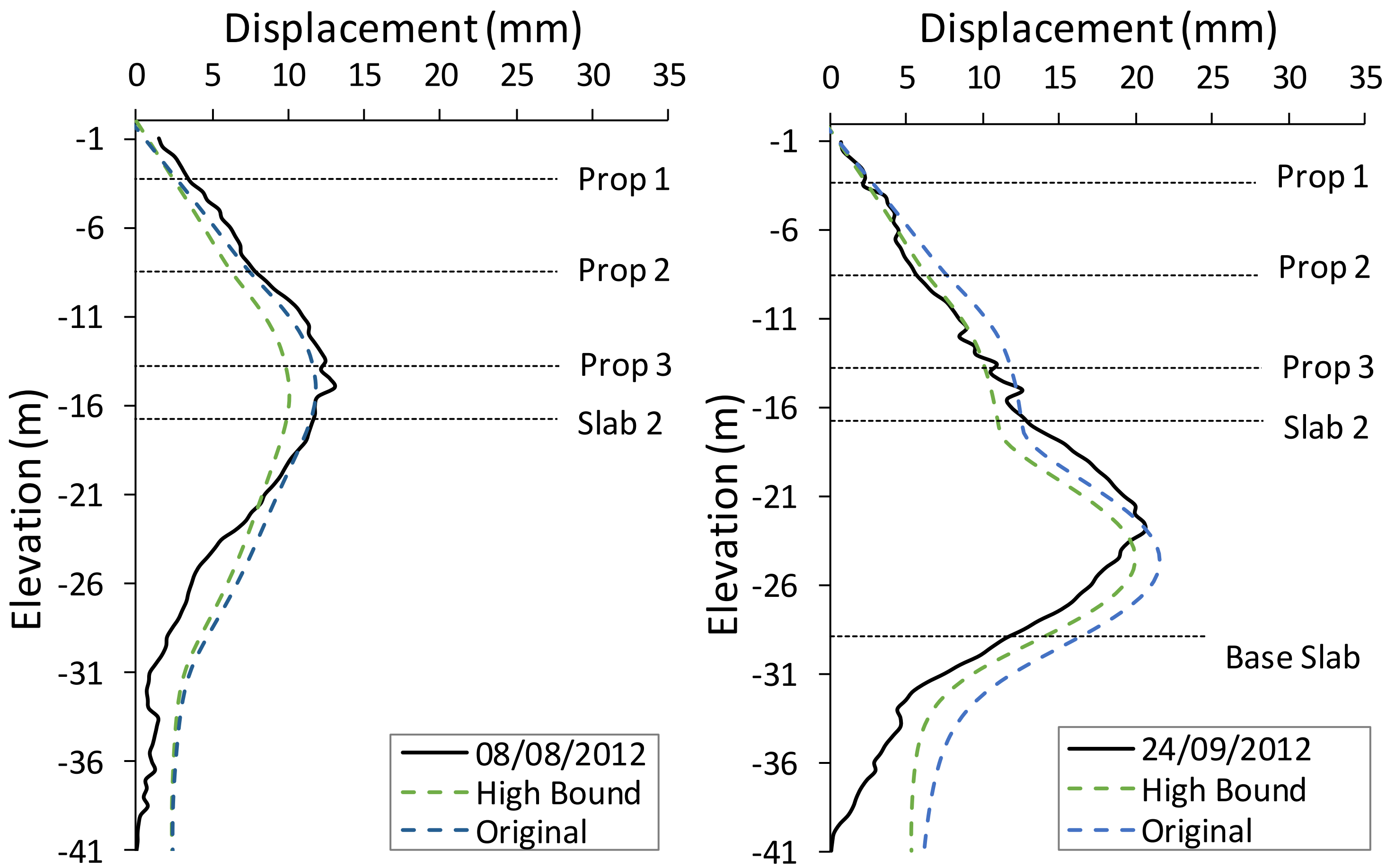

Displacement (mm)
0
5
10
15
20
25
30
35
-1
-6
-11
-16
-21
-26
-31
-36
-41
Elevation (m)
Prop 1
Prop 2
Prop 3
Slab 2
08/08/2012
High Bound
Original
Displacement (mm)
0
5
10
15
20
25
30
35
-1
-6
-11
-16
-21
-26
-31
-36
-41
Elevation (m)
Prop 1
Prop 2
Prop 3
Slab 2
Base Slab
24/09/2012
High Bound
Original

Figure 24

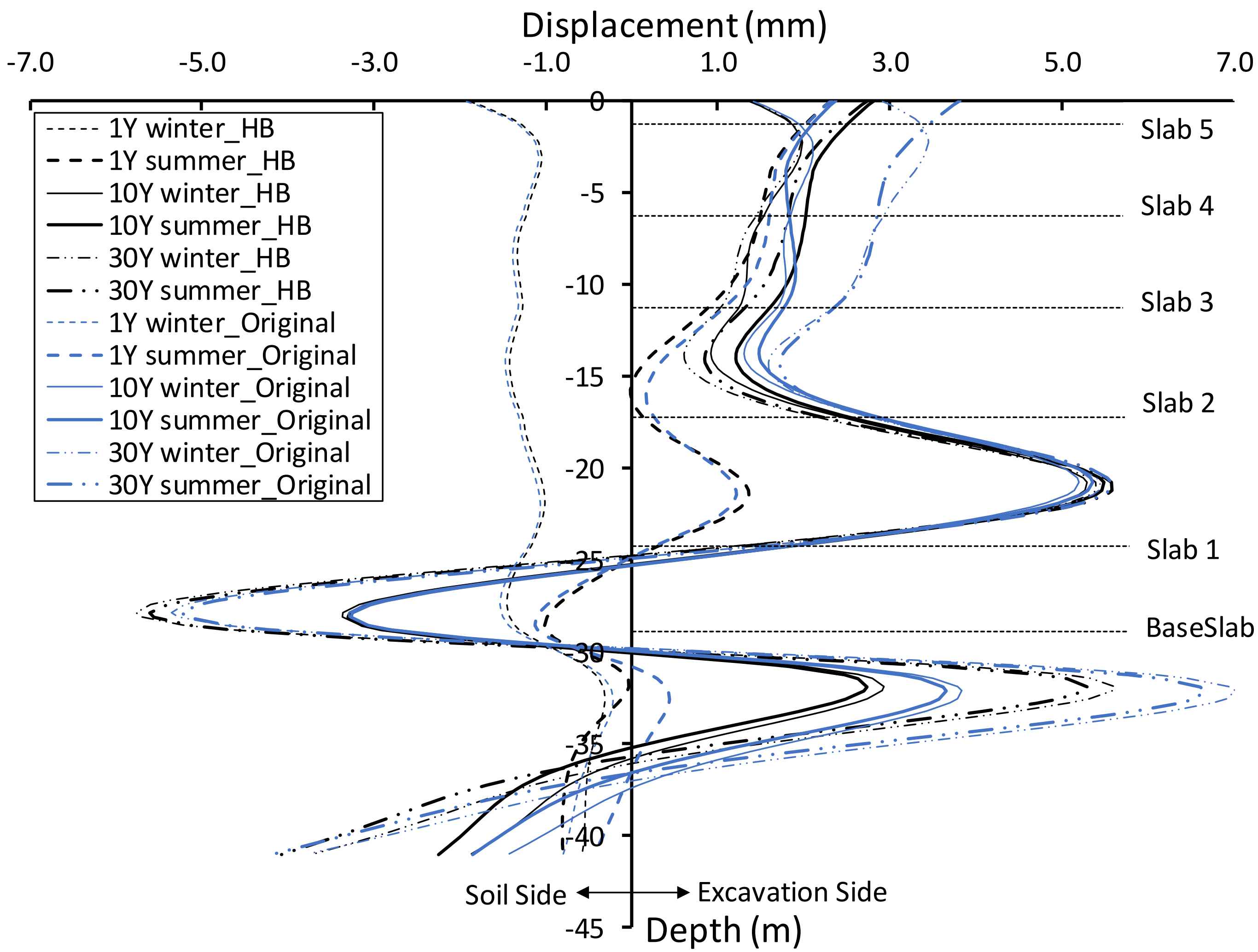
Displacement (mm)
-7.0
-5.0
-3.0
-1.0
1.0
3.0
5.0
7.0
0
-5
-10
-15
-20
-25
-30
-35
-40
-45
1Y winter_HB
1Y summer_HB
10Y winter_HB
10Y summer_HB
30Y winter_HB
30Y summer_HB
1Y winter_Original
1Y summer_Original
10Y winter_Original
10Y summer_Original
30Y winter_Original
30Y summer_Original
Slab 5
Slab 4
Slab 3
Slab 2
Slab 1
BaseSlab
Soil Side
Excavation Side
Depth (m)

Table 1 – Prop (steel) properties (Zdravkovic et al., 2005)

Material type	**E, kPa**	**D_e, m**	**Thickness, mm**	**EA, kN**	**Spacing, m**
Elastic	2.05×10^8	1.0	16	1×10^8	2

Table 2 – Wall and slab properties (Gaba et al., 2003)

Material set	**γ, kN/m³**	**E, kPa**	**ν**	**C_s, kJ/t/K**	**λ_s, kW/m/K**	**ρ_s, t/m³**	**α, 1/K**	**K_0**
Linear elastic, non-porous	24.0	2.59×10^7	0.2	920.0	1.75×10^{-3}	2.50	1×10^{-5}	1.0

Table 3 – Mechanical properties of soil layers (Hight et al., 2004, Rui, 2014)

Soil Description	E, kPa	Material set	ν	c, kPa	ϕ, °	ψ, °
Made Ground	9600	MC, drained, saturated	0.2	0	25	0
Terrace Ground	48000	MC, drained, saturated	0.2	0	35	0
London Clay A3	see Table 5	HSS, undrained A, saturated	0.2	5	25	0
London Clay A2	see Table 5	HSS, undrained A, saturated	0.2	5	25	0
Lambeth Group UMC	see Table 5	HSS, undrained A, saturated	0.2	230	28	0
Lambeth Group LMC	see Table 5	HSS, undrained A, saturated	0.2	230	28	0
Thanet Sand	400800	MC, drained, saturated	0.2	0	27	0
Chalk	400800	MC, drained, saturated	0.2	0	32	0

Table 4 – Thermal properties of soil layers (Rui, 2014)

Soil description	**γ, kN/m³**	**k, m/day**	**C_s, kJ/t/K**	**λ_s, kW/m/K**	**ρ_s, t/m³**	**α, 1/K**	**k_0**
Made Ground	20	8.64	1400	1.25×10^{-3}	2.0	1.0×10^{-5}	0.6
Terrace Ground	21	8.64	1333	1.80×10^{-3}	2.1	1.0×10^{-5}	0.4
London Clay A3	20	8.64×10^{-6}	1600	1.60×10^{-3}	2.0	1.0×10^{-5}	1.0
London Clay A2	21	8.64×10^{-6}	1524	1.60×10^{-3}	2.1	1.0×10^{-5}	1.0
Lambeth Group UMC	21	8.64×10^{-6}	1524	2.10×10^{-3}	2.1	1.0×10^{-5}	1.0
Lambeth Group LMC	21	8.64×10^{-6}	1524	2.10×10^{-3}	2.1	1.0×10^{-5}	1.0
Thanet Sand	21	8.64×10^{-2}	1333	1.27×10^{-3}	2.1	1.0×10^{-5}	1.0
Chalk	19	8.64×10^{-2}	1263	1.27×10^{-3}	1.9	1.0×10^{-5}	1.0

Table 5 – Properties in HSS soil models (Gasparre, 2005, Hight et al., 2004)

Soil description	**Hardening soil model with small-strain stiffness**							
	R_f	m	E_{50}^{ref}, kPa	E_{oed}^{ref}, kPa	E_{ur}^{ref}, kPa	$\gamma_{0.7}$	G_0^{ref}, kPa	p^{ref}, kPa
London Clay A3	0.9	0	6000	6000	110000	3.0×10^{-4}	65000	170
London Clay A2	0.9	0	8500	8500	145000	5.0×10^{-4}	90000	287
Lambeth Group UMC	0.9	1	30000	30000	500000	1.3×10^{-5}	580000	394
Lambeth Group LMC	0.9	1	35000	35000	700000	8.0×10^{-6}	780000	501

Table 6 – Properties in HSS soil models as high bound

Soil description	Hardening soil model with small-strain stiffness							
	R_f	m	E_{50}^{ref}, kPa	E_{oed}^{ref}, kPa	E_{ur}^{ref}, kPa	$\gamma_{0.7}$	G_0^{ref}, kPa	p^{ref}, kPa
London Clay A3	0.9	0	80000	80000	160000	3.0×10^{-4}	75000	170
London Clay A2	0.9	0	70000	70000	145000	5.0×10^{-4}	100000	287
Lambeth Group UMC	0.9	1	200000	200000	500000	1.3×10^{-5}	800000	394
Lambeth Group LMC	0.9	1	200000	200000	700000	8.0×10^{-6}	950000	501